UNIVERSITY OF BELGRADE
FACULTY OF TECHNOLOGY AND METALLURGY

Jelena B. Pavlović

SYNTHESIS AND CHARACTERIZATION OF NOVEL ADSORBENTS AND CATALYSTS BASED ON NATURAL ZEOLITE, APPLICABLE IN USE OF BIOMASS

Doctoral Dissertation

Belgrade, 2020

UNIVERZITET U BEOGRADU
TEHNOLOŠKO-METALURŠKI FAKULTET

Jelena B. Pavlović

SINTEZA I KARAKTERIZACIJA NOVIH ADSORBENASA I KATALIZATORA NA BAZI PRIRODNOG ZEOLITA PRIMENLJIVIH U PROCESU KORIŠĆENJA BIOMASE

doktorska disertacija

Beograd, 2020

Mentor/Advisor:

Dr. Nevenka Rajić, Full Professor

University of Belgrade, Faculty of Technology and Metallurgy

Committee Members:

Dr. Snežana Gojković, Full Professor

University of Belgrade, Faculty of Technology and Metallurgy

Dr. Margarita Popova, Full Professor

Bulgarian Academy of Sciences, Institute of Organic Chemistry with Centre of Phytochemistry

Date of defense:

Mentor:

Dr Nevenka Rajić, redovni profesor

Univerzitet u Beogradu, Tehnološko-metalurški fakultet

Članovi komisije:

Dr Snežana Gojković, redovni profesor

Univerzitet u Beogradu, Tehnološko-metalurški fakultet

Dr Margarita Popova, redovni profesor

Bugarska akademija nauka, Institut za organsku hemiju sa centrum za fitohemiju

Datum odbrane:

ACKNOWLEDGMENTS

This thesis was done at the Department of General and Inorganic Chemistry, Faculty of Technology and Metallurgy, University of Belgrade, as part of the project (No. 172–018) entitled "Oxide-Based environmentally-friendly porous materials for genotoxic substances removal" funded by Ministry of Education, Science and Technological Development of Republic of Serbia.

I would like to express my sincere gratitude to my mentor Prof. Nevenka Rajić for accepting me and giving me the opportunity of being part of her research group, for her dedicated supervision, valuable guidance, and useful advice during all these years.

The part of research work has taken place at the Department of Environmental Sciences, Faculty of Environmental Science and Technology, Norwegian University of Life Sciences, Ås, Norway. I would like to thank Prof. Tore Krogstad and all the people from his research group who have contributed to my research work and to make my time enjoyable.

The part of research work was done in the Institute of Organic Chemistry with Centre of Phytochemistry, Bulgarian Academy of Sciences, Sofia. I would like to thank Prof. Margarita Popova for great scientific discussions and guidance and all the colleagues from her research group who created a productive work environment.

Sincerely, I would like to express my gratitude to the members of my dissertation committee: Prof. Margarita Popova and Prof. Snežana Gojković for their careful, constructive and insightful comments in relation to this thesis.

I would like to thank colleagues from the National Institute of Chemistry, Laboratory of Inorganic Chemistry and Technology, Ljubljana, for their support in the experimental analysis of the samples.

My sincere gratitude to Prof. Đorđe Stojaković for helpful discussion, all useful comments, suggestions and engagement during these years.

I am thankful to all the current and former colleagues at the Department of General and Inorganic Chemistry.

Last but not least my thanks are reserved for my family and friends for supporting me throughout my studies and believing in me.

Synthesis and characterization of novel adsorbents and catalysts based on natural zeolite, applicable in use of biomass

ABSTRACT

The thesis has two interconnected general goals. The first one was to develop novel, environmentally friendly and cost-efficient soil supplements using natural zeolite (clinoptilolite, CLI) which will retain plant nutrients (nitrogen, potassium and phosphorus) in different soil types and accordingly increase biomass production. The second one was to develop effective clinoptilolite-based catalysts for biomass conversion into industrial valuable chemicals.

To achieve the first aim, nitrate and phosphate adsorption onto CLI modified with several oxides were studied. The obtained results showed that the oxide coverage of CLI surface makes it accessible for effective binding of nitrate and phosphate ions. The best adsorption ability was obtained for Fe(III)-enriched CLI (FeCLI). FeCLI shows significantly better retention effect than CLI but the leaching depends on soil types. Nitrate retention increases by the zeolite addition only for silty loam and silty clay soils whereas potassium retention increases in the following order: silty loam < silty clay << sandy soil. FeCLI shows a retention effect in phosphate leaching only from sandy soil.

The second goal was development of a CLI-based catalyst effective in the esterification of levulinic acid (LA) which can be obtained from biomass. The catalysts were prepared from CLI and SnO_2 or sulfated SnO_2. Sulfated catalysts are more active than nonsulfated ones. Nonsulfated catalysts showed a high activity in the conversion of LA into octyl levulinate (55%) and moderate activity in the conversion into ethyl levulinate (22%), whereas sulfated catalysts led to a total conversion of LA to esters.

Keywords: clinoptilolite, natural zeolite, oxide-modified clinoptilolite, adsorption, soil supplements, leaching, biomass, catalysts, levulinic acid, esterification.

Scientific field: Scince of Chemistry

Scientific subfield: Inorganic Chemistry

Sinteza i karakterizacija novih adsorbenasa i katalizatora na bazi prirodnog zeolita primenljivih u procesu korišćenja biomase

SAŽETAK

Teza ima dva međusobno povezana opšta cilja. Prvi cilj je dobijanje novog, ekološki prihvatljivog i jeftinog zemljišnog suplementa korišćenjem prirodnog zeolita (klinoptilolit, CLI) koji će zadržati biljne nutrijente (azot, kalijum i fosfor) u različitim vrstama zemljišta i shodno tome povećati proizvodnju biomase. Drugi cilj je dobijanje efikasnog katalizatora na bazi klinoptilolita za konverziju biomase u industrijski važne hemikalije.

Za postizanje prvog cilja, proučavana je adsorpcija nitrata i fosfata na CLI koji je bio modifikovan sa nekoliko oksida. Dobijeni rezultati pokazali su da oksidna prevlaka na površini CLI omogućava efikasno vezanje nitrata i fosfata. Najbolja adsorpciona sposobnost dobijena je za Fe(III)-obogaćen CLI (FeCLI). FeCLI pokazuje značajno bolji efekat zadržavanja ispitivanih jona u odnosu na CLI, ali izluživanje zavisi od vrste zemljišta. Zadržavanje nitrata povećava se dodatkom zeolita u praškastu glinu i praškastu ilovaču, dok se zadržavanje kalijuma povećava sledećim redosledom: praškasta ilovača < praškasta glina << peskuša. FeCLI pokazuje efekat zadržavanja fosfata samo za peskuše.

Drugi cilj teze bio je razvoj efikasnog katalizatora zasnovanog na CLI, za primenu u esterifikaciji levulinske kiseline (LA) koja se može dobiti iz biomase. Katalizator je pripremljen iz CLI i SnO_2 ili sulfatiranog SnO_2. Sulfatirani katalizatori pokazali su veću aktivnost u odnosu na nesulfatirane. Nesulfatirani katalizatori pokazali su aktivnost u konverziji LA u oktil levulinat (55%) i umerenu aktivnost u konverziji u etil levulinat (22%), dok su sulfatirani katalizatori LA u potpunosti konvertovali u estre.

Ključne reči: klinoptilolit, prirodni zeolit, oksidom-modifikovan klinoptilolit, adsorpcija, zemljišni suplementi, izluživanje, biomasa, katalizatori, levulinska kiselina, esterifikacija.

Naučna oblast: Hemijske nauke

Uža naučna oblast: Neorganska hemija

TABLE OF CONTENTS

LIST OF FIGURES

LIST OF TABLES

ABBREVIATIONS

BH	Silty clay soil from Bosnia and Hercegovina
CLI	Clinoptilolite
DRS	UV/Visible diffuse reflectance spectroscopy
EDS	Energy dispersive X-ray spectroscopy
ELA	Ethyl levulinate
Et	Ethanol
FeCLI	Iron(III)-containing clinoptilolite
FTIR	Fourier transform infrared spectroscopy
HCLI	Hydrogen form of clinoptilolite
HDTMA	Hexadecyltrimethylammonium-bromide
LA	Levulinic acid
LE	Esters of levulinic acid
MCLI	Metal containing samples (M – Fe, Mg or Mn)
MgCLI	Magnesium-containing clinoptilolite
MnCLI	Manganese-containing clinoptilolite
NaCLI	Na-containing form of clinoptilolite
NMR	Solid-state nuclear magnetic resonance
NW	Sandy soil from Norway
Oc	Octanol
OLA	Octyl levulinate

PXRD	Powder X-ray powder diffraction
SEM	Scanning Electron Microscopy
SMO	Sulfated metal oxides
SnHCLI	SnO_2-containing clinoptilolite
SRB	Silty loam soil from Serbia
SSnHCLI	Sulfated SnO_2-containing clinoptilolite
TG/DTG	Thermal analysis
XPS	X-ray photoelectron spectroscopy

1. INTRODUCTION

XXI century has been declared a century of Green chemistry. Thus, many efforts have been devoted to prevent and minimize the adverse effects on the environment and human health caused primarily by population growth and industrialization progress. A large amount of hazardous waste has been produced leading to deterioration of water, air and soil and affecting human health.

Water pollution is a worldwide problem. Both surface and groundwater sources are severely polluted by various contaminants. An increasing concern is associated with a high concentration of plant nutrients such as nitrate and phosphate. The most common sources of these plant nutrients are municipal and industrial wastewater, and wastewater from landfills. Agricultural activities usually result in the overuse of nitrate and phosphate fertilizers and improper storage of animal waste. Thus, an excessive use of nitrate fertilizers does not lead to the increase of soil fertility and crop yields. Due to the high solubility of nitrate compounds in water and low adsorption onto soil particles, nitrate ions move freely through soil and readily leach to groundwater. Leaching of phosphates occurs to a lower extent due to their higher adsorption onto soil particles. High concentrations of nitrates and phosphates promote not only eutrophication of water bodies but also deterioration of groundwater quality. This is of a great concern primarily of countries that use groundwater for drinking water supply. Accordingly, there is an increasing interest for the uses of soil amendments which not only improve agricultural production but also prevent degradation of groundwater quality through the reduction of nutrients leaching.

Moreover, high concentrations of hazardous gases, toxic volatile organic compounds, particulate matter etc. in the atmosphere, generation of large amounts of solid waste and their inappropriate disposal, an excessive energy consumption have directed many scientific investigations towards development of new, green and sustainable materials as well as to more effective technological processes based on renewable sources of energy. In this regard, great benefits have been expected through valorization of biomass. Biomass is organic material origins from plants and animals. Biomass is an ideal, abundantly available, inexpensive and renewable source that can be converted to either energy or a variety of valuable chemicals. Several chemicals that can be obtained from biomass are

recognized as platform chemicals. They can be converted to other types of chemicals that are considered as a replacement for the fossil-based chemicals. One of the twelve platform chemicals is levulinic acid (LA). LA is a reactive organic acid that can be converted to valuable industrial chemicals. Thus, great efforts are directed to the synthesis of esters of levulinic acid. The physicochemical properties of levulinate esters make them applicable as solvents, plasticizers, fuel additives and biolubricants.

Natural zeolites as abundant, inexpensive, environmentally friendly and harmless minerals have been recognized as perspective materials for different applications. Zeolites are crystalline, hydrated aluminosilicates with a porous structure. Due to their unique structural features, they have been used as ion-exchanger, adsorbents and catalysts. All of these performances can be improved by a rather simple modification which makes their use more attractive. Traditionally, zeolites have been used in different areas including environmental protection, industrial processes, agriculture, veterinary, pharmacy and medicine. Nowadays, natural zeolites have been studied as starting materials for green and sustainable processes including biomass production and biomass conversion to valuable chemicals and biofuels.

The aims of this doctoral thesis are as follows:

1) Development of novel, environmentally friendly and cost-effective soil supplements based on clinoptilolite as the most abundant natural zeolite. To achieve this goal natural clinoptilolite from deposits in R. Serbia was modified with several oxides and obtained products were characterized in detail. Their adsorption capacity, the influence of the specific parameters on the adsorption of several plant nutrients were studied in batch experiments. Adsorption kinetics and mechanism were examined by commonly used adsorption models. The most efficient products were tested as soil supplements in column systems using three typical soil types: sandy, silty loam and silty clay soil.
2) Development of an effective, reusable and environmentally friendly catalyst based on clinoptilolite applicable for esterification of levulinic acid. The catalyst was prepared from natural clinoptilolite and SnO_2 or sulfated SnO_2. Catalytic activity was studied in the esterification of levulinic acid with octanol and ethanol, by batch method under mild reaction conditions. Applicability of the obtained catalysts was additionally confirmed in the recyclability tests.

2. THEORETICAL PART

2.1 Structure of zeolites

Zeolites are crystalline, hydrated aluminosilicate minerals. They are composed of three-dimensional frameworks consisting of $[SiO_4]^{4-}$ and $[AlO_4]^{5-}$ tetrahedral units linked *via* oxygen atoms (Figure 1). The lattice of zeolites is negatively charged, and its electroneutrality is achieved by extraframework cations - alkali and earth alkaline cations.

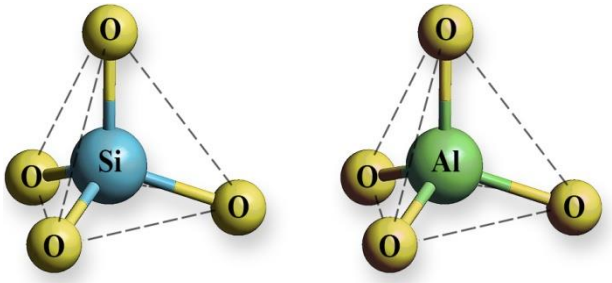

Figure 1. $[SiO_4]^{4-}$ and $[AlO_4]^{5-}$ tetrahedral units of zeolite lattice.

These cations are present inside cavities and channels of zeolite lattice accompanied with water molecules. The cations are mobile and can be substituted with other cations from the solution giving zeolites an ion-exchange property. Ion-exchange takes place to varying degrees depending on nature of zeolites, nature of cations present in zeolite lattice and solution as well as on experimental conditions (static or dynamic regime, solid:liquid ratio, contact time, reaction temperature, initial concentration, pH, contact time). Water molecules can be removed from zeolite lattice reversibly giving zeolites properties of drying agent.

Since the lattice of zeolites is porous, consisting of channels and cages, its specific surface area is large being several hundred to thousand square meters per gram. Consequently, zeolites possess good adsorptive and molecular sieve properties. The shape and size of apertures on cavities and channels influence the adsorptive behavior. Thus, only molecules with a diameter less than that of the apertures can enter the zeolite lattice. This gives to zeolites molecular sieving property.

Moreover, zeolite lattice can accommodate not only metal cations but also hydrogen ions. Their presence in the zeolite lattice gives to zeolites properties of solid acids with catalytic activity in various chemical reactions.

The acidity of zeolites is expressed as Brönsted and Lewis acidity (Figure 2). The Brönsted acid sites originate from the bridging hydroxyl groups (Si–OH–Al) whereas the Lewis acid sites are associated with three-coordinate framework Al or/and extra-framework Al species. The acidity of zeolites can be significantly enriched by chemical or thermal treatment of zeolites.

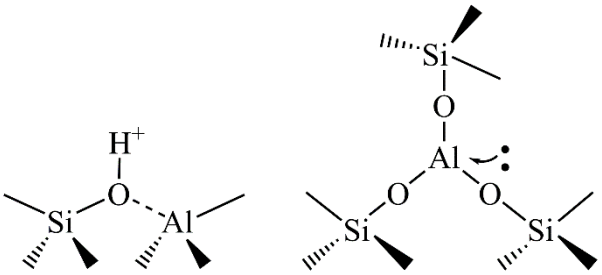

Figure 2. The Brönsted (left) and Lewis (right) acid sites in zeolite lattice.

2.1.1 Clinoptilolite - the most abundant natural zeolite

According to the structural database of the International Zeolite Association (IZA) from 2019, about 60 different zeolite structures belong to natural zeolites and 237 for synthetic ones (https://europe.iza-structure.org/IZA-SC/ftc_table.php). Among the natural zeolites, clinoptilolite is the most abundant one. Deposits of zeolitic tuff rich with clinoptilolite are found in many countries. In R. Serbia, several deposits including Zlatokop (Vranjska Banja), Igroš (Brus), Beočin (Fruška gora) and Slanci (Belgrade) are rich with clinoptilolite making that clinoptilolite is a mineral resource of R. Serbia.

Based on the IZA classification, clinoptilolite (CLI) is a member of the heulandite (HEU) group of zeolites. However, both Si/Al molar ratio and thermal stability make CLI different from HEU. The Si/Al ratio of CLI is in the range 4.0–5.3 whereas for HEU this ratio is lower than 4.0. Additionally, CLI is thermal stable up to 800 °C whereas the thermal stability of HEU is lower - up to 550 °C.

The framework of the CLI (Figure 3) consists of three types of channels: A - formed from 10-membered rings, B - formed from 8-membered rings and C - formed from 8-membered rings. The channels A (0.3 x 0.76 nm) and B (0.33 x 0.46 nm) are parallel to

the *c*-axis, while the C channel (0.26 x 0.47 nm) is parallel to the *a*-axis (Godelitsas and Armbruster, 2003; Dziedzicka *et al*., 2016).

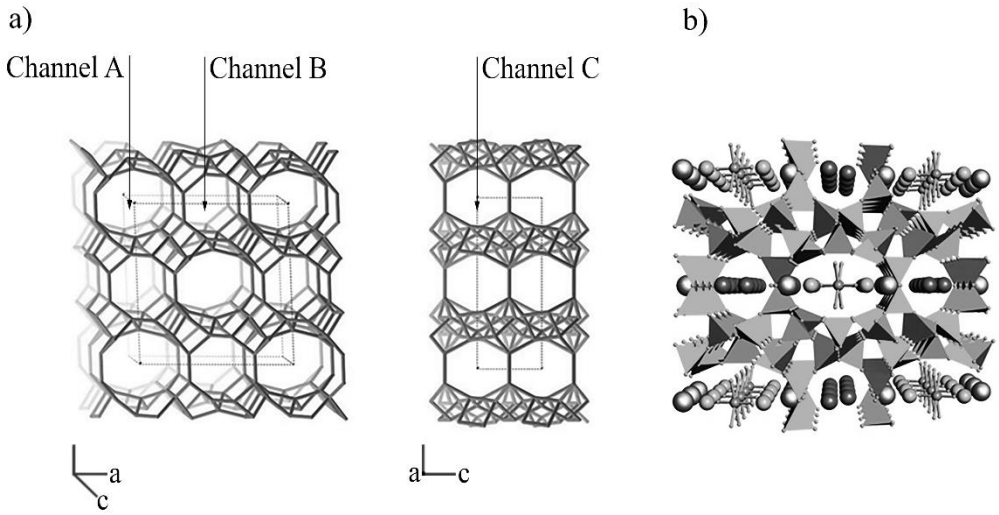

Figure 3. Schematic view of: a) 3D-structure of clinoptilolite lattice (International Zeolite Association, IZA Structure Commission, https://europe.iza-structure.org/IZA-SC/framework.php?STC=HEU) and b) Cavities and channels inside the clinoptilolite lattice (tetrahedra represent the $[SiO_4]^{4-}$ and $[AlO_4]^{5-}$ building units); balls show ion-exchangeable cations (Rajic *et al*., 2011).

2.2 Use of clinoptilolite

Due to its structural features and availability, CLI has been recognized as a perspective, cost-effective and environmentally friendly material for the synthesis of different types of materials that have been used in ion-exchange, adsorption and catalysis.

CLI has been studied for water and wastewater treatments. It can be used in removal of different cations (Ca^{2+}, Mg^{2+}, Cu^{2+}, Zn^{2+}, Co^{2+}, Cd^{2+}, Ni^{2+}, Pb^{2+}, Fe^{2+} etc.), anions (NO_3^-, PO_4^{3-}, AsO_4^{3-}, CrO_4^{2-}, $Cr_2O_7^{2-}$, etc.) as well as different types of organic compounds (including dyes, phenols, pesticides and different pharmaceuticals) from water and wastewaters (Rajić *et al.*, 2010; Wang and Peng, 2010; Camacho *et al.*, 2011; Hailu *et al*., 2019).

CLI and its modified forms have been also investigated for application in medical and pharmaceutical purposes. Thus, CLI has been studied as a gastric antacid, antidiarrheic as well as an adjuvant in anticancer therapy (Pavelić *et al*., 2001; Tomečková *et al*.,

2012). It has been tested also as a drug carrier for salicylate anion or diclofenac (Jevtić *et al*., 2012; Gennaro *et al*., 2015). Antibacterial and antimicrobial activity of metal-containing CLI have also been reported and explained by slow release of Ag^{+}, Cu^{2+} or Zn^{2+} from the CLI lattice (Top and Ülkü, 2004; Hrenović *et al*., 2013).

CLI has properties which are beneficial for agriculture and soil chemistry. The addition of CLI to the soil can improve the physicochemical properties of soils (especially sandy soil) and contribute to the remediation of the soils contaminated by toxic metals such as Cd, Ni, Pb, Zn, Co (Andronikashvili, 2012; Yi *et al*., 2019). Moreover, the addition of CLI to soil can improve (prolong) the retention of plant nutrients in the soil providing their better utilization by plant, which leads not only to decrease of the fertilizer usage but also to prevention of groundwater pollution caused by leaching of usual plant nutrients (Reháková *et al*., 2004).

CLI can be catalytic active in different organic reactions such as isomerization, hydrocracking, esterification or oxidation (Soylu *et al*., 2010; Akgül and Karabakan, 2010). The catalytic activity and selectivity of CLI are attributed to its structural features and acidity as well as to the possibility to adopt its structural features by different treatments. Nowadays, great efforts are directed to the use of CLI in catalysis for new, green and sustainable processes. Among others, these processes include biomass conversion to high-value chemicals and biofuels by using CLI as catalyst or catalyst support (Akgül *et al*., 2013; Rajić *et al*., 2013).

2.2.1 Adsorptive properties

In recent years, the adsorption has been proven to be an effective method in environmental protection. The process is usually simple, low cost for maintenance and many available adsorbents can be applied. Thus, naturally occurring materials (chitin, clays, natural zeolites), different types of agricultural wastes (corncob, fruits stones, straw, coffee), as well as industrial waste (fly ash, red mud, sugarcane bagasse) have been recognized as perspective adsorbents (Singh *et al*., 2018). The main criteria in an adsorbent selection are cost effectiveness, availability, adsorption capacity as well as its recyclability. Taking this into account, CLI has been studied as a promising adsorbent.

a) Ion-exchange

Due to the weak electrostatic interactions between hydrated extraframework cations and aluminosilicate lattice, these cations can be readily exchanged with other cations from solution through an ion-exchange reaction. Various parameters including chemical nature of cations both in lattice and in solution, pH of the solution, temperature, as well as contact time affect the ion-exchange process. High selectivity of CLI has been reported toward cations such as Cs^{+}, NH_4^{+}, K^{+}, Na^{+}, Ca^{2+}, Mg^{2+} (Jaskūnas *et al*., 2015) but also to heavy metal cations including Pb^{2+}, Cd^{2+}, Zn^{2+}, Cu^{2+}, Ni^{2+} (Inglezakis *et al*., 2003; Rajić *et al*., 2010; Wang and Peng, 2010). Moreover, the ion-exchange capacity of CLI can be significantly enriched by its modification. The most common procedure includes the preparation of the homoionic-form of CLI (mainly Na-containing form, NaCLI) by treating CLI with a concentrated solution of NaCl (Tarasevich *et al*., 2008; Mozgawa *et al*., 2009; Rajić *et al*., 2010; Mihaly-Cozmuta *et al*., 2014).

Mechanism of ion-exchange usually includes two steps:

1) fast ion-exchange reaction between easily available cations from CLI and cations present in solution, and
2) cation diffusion within the CLI lattice, which is usually a rate-controlling step.

Transition metal (TM) cations readily form complexes in water media and accordingly, mechanism of ion-exchange by TM can include chemisorption or inner-sphere complexation (Doula and Ioannou, 2003; Çoruh, 2008). In addition, an increasing of the adsorbed TM amounts on zeolite surface can result in formation of TM complex species and their surface precipitation.

The regeneration of saturated CLI adsorbent usually includes a reverse ion-exchange reaction in which CLI reacts with aqueous solution of NaCl, KCl, Na_2CO_3 or NaOH. The regeneration efficiency is affected by the cation concentration, temperature, contact time and pH (Turan *et al*., 2005; Gedik and Imamoglu, 2008; Katsou *et al*., 2011). Usually, the regeneration process does not influence the CLI crystal structure.

b) Adsorption of anionic species

Due to negatively charged aluminosilicate lattice, CLI does not show an affinity toward anions. Also, its hydrophilic surface does not attract non polar organic species.

However, surface charge and polarity can be altered by using appropriate modification procedures.

The most commonly used modification includes the use of different surfactants. Quaternary ammonium compounds such as tetraethylammonium-, hexadecyltrimetylammonium-, cetylpyridinium- or octadecyltrimethylammonium-ion (Guan *et al*., 2010; Schick *et al.*, 2010) are usually applied. Depending on the surfactant concentration, modification of CLI can lead to the formation of monolayer or bilayer surfactant coverage (Figure 4). By bilayer surfactant coverage, negatively charged CLI surface becomes positively charged and thus available for various anions such as arsenates, iodide, nitrates, sulfates, chromates, phosphates, etc. as well as organic species such as pharmaceuticals or pesticides (Rivera and Farías, 2005; Guan *et al*., 2010; Schick *et al.*, 2010; Jevtić *et al.*, 2012).

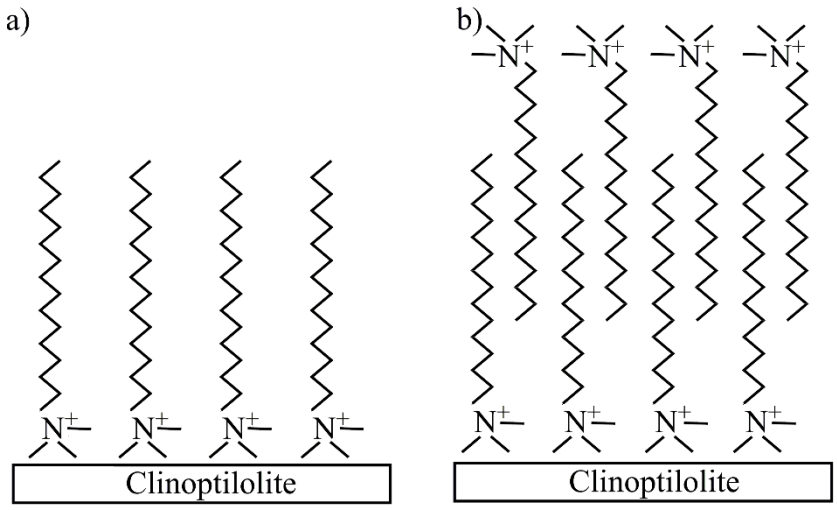

Figure 4. Schematic presentation of surfactant coverage formation on the clinoptilolite surface: a) monolayer and b) bilayer (modified from Figueiredo and Quintelas, 2017).

Moreover, different oxides present on the CLI surface can also improve or change its adsorption capacity and affinity. It has been shown that oxide coverage can improve the CLI adsorption capacity toward cations (such as lead, copper, manganese or zinc), and also its affinity for different anions (arsenates, selenite and selenate, phosphates) (Kragović *et al*., 2013; Jevtić *et al.*, 2014; Kaplanec *et al.*, 2017).

The most common oxide modification includes modification with Fe(III). Usually, the modification included two steps:

1) conversion of CLI to Na-containing form (NaCLI) by using a concentrated solution of NaCl, and
2) NaCLI conversion to Fe(III)-containing CLI (FeCLI) by treating NaCLI with Fe(III)-containing solution (Huo *et al.*, 2012; Guaya *et al.*, 2016). The addition of NaOH in this step promotes the formation of iron oxides on the CLI upon dehydration or calcination.

Various Fe(III) species have been found at the CLI surface after the modification (Doula, 2007; Kragović *et al*., 2013; Jevtić *et al*., 2014):

1) isolated Fe(III) ions in the lattice or at the lattice positions in the CLI structure,
2) Fe(III) complexes at the extraframework positions,
3) Fe(III) nanooxide particles at the CLI surface,
4) bulk Fe(III) oxide coverage.

Modification of CLI with Fe(III) affects the textural properties of the CLI increasing specific surface area over 100 m^2 g^{-1} – that is about three times higher than for parent CLI (Jevtić *et al.*, 2014) or over 50 m^2 g^{-1} (Kragović *et al*., 2013) depending on crystallinity of Fe(III) coating.

The adsorption capacity of FeCLI has been studied for different oxyanions including chromate, phosphate, arsenite and arsenate, as well as selenite and selenite (Jeon *et al*., 2009; Du *et al*., 2012; Jevtić *et al*., 2014; Guaya *et al.*, 2016). In general, the adsorption is influenced by chemical nature of the oxyanions and reaction conditions (amount of FeCLI, initial concentration, presence of competition anions, reaction temperature and pH).

Adsorption of oxyanions proceeds through the formation of oxo-complexes with Fe(III). Also, pH has an important factor in the adsorption process. Under acidic conditions (pH below pH_{PZC}[1]), the adsorption mechanism is considered to be an electrostatic attraction between the positively charged surface of FeCLI and negatively charged oxyanions. The

[1] pH_{PZC} (Point of zero charge pH) represents the pH value for which the net surface charge of adsorbent is equal to zero.

adsorption of $H_2AsO_4^-$ was therefore proposed to proceed by the following reactions (Jeon *et al*., 2009):

$$CLI–Fe–OH_2^+(s) + H_2AsO_4^-(aq) \rightarrow CLI–Fe–O–AsO_3H(s) + H_2O(l)$$

At pH above $pH_{PZC,}$ the surface of FeCLI is mainly negatively charged indicating the formation of oxo-complexes *via* a ligand-exchange reaction rather than electrostatic attraction. The oxyanions present in the aqueous solution replace the hydroxyl ions from the FeCLI surface without affecting its crystal structure. In this regard, the adsorption of As(V) onto FeCLI was proposed to occur through the following reactions (Jeon *et al*., 2009):

$$CLI–Fe–OH(s) + H_2AsO_4^-(aq) \rightarrow CLI–Fe–OAsO_3H(s) + OH^-(aq)$$

$$CLI–Fe–OH(s) + HAsO_4^{2-}(aq) \rightarrow CLI–Fe–O_2AsO_2H^-(s) + OH^-(aq)$$

$$2CLI–Fe–OH(s) + HAsO_4^{2-}(aq) \rightarrow 2CLI–FeO–AsO_2H(s) + 2OH^-(aq)$$

The ligand-exchange reaction leads to the formation of inner-sphere monodentate and bidentate (mononuclear and binuclear) Fe(III) complexes (Figure 5).

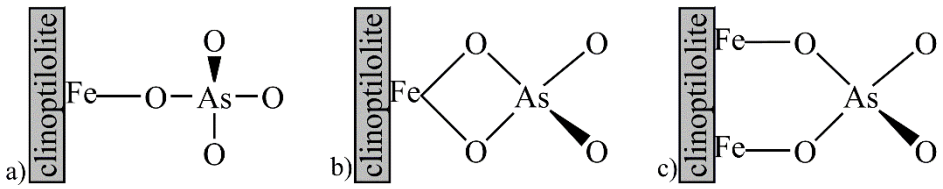

Figure 5. Schematic presentation of monodentate (a), bidentate mononuclear (b) and bidentate binuclear complexes (c) formed onto FeCLI.

The influence of the pH on the adsorption of oxyanions onto FeCLI has been widely studied. The adsorption of As(V) has been reported to remain unaffected in the pH range from 3 up to 8 (Jeon *et al*., 2009; Nekhunguni *et al*., 2017). However, at pH>8 adsorption capacity of As(V) decreases. Moreover, the adsorption of Cr(VI) also shows dependence on pH: 50% decrease of capacity has been found by increasing pH from 3 to 7 (Du *et al*., 2012). Similarly, the adsorption of both Se(IV) and Se(VI) decreases with pH

increase due to competition of hydroxyl ions with Se-oxyanions for the adsorption sites onto FeCLI (Jevtić *et al*., 2014).

At comparable reaction conditions, the adsorption of oxyanions such as As(V) onto FeCLI is lower than that on CLI modified with cationic surfactants (Chutia *et al*., 2009). However, leaching of the surfactant molecules from CLI is difficult to control and therefore limits their use especially in the treatment of drinking water. However, FeCLI shows a higher adsorption capacity toward As(V) than Mn-containing CLI (Jiménez-Cedillo *et al.,* 2009).

Regeneration of saturated FeCLI mainly includes a reverse ion-exchange. However, the tendency of oxyanions to bond strongly to the iron oxide species present onto FeCLI leads to its partial regeneration. Thus, the adsorption of both As(III) and As(V) is reported to be practically irreversible with HCl (up to 3 mol dm^{-3}) suggesting the formation of strong covalent bonds between these atoms and FeCLI (Šiljeg *et al*., 2009). Similarly, FeCLI is partially regenerated by NaOH, $NaHCO_3$ or Na_2CO_3 after adsorption of phosphate (Guaya *et al.,* 2016; Kaplanec *et al*., 2017). In addition, a partial regeneration of FeCLI by phosphate buffer is obtained after adsorption of Se(IV) and Se(VI) showing the higher regeneration for Se(VI) due to the formation of a more labile complex with the surface of FeCLI (Jevtić *et al*., 2014).

1. Adsorption of nitrate ions

The most commonly used modification method of CLI for nitrate adsorption is loading of different surfactant molecules at the CLI surface. Hexadecyltrimethylammonium-bromide (HDTMA) is one of the most commonly used cationic surfactants.

The amounts of HDTMA on the surface of CLI differ depending on CLI origin as well as the initial concentration of HDTMA (Guan *et al*., 2010). The modified CLI (HDTMACLI) exhibits different nitrate adsorption capacity depending on HDTMA amounts: for the HDTMA amounts ranging from 75 to 219 mmol HDTMA kg^{-1}, the nitrate adsorption capacity varies (being 8 to 18 times higher than for parent CLI). This was explained by the fact that low amounts of HDTMA onto CLI results mainly in the formation of HDTMA monolayer which is not accessable for nitrate bonding. At higher HDTMA amounts, HDTMA double layers are formed which significantly improve nitrate adsorption efficiency. Thus, HDTMACLI with the HDTMA amount being 120% of the CLI effective cation exchange capacity approaches the adsorption equilibrium for

60 min and removes 80% of nitrate from solution with initial concentration of 2.42 mmol dm^{-3} (Schick *et al.*, 2010). The presence of competition anions such as chloride, sulfate and bicarbonate does not influence significantly the nitrate removal rate but influences the adsorption kinetics. However, despite the fact that HDTMACLI shows high removal rate, use of HDTMA in the CLI modification is under review due to toxicity of HDTMA. The reported results show that the leaching of HDTMA from the CLI occurs in the concentrations that exceed the ecotoxic level (Schick *et al.*, 2011). The problem could be overcome by filtration of effluents through activated carbon beds but this significantly increases operational costs.

Cetylpyridinium bromide (CPB) is also used for the modification of CLI (Zhan *et al*., 2011). The presence of chloride sulfate or bicarbonate influences the adsorption rate leading to slight reduce pf the nitrate adsorption rate.

Recently, the modification of CLI with chitosan has been shown as an effective method for nitrate removal (Arora *et al*., 2010; Yazdi *et al*., 2019). Chitosan is a polysaccharide (Figure 6) obtained from chitin which is one of the most abundant biopolymers (after cellulose).

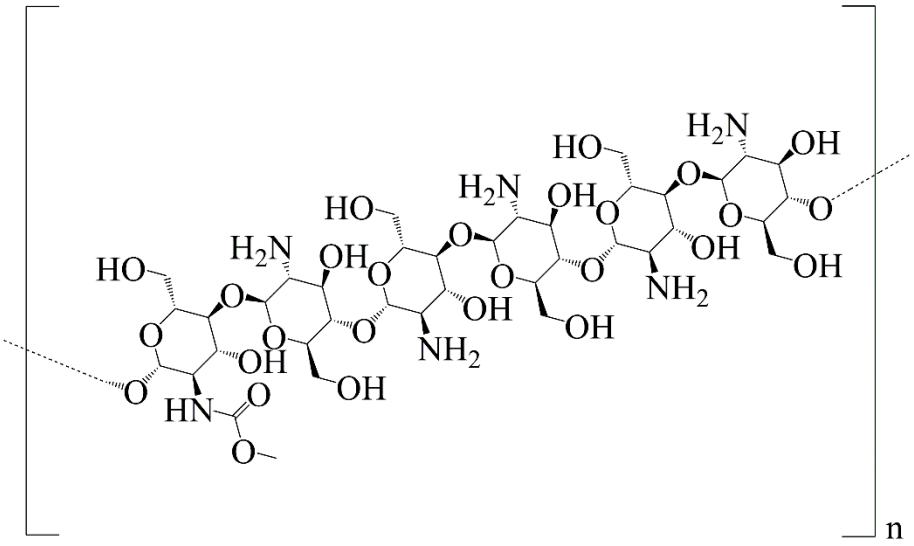

Figure 6. Structural formula of chitosan.

This biopolymer possesses numerous binding sites - functional groups such as amine and hydroxyl groups - giving the chitosan ability for cation bonding (Figure 6). Furthermore, nitrate adsorption onto CLI loaded with chitosan (CLICH) can be

significantly enhanced through chitosan protonation by hydrochloric acid or by its functionalization with pentaethylenehexamine (Arora *et al*., 2010; Yazdi *et al*., 2019). Both methods provide additional binding sites for interaction with nitrate ions. However, the efficacy of CLICH for nitrate adsorption is limited by the presence of chloride, sulfate, carbonate and hydroxyl anions. Moreover, although the spent CLICH can be regenerated using the NaOH solution, the adsorption capacity of the regenerated CLICH decreases after each reaction cycle due to incomplete regeneration.

Modification with polydopamine (PDA, Figure 7) is a relatively novel approach (Gouran-Orimi *et al*., 2018). The formation of PDA onto CLI (CLIPD) involves spontaneous oxidative polymerization of PDA in an alkaline media. The adsorption ability of CLIPD has been studied in fixed-bed column experiments. The adsorption capacity depends on reaction conditions such as pH, bed height, temperature, flow rate and presence of anions. By passing the NaOH solution through the column with spent CLIPD, it can be regenerated and reused at least three times for nitrate adsorption.

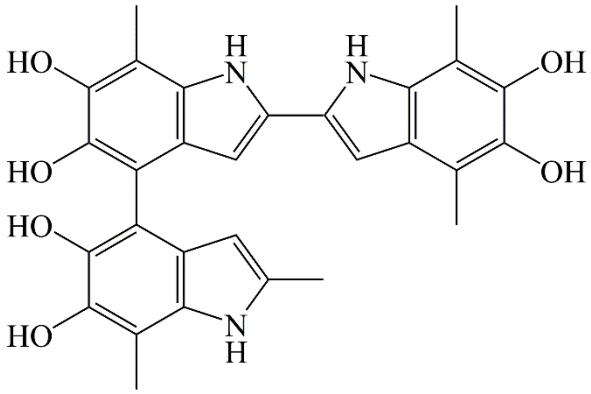

Figure 7. Structural formula of polydopamine.

Finally, modification of CLI can also be performed with zero valent nano Fe particles (NZVFeCLI). The modification is based on sodium borohydride reduction method (Fateminia and Falamaki 2013; Sepehri *et al.*, 2014). This method increases the specific surface area of CLI (from 17.8 to 49.7 m^2 g^{-1}) and leads to the formation of uniformly dispersed nano/sized NZFe particles (45 nm) on the CLI surface (Sepehri *et al.*, 2014). Nitrate adsorption onto NZVFeCLI occurs through several steps including nitrate reduction to ammonium ions which bind to NZVFeCLI in the final step. Batch

adsorption experiments showed that 84% of nitrate can be reduced to ammonium from the initial concentration of 100 mg dm^{-3} after 24 h.

2. Adsortion of phosphate ions

Phosphate ions are also attracted by cationic surfactant modified CLI (Naghash and Nezamzadeh-Ejhieh, 2015). However, the adsorption efficiency is related to the type of cationic surfactant. CLI modified by HDMTA exhibits a significantly higher adsorption capacity towards phosphate ions than the CLI modified by CPB. This is due to higher amount of HDTMA (298.9 mmol HDTMA per kg CLI) than CPB (208.6 mmol HDTMA per kg CLI). Moreover, the adsorption of phosphate is more favorable in alkaline media. In alkaline media, PO_4^{3-} is the predominant form of phosphate species in aqueous solution, which causes strong attractions between positively charged head of the surfactant. Due to the competition for adsorption active sites, phosphate adsorption decreases in the presence of arsenate, nitrate and sulfate (Naghash and Nezamzadeh-Ejhieh, 2015).

However, recent studies show that the adsorption capacity of CLI towards phosphate ions can be improved by CLI treating with $Ca(OH)_2$ solution (Mitrogiannis *et al.*, 2017). This is an economical approach due to the low-cost of $Ca(OH)_2$ and the fact that treatment of CLI involves only the cation-exchange reaction at room temperature. More than 90% of phosphate can be removed by $Ca(OH)_2$-treated CLI (CaCLI) from low concentrated solutions (up to 10 mg dm^{-3}) (Mitrogiannis *et al.*, 2017). The adsorption process is endothermic, pH-independent and slow reaching equilibrium after 120 h. The half of the removed phosphate occurs in the first 8 h. The adsorption process occurs through the precipitation due to the strong affinity of calcium ions to phosphate.

Modification of CLI with metal oxides species has been also considered as an effective method (Huo *et al.*, 2012; Guaya *et al.*, 2015; Guaya *et al.*, 2016). Compared to parent CLI, Fe(III)-containing CLI (FeCLI) shows six times higher phosphate adsorption capacity, whereas Al(III)-containing CLI (AlCLI) exhibits twelve times higher adsorption capacity (Guaya *et al.*, 2015; Guaya *et al.*, 2016). Depending on the pH_{PZC}, the phosphate adsorption proceeds through the formation of complexes with the hydroxyl surface groups present onto the surface of CLI or by electrostatic attractions. Adsorption kinetics data for both FeCLI and AlCLI indicates that about 3 h is needed to

reach the adsorption equilibrium. The regeneration efficiency of both FeCLI and AlCLI is affected by solution applied for regeneration. The effect increases in the following order: $NaHCO_3$ < NaOH < $NaHCO_3/Na_2CO_3$ < Na_2CO_3. Incomplete regeneration is explained by strong complexation of phosphate by iron/aluminum oxide species that are primarily responsible for the adsorption. The adsorption capacity of the regenerated FeCLI and AlCLI significantly decreases in the second adsorption cycle suggesting that the re-impregnation is necessary before the next adsorption step.

2.2.1.1 Clinoptilolite as soil supplement

Good ion-exchange and adsorptive properties of zeolites recommend them for application in agriculture. In order to increase the quantity of agricultural production, a large amount of mineral and organic fertilizers are utilized. However, this does not lead to their effective utilization by plants and increase of crop yield. Only a small amount of fertilizer can be effectively taken by plants whereas the rest is lost in environment causing environmental damages.

Many studies have been performed to find a cost effective and environmentally friendly solution to increase soil fertility and agricultural production without an excessive use of fertilizers. In this regard, the use of various soil supplements has received great attention. Soil supplements (organic or inorganic) increase soil fertility by improving physico-chemical properties of the soil such as water retention capacity, ion-exchange capacity and acidity. In addition, soil supplement can act as a carrier of plant nutrients enabling slow release of nutrients. Gradual release of plant nutrients contributes to prolong retention of nutrients in the soil increasing their effectiveness. Also, the use of such fertilizing agents decreases possibility of contamination of groundwater.

Various soil supplements have been studied taking into account their environmental and economical impacts including organics such as compost, biochar, nutrient rich waste – manure, and natural minerals (bentonite, dolomite, gypsum, zeolites) (Reháková *et al*., 2004; El Sharkawi *et al*., 2018).

Nitrogen, phosphorus and potassium are essential plant nutrients supplied through fertilizers to agricultural soils. These nutrients are included in almost all metabolic and growth processes, and they are necessary for the growth and production of plants.

Nitrogen is both an essential nutrient for all living organisms and widespread water pollutant. A high concentration of nitrogen in water in form of ammonium, nitrate and nitrite ions, can cause not only degradation of surface and groundwater ecosystems but also affects the public health. The most common nitrate sources in water are municipal and industrial wastewater, septic tanks as well as wastewater from landfills. In addition, agricultural activities (use of the excess amount of nitrate fertilizers, improperly storage of animal waste on farms, discharge of wastewater directly to a water body) contribute significantly to the water pollution by nitrates.

Due to a high leaching rate of nitrate ions through the soil, excessive use of nitrate fertilizers directly threatens groundwater. The nitrate leaching is a complex process (Figure 8) which occurs due to a high solubility of nitrate in water and low adsorption of negatively charged nitrate ions onto negatively charged soil particles. Therefore, nitrate ions present in the soil solution move freely through soil to groundwater by percolating rainfall or irrigation. Many factors affect the leaching rate including the amount and frequency of applied nitrate fertilizers, physico-chemical properties of soil, irrigation and precipitation amount. As an example, sandy soils that are characterized by a low ion-exchange capacity and low water holding capacity are particularly exposed to nitrate leaching (Brady and Weil, 2009; Colombani *et al*., 2015). Also, the leaching of nitrate is enhanced under humid conditions and irrigated cropping areas.

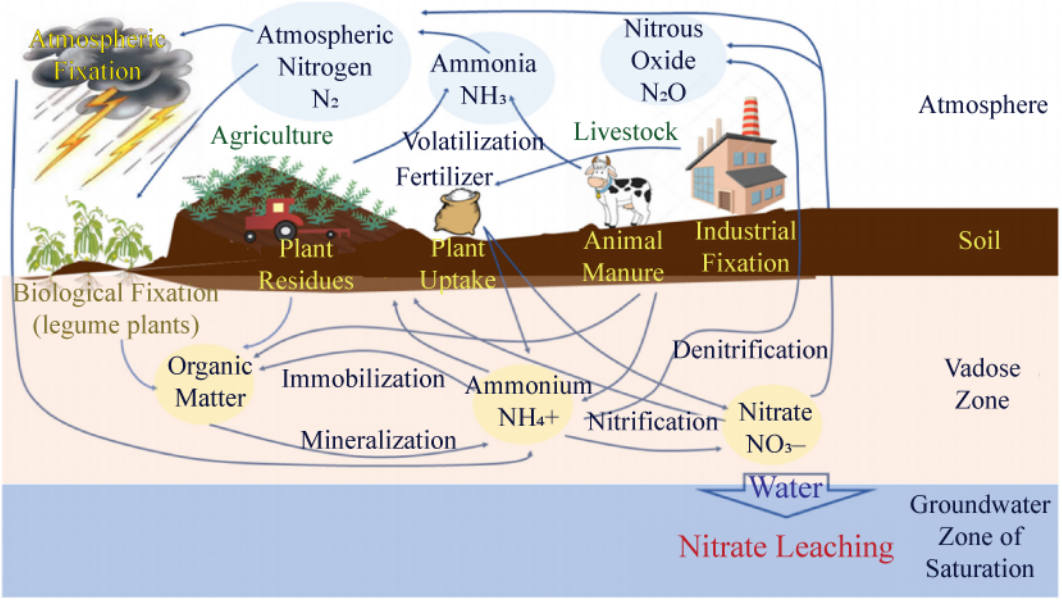

Figure 8. The nitrogen cycle and nitrate leaching (Padilla *et al.*, 2018).

Phosphorus is also an essential plant nutrient. Phosphorus is present as phosphate ions. In contrast to leaching of nitrate ions, phosphate leaching occurs to a lower extent due to the strong binding of phosphate to soil particles. Thus, binding of phosphate ions onto particles of acidic soils is directly related to the presence of different oxides (iron, aluminum and manganese) whereas in alkaline soils, oxides and salts of calcium and magnesium are responsible for the phosphate adsorption (Brady and Weil, 2009).

Potassium is an essential plant nutrient. It attracts less attention than nitrogen and phosphorous since potassium leaching does not contribute directly to eutrophication. Depending on potassium availability to plants, potassium present in soil can be classified as non-exchangeable, exchangeable, structural (present in minerals) and water soluble. Exchangeable and water soluble potassium primarily contribute to its leaching (Brady and Weil, 2009). The leaching rate is generally affected by soil physicochemical properties. Thus, the potassium leaching is characteristic for soils with low cation exchange capacity such as sandy soils. In addition, factors including precipitation and irrigation rate, applied amount of K fertilizers as well as the concentration of other cations in the soil (especially Ca^{2+}) enhance the K leaching (Alfaro *et al.*, 2004; Kolahchi and Jalali, 2007).

Since these plant nutrients, especially nitrate and phosphate, reach both surface and groundwaters, monitoring of their concentration is necessary. According to World Health Organization (WHO), maximum permitted concentration (MPC) of nitrate in public drinking water supplies is 50 mg dm^{-3} and 12 mg dm^{-3} for potassium (WHO, Guidelines for drinking-water quality). These values are accepted in the legislation of the Republic of Serbia (Pravilnik o higijenskoj ispravnosti vode za piće). Since phosphates are not recognized as high toxic to human health, WHO is not recommended MPC for phosphorous. However, in order to control eutrophication, there are some recommendations for the phosphate concentration that can be discharge in a water body such as 0.025 mg dm^{-3} for reservoirs used as drinking water sources. In the Republic of Serbia, MPC of phosphate concentration in drinking water is 0.15 mg dm^{-3} (Pravilnik o higijenskoj ispravnosti vode za piće).

According to the monitoring performed by the Serbian Environmental Protection Agency, concentration of nitrate in surface water are within the permitted concentration (up to 2 mg dm^{-3}) for a period of 2007–2016 with slight increasing trend during 2014–

2016 (The report on the environmental situation in the Republic of Serbia for 2017). Additionally, nitrate concentrations in groundwater were significantly higher, up to 30 mg dm^{-3}, but still below MPC. However, during 2016 nitrate concentration higher than 50 mg dm^{-3} was observed in the region of Velika Morava (96.5 mg dm^{-3}), Srem (95.7 mg dm^{-3}) and Bačka (104.7 mg dm^{-3}). For the same period, concentration of phosphate in surface waters was in the range of 0.02 to 0.1 mg dm^{-3}. The highest phosphate concentration was found in Vojvodina reaching concentration six times higher than MPC (The report on the environmental situation in the Republic of Serbia for 2017). Furthermore, Devic *et al*. studied in detail quality of groundwaters in Vojvodina and Central Serbia for the summer period of 2009 (Devic *et al*., 2014). The results showed great variations in nitrate concentration from 0.02 to 42.45 mg dm^{-3}. These results also demonstrated that the groundwaters of the Velika, Zapadna and Južna Morava Rivers and partly of the Mačva region are severely polluted by the nitrate. These areas are typical agriculture areas and high concentration of nitrates in groundwater can be ascribed to agricultural activities. Spatial variations in the nitrate concentration among the different studied sites were attributed to the soil properties, hydrological conditions, but also to the different fertilizer applications (type and amounts). In addition, the results showed that concentration of potassium varied significantly from 0.4 to 38.7 mg dm^{-3} among the studied sites showing that in some area potassium concentrations are above MPC (12 mg dm^{-3}).

High concentration of nitrate was also reported for waters from Rasina district (Pantelić *et al*., 2017) which is in the southern part of Central Serbia, bounded by several mountains. Water samples were collected from wells (in the period of June–August 2016) of municipalities of Kruševac, Aleksandrovac, Trstenik, Brus, Varvarin and Ćićevac. The results showed that the nitrate concentration varied depending of locality and being two or three times higher than MPC which was due to agricultural activities.

Nitrate and phosphate concentrations that are higher than MPC cause serious environmental and economic problems around the world. These nutrients stimulate heavy algal growth (algal blooms) such as *Cyanophyta* (blue-green algae) and *Chlorophyta* (green algae) leading to depletion of dissolved oxygen in the water bodies and reduction of light penetration. This process is known as eutrophication. Eutrophication has a negative impact on aquatic organisms causing death of plants and

animals. Moreover, eutrophication affects human causing restriction in drinking water supply.

For many years, waters of the Republic of Serbia suffer from the high concentrations of these nutrients and thereby from eutrophication. Vojvodina primarily uses groundwater for drinking water supply whereas central part of Serbia uses also surface reservoirs. From 2007 nine of twenty reservoirs suffer from permanent eutrophication (Svirčev *et al*., 2017).

Eutrophication has been observed in Ćelije reservoir (Central Serbia) which is used as a source of drinking water for Kruševac city and its surroundings (Figure 9). The cyanobacterial blooms have been detected since summer 1998 due to uncontrolled nutrient and organics inflow, primarily from Rasina and Blatašnica rivers (Čađo *et al*., 2017). Water analysis showed the presence of *Chlorophyta* and *Bacillarophyta* algae, but also cyanobacteria including *Aphanizomenon, Anabaena and Microcystis* (Svirčev *et al*., 2009).

Figure 9. Eutrophic reservoirs used for drinking water supply of a) Užice (Vrutci reservoir) and b) Kruševac (Ćelije reservoir) (https://www.rtk.rs/66965/celije-cvetanje-jezera-voda-iz-vodovoda-je-ispravna-za-pice/).

Eutrophication has also been observed in the Vrutci, accumulation on the Đetinja river in Western Serbia that supplies Užice with drinking water (Figure 9). The analysis revealed the presence of 65 taxa and 7 blue-green algae (*Bacillariophyta, Chlorophyta, Chrysophyta, Cryptophyta, Cyanobacteria, Dinophyta and Euglenophyta* (Đeković *et al.*, 2017). In 2013, dominant species in the accumulation was cyanobacteria *Planktothrix rubescens* responsible for production of cyanotoxin with negative impacts on human health. As a consequence, the use of water from Vrutci accumulation has been

prohibited. Moreover, eutrophication has also been observed in other Serbian reservoirs of drinking water including Ključ (Požarevac), Garaši and Bukulja (Aranđelovac), Grlište (Zaječar) and Gruža (Kragujevac) (Ostojić *et al*., 2005; Pešić 2006; Karadžić *et al*., 2010; Vujasinović *et al*., 2014; Gavrilović *et al*., 2014). Concentrations of nitrate and phosphate higher than MPC have led to the growth of different algae species including *Planktothrix agardhii, Aphanizomenonflos-aquae, Microcystis aeruginosa and Anabaena affinis*, *Bacillariophyta*, *Chlorophyta* and *Cyanobacteria*. Due to harmful effect, a water supply restriction of city and surrounding villages becomes a common problem in Serbia.

Besides reservoirs used for drinking water supply, lakes such as Palić and Ludaš suffer from constantly blooming of cyanobacteria. Both lakes are located in Vojvodina, near Subotica. Based published reports, presence of toxic cyanobacteria such as *Limnothrix redekei, Pseudanabaena limnetica, Planktothrix agardhii and Microcystis spp.* were found in these lakes (Svirčev *et al*., 2017; Tokodi *et al.*, 2018).

Taking all of these into account, CLI has been considered as a good candidate for a soil supplement, which could prevent not only nutrient leaching but also contributes soil remediation. To date, it has been reported that the addition of CLI to different soil types can improve physical and chemical properties of soils such as water retention capacity, which is of particular importance for sandy soils, acidity of sandy soils (Andronikashvili, 2012), or to be used in remediation of soils polluted by heavy metals such as Cd, Ni, Pb, Zn, Co (Usman *et al*., 2006; Mahabadi *et al*., 2007; Yi *et al*., 2019). As an example, the CLI addition to soil polluted by Pb(II) enables that the metal cations are captured *via* surface complexation and precipitation (Wei-yu *et al*., 2009) at the CLI. One of the main beneficial effects of CLI addition to soils is its ability to prolong retention of plant nutrients (Latifah *et al.*, 2017; Souza *et al*., 2018). Improvement of potassium retention was observed for different soil types. The effect is more noticeable for acidic sandy soils. It has been explained by the fact that alkaline soils contain larger amount of calcium and magnesium and accordingly these cations are in competition for adsorption sites on CLI (Rezaei and Mohavedi Naeini, 2009; Najafi-Ghiri, 2014). For instance, the effect of CLI addition on potassium retention was studied for sandy soil amended with municipal compost as a source of potassium (Moraetis *et al*., 2015). Leaching of potassium was monitored by simulating the artificial rain during the seven

days. The obtained results showed that addition of CLI increases potassium retention up to six times showing that potassium leaching does not change after the fourth day.

Similar effect of CLI addition to sandy soil was observed for retention of nitrates (Malekian *et al.*, 2011; Moradzadeh *et al.*, 2014). The retention of nitrates has been improved by the addition of K-rich zeolite (Moradzadeh *et al.*, 2014). Depending of the applied amount, nitrate leaching was reduced for 21, 36 and 43% by applying 2, 4 and 8 g K-rich natural zeolite per kg soil, respectively.

It has been also found that HDTMACLI has higher retention efficiency than CLI in the sandy loam soil due to its high affinity toward nitrates (Malekian *et al.*, 2011). In addition, retention efficiency was affected by the amount of the applied zeolites: highest retention efficiency was achieved by the highest zeolite amount.

2.2.2 Catalytic properties

The unique porous structure and acidity of CLI are responsible for its catalytic activity. In order to enhance the acidity the procedures for preparation of "hydrogen form of CLI" (HCLI) have been developed. Usually, the procedures consist of the following steps (Figure 10):

1) An ion-exchange reaction in which NH_4^+ ions replace parent cations from CLI lattice (Na^+, K^+, Ca^{2+}, Mg^{2+});
2) Conversion of NH_4-containing CLI to HCLI by calcination at about 500 ^oC.

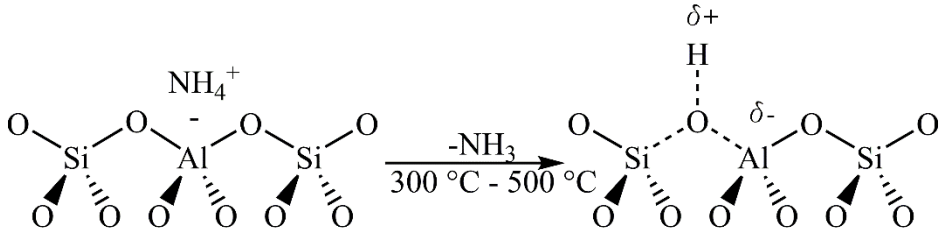

Figure 10. Shematic presentation of HCLI preparation.

HCLI can also be obtained by treating CLI with an acid solution (usually HCl). In the treatment exchangeable cations from CLI lattice are replaced by hydronium ions from solution but a partial dealumination of CLI occurs simultaneously due to leaching of Al^{3+} from the CLI lattice (Figure 11). During the dealumination, breaking of Si–O–Al

bonds occurs and vacancies are formed in the lattice. This provides an additional porosity and increase of acidity of the CLI lattice but can also affect crystallinity.

The conversion of CLI to HCLI is accompanied with considerable increase of specific surface area (up to 259.2 $m^2\ g^{-1}$), micropore volume and external surface area (Garcia-Basabe *et al.*, 2010; Dziedzicka *et al.*, 2016). This is caused by the leaching of a significant amount of Al^{3+} (up to 46%) from the CLI framework. The conversion also causes the formation of extra-framework aluminum species (such as octahedrally- and five-coordinated Al species) which can improve catalytic activity (Farías *et al.*, 2009; Garcia-Basabe *et al.*, 2010).

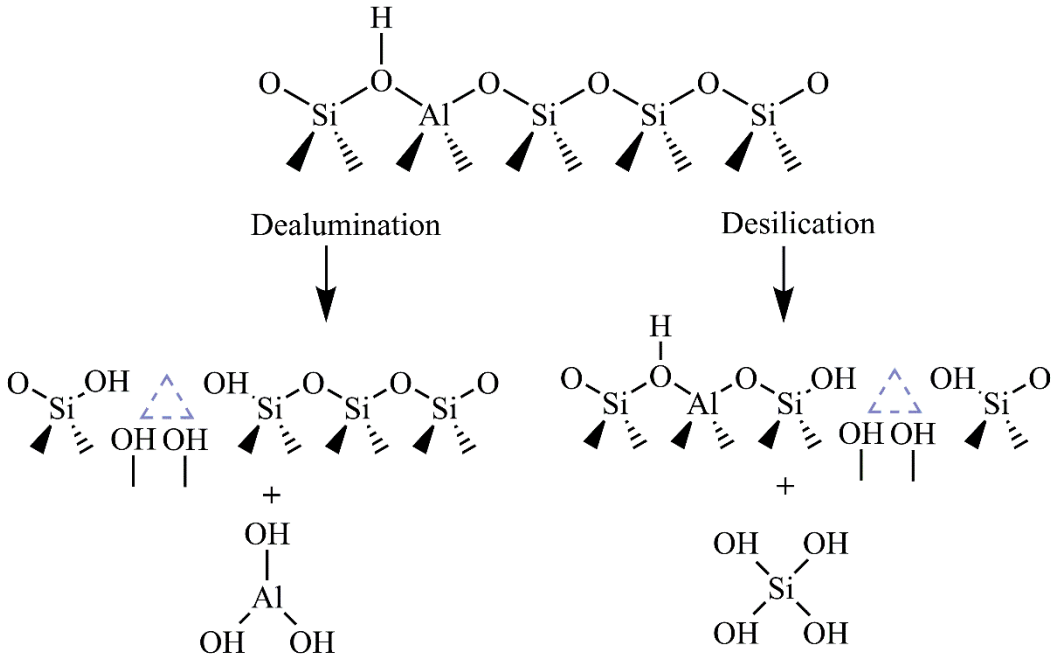

Figure 11. Schematic illustration of dealumination and desilication during transformation of CLI into HCLI.

Figure 11 shows that acidic properties of zeolites can be improved also by desilication. The method includes a partial removal of Si^{4+} which occurs in an alkaline solution (usually NaOH). This method has been usually applied for synthetic zeolites (such as ZSM–5, MOR, BETA).

The CLI desilication using NaOH in different concentration resulted in the Si removal in different extents: from 0.49 wt.% (using 0.05 mol NaOH dm^{-3}) to 7.64 wt.% (0.8 mol

NaOH dm^{-3}). However, the Si leaching in the highest degree caused a partial loss of the CLI crystallinity (Lin *et al*., 2015; Ates, 2018; Souza *et al*., 2018; Wang *et al*., 2019) and do not result in significant increasing of CLI specific surface area (about 60 $m^2 g^{-1}$) such as after dealumination (Lin *et al*., 2015). Desilication, however, contributes to the acidity increasing both Brönsted and Lewis acidity due to preservation of Al in the CLI lattice (Souza *et al.*, 2018).

Catalytic activity can be also significantly improved by the introduction of transition metals such as Sn, Ga, Ti or Zr into the zeolite lattice (Yang *et al*., 2013; Zhang *et al*., 2017). This method is applied mainly for synthetic zeolites. Incorporation of transition metal cations into aluminosilicate lattice leads to the formation of additional acid sites due to formation of Si–O–M(II) bonds (Dijkmans *et al*., 2015; Guan *et al.*, 2018).

2.2.2.1 Catalytic performance of zeolites in biomass valorization

XXI century has been declared a century of Green chemistry. Thus, many efforts have been devoted to usage of renewable sources. According to the Europe 2020 strategy, 20% of consumed energy should be used from renewable sources in 2020, and at least 27% in 2030 (A European strategy for smart, sustainable and inclusive growth, Communication from the commission Europe 2020). Sweden is the leading Europen country covering about 55% of the final bioenergy consumption from renewable sources, followed by Finland, Denmark and Austria (Stec and Gruebyk, 2018). Among other renewable sources, biomass valorization received increased attention in the last decade.

The term biomass describes organics originate from plants and animals. Biomass is an ideal low-cost source of various value-added products. Sweden is known as a country with biomass import. On the contrary, in R. Serbia, a large amount of waste biomass leaves unused on agricultural lands.

It has been estimated that in R. Serbia biomass participates with about 60% among the total renewable energy sources (Grahovac *et al.*, 2012; Bojic *et al.*, 2018). About 12.5 million tons are produced every year, 9 million tons come from the area of Vojvodina and only 19% are used mainly for the heating (Dodić *et al.*, 2010). The left biomass is still treated as a waste.

In the last decade, in European countries, lignocellulosic biomass has been used for the synthesis of many different important chemicals. Lignocellulosic biomass is mainly composed of cellulose, hemicellulose and lignin (Figure 12).

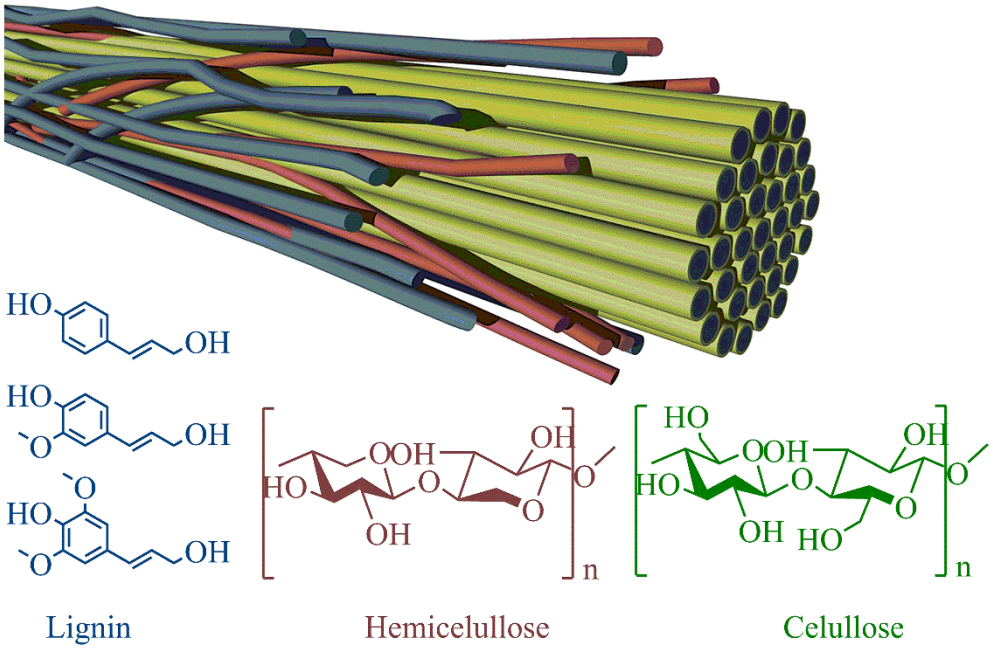

Figure 12. The main components of lignocellulosic biomass (adopted from Wakerley *et al.*, 2017).

Cellulose is the major component of lignocellulosic biomass with a contribution of about 40–55 wt.%. It is a polysaccharide consisting of linear chains of several hundred to many thousands of *β*-(1→4) linked D-glucose units. The chains are linked via hydrogen bonds forming microfibrils covered with lignin and hemicellulose.

Hemicellulose is a complex polymer that participates with approximately 25–35 wt.% It is based on polysaccharides with a branched structure with short lateral chains composing of different sugars such as monosaccharides, pentoses (arabinose, xylose and rhamnose), hexoses (glucose, mannose and galactose) and uronic acids (*D*-glucuronic, *D*-galacturonic acids and 4-o-methylglucuronic).

Lignin is a complex cross-linked phenolic polymer that constitutes 15–20 wt.% of the lignocellulosic biomass. It is responsible for rigidity and strength of the cell wall, especially in wood and bark. Lignin consists of three phenylpropane building units

including coniferyl alcohol (guaiacyl propanol), coumaryl alcohol (*p*-hydroxyphenyl propanol) and sinapyl alcohol (syringyl alcohol). It fills the spaces in the cell wall between cellulose, hemicellulose, and pectin components.

It is worth to mention that biomass sources are diverse, and they include products and residues from agriculture and forestry, herbaceous crops and grass, aquatic biomass and wastes (municipal sewage sludge and solid waste, animal and industrial waste).

Biofuels are renewable energy resources, which replace traditional and limited fossil fuels. The use of biofuels contributes to reduction of CO_2 emission and toxic compounds making them an environmentally friendly alternative to fossil fuels. Biofuels can be used without any treatment of biomass, and such biofuels are classified as primary biofuels. In this form, they are usually used for heating, cooking or for production of electricity (wood, wood chips and pellets). In contrast, secondary biofuels are produced by treatment of biomass and can be used for different industrial applications. Since that they can be produced from different biomass sources and by different technology, secondary biofuels are divided into three generations. The first generation of biofuels (bioethanol and biomethanol) is produced through relatively simple technology by fermentation of food crops rich in starch (corn, potato, wheat or barley) or sugars (sugar beet or sugarcane). Additionally, biodiesel is produced by transesterification of crops such as soybeans, sunflowers, rapeseed etc. Because the feedstocks of these biofuels are also a source for the food industry, second generation biofuels are developed. These biofuels are produced from lignocellulosic biomass which includes non-food crops or non edible plant biomass such as grass, fruit skin or wood chips. The third generation of biofuels is produced from algal biomass due to high amount of lipids.

Bio-based chemicals are recognized as highly desirable alternative chemicals in replacing of petrochemicals. The US Department of Energy (National Renewable Energy Laboratory) has been reported twelve building block chemicals (so called platform chemicals) that can be obtained from biomass (Werpy and Patersen, 2004):

1) *1,4-diacids (succinic, fumaric and malic)*
2) *2,5-furan dicarboxylic acid*
3) *3-hydroxy propionic acid*
4) *3-hydroxybutyrolactone*
5) *aspartic acid*

6) *glucaric acid*
7) *glutamic acid*
8) *itaconic acid*
9) *levulinic acid*
10) *glycerol*
11) *sorbitol and*
12) *xylitol/arabinitol.*

The platform chemicals are converted to many important industrial chemicals and used as farmaceuticals, agrochemicals, bioadditives, green solvents, polymeric or coating materials.

Levulinic acid

Levulinic acid (LA), 4-oxopentanoic acid or γ-ketovaleric acid ($C_5H_8O_3$) is a short chain fatty organic acid (Figure 13). LA has a ketone and a carboxylic group and is reactive to other functional groups making it an important platform chemical.

LA can be used as precursor for the synthesis of various important derivatives including polymers, resins, pharmaceutical and fragrance compounds, herbicides, solvents, plasticizers and biofuels (Rackemann and Doherty, 2011).

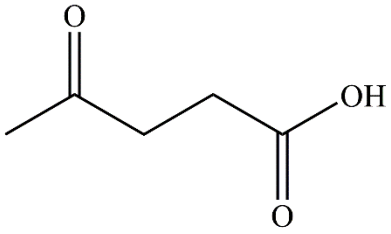

Figure 13. Structural formula of levulinic acid.

LA can be produced by an acid-catalyzed decomposition of lignocellulosic biomass. Feedstocks such as sugars (monosaccharides and polysaccharides), renewable resources (starch-rich materials) and lignocelluloses biomass (woods, crop residues, cellulose) have been used for the synthesis of LA.

Usually, the synthesis of LA from biomass includes several steps (Figure 14):

– *Pretreatment of biomass:* it is an important step which improves the conversion of biomass into LA. It results in the fractionation of the polymeric

components and increases reactivity of cellulose. Various pretreatment methods have been used including physical, chemical or biological treatments (Mood *et al*., 2013).

– *Formation of monomeric sugars:* The step includes hydrolysis of cellulose to glucose, the most ideal hexose sugar for synthesis of LA (Kang *et al*., 2018). Reaction is usually occurring under mild conditions in the presence of a homogenous or heterogeneous catalyst.
– *Conversion of glucose to LA:* The step consists of the isomerization of the obtained glucose to fructose, followed by dehydration of the fructose to the intermediate 5-hydroxymethylfurfural (HMF). Finally, LA can be obtained by rehydration of HMF (Kang *et al*., 2018).

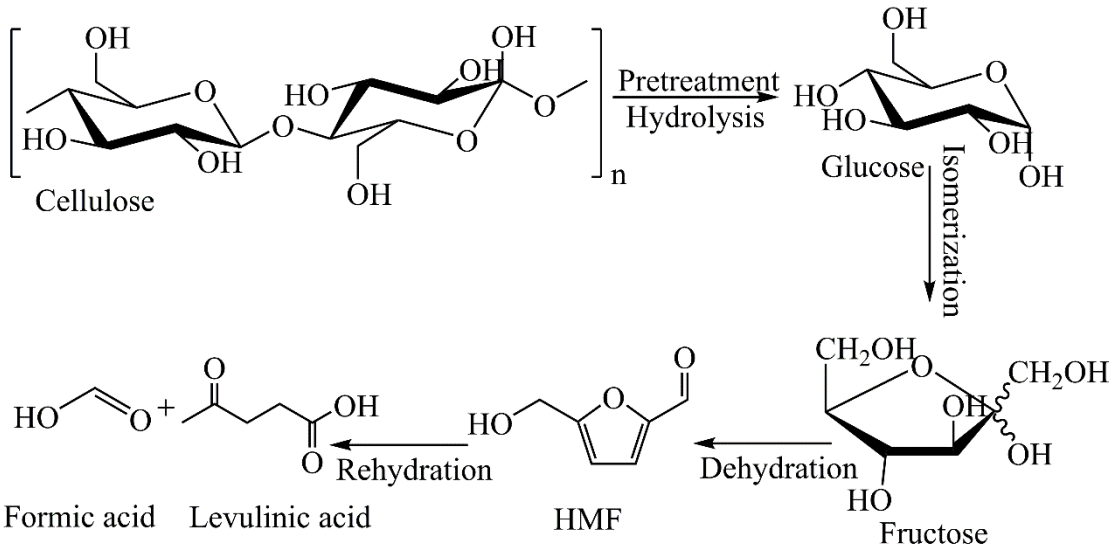

Figure 14. Shematic presentation of LA synthesis from biomass.

Efficient conversion of biomass to LA is affected by different parameters including biomass source, pretreatment and reaction conditions (Morone *et al*., 2015). Moreover, the conversion is necessary to be catalyzed by Lewis or Brönsted acid sites. In the conventional procedures, mineral acids such as HCl, HNO_3, H_3PO_4 and H_2SO_4 have been used. Their catalytic activity was reported in LA synthesis from sugars (glucose, fructose) but also from complex biomass sources such as wheat straw, pulp, bagasse etc. (Chang *et al*., 2007; Yan *et al*., 2008; Morone *et al*., 2015). The yield of LA production

from C6-sugars is around 64.5 wt.% because of the formation of formic acid and water (Pulidindi and Kim, 2018).

Biofine process developed by Biofine Renewables (Bozell *et al*., 2000; Girisuta *et al*., 2008; Hayes *et al*., 2008) involves two acid catalyzed steps:

1) fast synthesis of HMF from hexose in presence of dilute H_2SO_4 at 200–230 °C and pressure 20–25 bar and
2) conversion of HMF to LA at 190–220 °C and p= 10–15 bar for 15–30 min.

Use of mineral acids as catalyst results not only in incomplete conversion of biomass to LA but also in serious problems such as equipment corrosion, necessity of introducing procedure for separation of product mixture, nonreusability of catalyst and in environmental problems. Therefore, many studies have been directed to the LA synthesis using heterogeneous catalysis as an economically and environmentally acceptable process.

Solid acid catalysts such as metals, acidic organic resins, mesoporous solids, clays and zeolites have been studied (Peng *et al.*, 2010; Lin *et al*., 2012; Hu *et al*., 2015; Zhi *et al*., 2015; Thapa *et al.,* 2017). For instance, Peng et al. studied the conversion of cellulose to LA in the presence of different metal chlorides (Peng *et al*., 2010) showing the superior catalytic activity of the salts of transition metals - $CrCl_3$, $FeCl_3$ and $CuCl_2$, $AlCl_3$ in comparison to usually applied salts of alkali and alkaline earth metals. Several types of zeolite also showed good catalytic performance due to acidity and mesoporosity (Zeng *et al*., 2010; Zhuang *et al*., 2013).

LA is considered as a green chemical and can be used in the synthesis of different compounds. An overview of products obtained from LA is shown in Figure 15.

LA can be converted to δ-amino levulinic acid that is useful herbicide, insecticide but also anti-cancer and anti-tuberculosis pharmaceuticals. Diphenolic acid and succinic acid are used for the production of polymers, plasticizers and textile chemicals. Additionally, γ-valerolactone is used as an environmentally safe solvent but also as a fuel additive (Ding *et al*., 2014). Moreover, methyltetrahydrofuran and angelica lactone are also used as fuel additives.

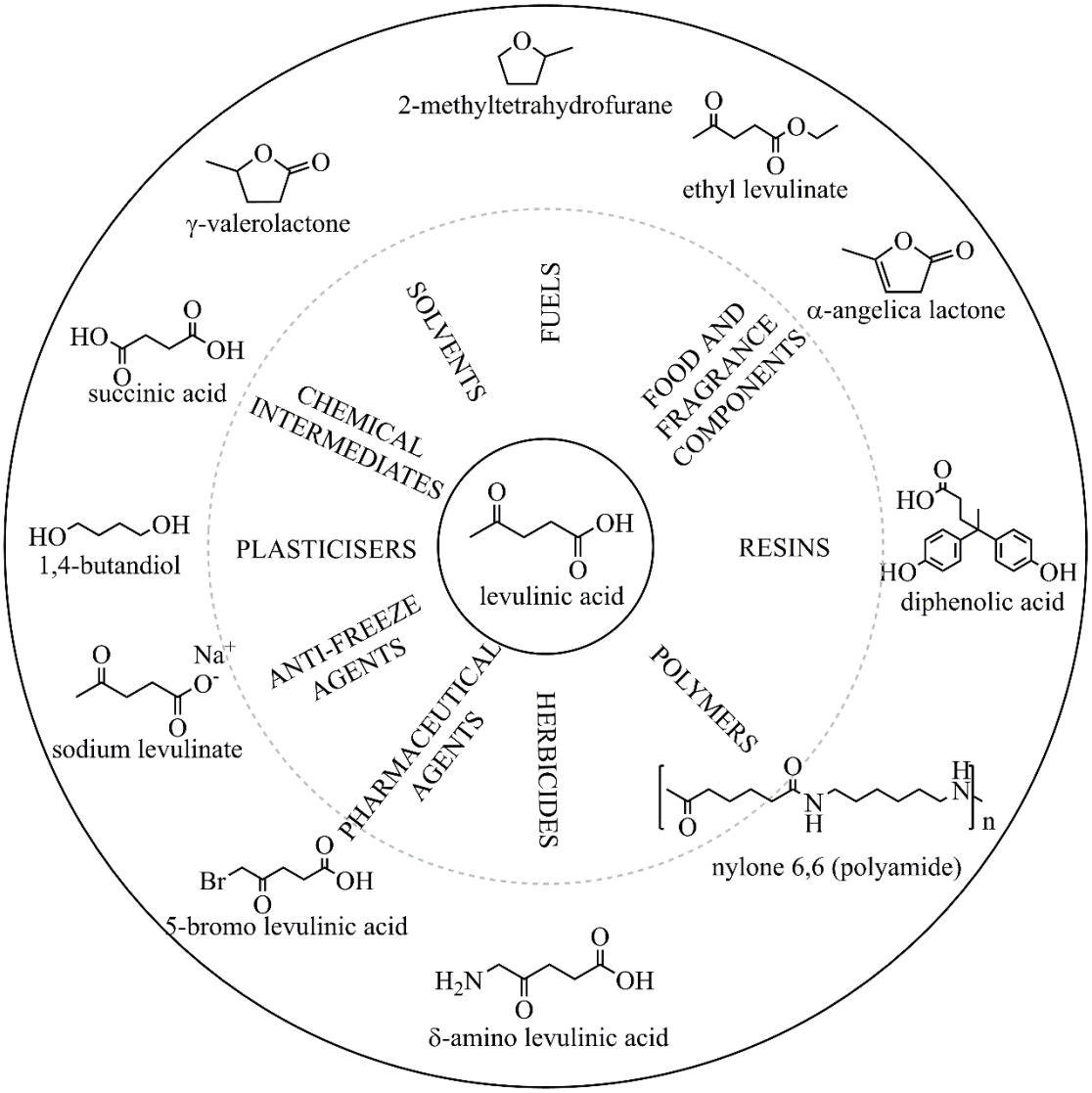

Figure 15. Shematic presentation of use of LA as a platform chemical in the synthesis of important industrial chemicals (Rackemann and Doherty, 2011).

In recent years, esterification of LA into esters (LE) has received a great attention. Alkyl levulinates are of particular interest due to their specific physicochemical properties making them applicable as second-generation biofuels and biofuel additives, alternative green solvents, plasticizers and fragrances (Christensen *et al.*, 2011; Joshi *et al*., 2011). Until now, the most attention has been directed to LA esterification with lower alcohol including methanol, ethanol and butanol (Fernandes *et al.*, 2012; Popova *et al*., 2016). The LE shows properties similar to the biodiesel fatty acid methyl esters that are used in some low-sulphur diesel formulations. However, their addition to the diesel would

improve the quality of fuel (reduction in toxicity and sulphur content, improvement in lubricity, stability in flash point and viscosity) (Joshi *et al*., 2011; Lei *et al*., 2016).

One of the most important LE is ethyl levulinate (ELA) which can be used as a blend component in diesel formulations. Investigations performed by Biofine and Texaco showed that ELA is promising oxygenate additive (ELA contains 33% of oxygen). It has been found that mixture containing 20% ELA, 79% diesel and 1% co-additive can be used in regular diesel engines due to its physicochemical properties similar to those of biodiesel. The mixture enables cleaner burning of diesel fuel decreasing sulphur emission. Therefore, ELA is a good candidate for decrease of consumption of fossil fuels (Joshi *et al*., 2011; Kuwahara *et al.,* 2014). Moreover, the use of ELA provides higher motor efficiency, long operation life, less carbon monoxide (CO) and NOx emissions. Diesel engines have a high exhaust and NOx emissions. The addition of oxygenates to fossil fuels is one of the most important methods for elimination of these problems.

Data on the esterification of LA with higher alcohol such as octanol have been rather scarce (Nandiwale *et al.*, 2014; Zhou *et al*., 2018) although octyl lavulinate (OLA) is an important biolubricant. OLA is promising alternative for synthetic and mineral-oil based lubricants due to its biodegradability, carbon-neutral and non-toxic properties, as well as needlessness to mix with various additives (anti-oxidants, pour point depressants, viscosity index improvers, detergents and emulsion stabilizers etc.) (Vasudevan and Briggs, 2008; Oh *et al*., 2013).

Synthesis of Levulinate Esters

Levulinate esters have been synthetized by different pathways (Figure 16). They can be synthetized directly from carbohydrate-based biomass (Pathway I) such as glucose, fructose, sucrose or cellulose in alcoholic medium in the presence of catalyst. The use of solid acid catalysts has more advantages in comparison to homogenous catalysts primarily due to their economical and environmental benefits. In this regard, sulfated oxides, ion-exchange resins and zeolites have been studied in the LA esterification (Peng *et al*., 2011; Saravanamurugan and Riisager, 2012; Liu *et al*., 2018). However, low yield of LE and poor selectivity accompanied with formation of multiple products limited the LE synthesis directly from biomass feedstocks.

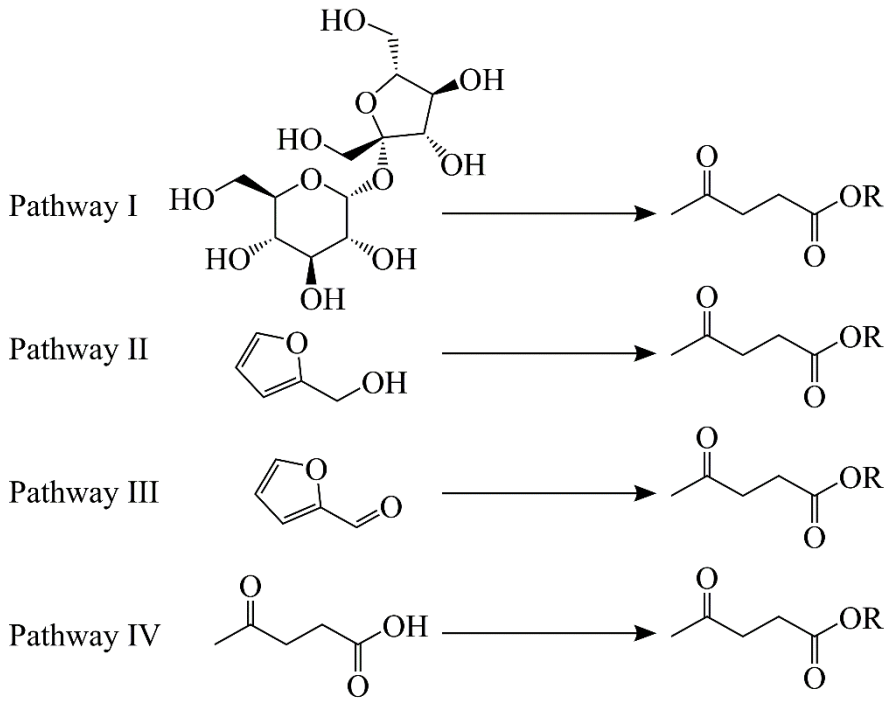

Figure 16. Shematic presentation of the LE synthesis (adopted from Badgujar *et al*., 2020).

The LE synthesis by the catalytic alcoholysis of furfuryl alcohol (Pathway II) offering high yield of esters at moderate reaction conditions. However, availability of furfuryl alcohol is the main restriction of the LE synthesis by this pathway (Badgujar *et al.*, 2020). Pathway III is based on the reduction of furfural to furfuryl alcohol followed by catalytic alcoholysis (Chen *et al*., 2016; Chen *et al.*, 2018; Gómez Bernal *et al*., 2019). The reduction using hazardous gases at high temperature and pressure restricts the LE synthesis by this pathway. Pathway IV shows direct esterification of LA with primary alcohols such as methanol, ethanol, *n*-butanol or *n*-octanol (Figure 17). This has been recognized as the most applicable, selective and sustainable method giving a high yield. However, very slow kinetics requires presence of a strong acidic catalyst. Usually, strong mineral acids such as HCl or H_2SO_4 have been used. Their use leads to high yield and short reaction time. However, due to the corrosive nature of the acids and their non-reusability, preference is given to heterogeneous catalysis. Different solid acid catalysts including heteropolyacids, ion-exchange resins, zeolites, sulfated metal oxides have been investigated for the esterification of LA with different alcohols.

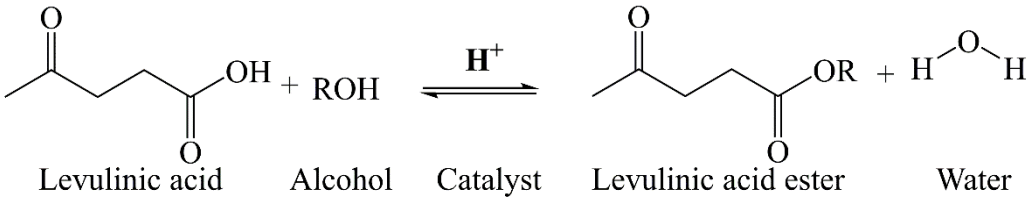

Figure 17. Shematic presentation of the esterification of LA with different alcohols (R – methyl, ethyl, *n*-butyl or *n*-octyl-).

Heteropolyacids (HPA) have been used in the esterification of LA primarily due to their strong Brönsted acidity. However, low specific surface area, poor chemical stability and high solubility in polar media restrict their use (Pasquale *et al*., 2012; Yan *et al.*, 2013). The HPA catalytic performance can be improved by their immobilization usually onto the porous supports. Thus, butyl levulinate was synthetized in a high yield (97%) by dodecatungestophosphoric acid (DTPA) supported on acid treated clay (Dharne and Bokade, 2011). Although highly catalytic active, the catalyst suffered from low stability: a drastic decrease in LA conversion rate was observed after the second reaction cycle due to DTPA leaching from the clay.

ELA was also synthetized using Well-Dawson HPA supported on silica. Decrease in yield from 72% (fresh catalyst) to 68% was reported during three reaction cycles (Pasquale *et al*., 2012). Methyl levulinate (MLA) and ELA were obtained by using Keggin type of HPA supported on silica showing 73% and 68% of yield, respectively (Yan *et al.*, 2013). A slight decrease in yield was observed during the repeated reaction cycle which was attributed to the HPA leaching. Better recyclability was reported for the HPA supported onto ZrO_2 (Ramli *et al*., 2017). About 97% ELA was obtained during four reaction cycles. In summary, despite a high LA conversion rate to LE using HPA-based catalysts, their recyclability still remains a major drawback.

Acidic ion-exchange resins (AIER) also show catalytic activity in the LA esterification. Due to strong acidity provided by the presence of sulfonated functional groups and well ordered mesoporosity, AIER are catalytically active in the LA esterification. Depending on the resin type, the yield of butyl levulinate (BLA) was in the range 64–94% showing that the LA esterification is influenced by the resin morphology (Tejero *et al*., 2016).

The unique properties of metal organic frameworks (MOF) such as porosity, high chemical and thermal stability as well as the possibility for modifications (such as increase of Brönsted acidity) make them promising candidates for the LA esterification (Cirujano *et al*., 2015; Guo *et al*., 2019). For instance, Zr-containing MOF is catalytically active in the LA esterification with different alcohol including ethanol, *n*-butanol and long chain biomass derived alcohols (C12–, C16– and C18–OH) (Cirujano *et al*., 2015). However, for the LA esterification with long chain alcohols high amount of catalyst is necessary. Moreover, the toxicity of metals incorporated into the MOF structure is also a limitation for their practical use.

Use of enzyme-based biocatalysts for the LA esterification has received a great attention as they are green and sustainable due to their biodegradability, minimal waste disposal and waste-free synthesis. Additionally, they are recognized as "energy saving" catalysts due to low energy consumption for activation as compared to traditionally used catalysts (Badgujar *et al*., 2020). Biocatalysts obtained from lipase *Candida Antartica* B (LCAB) are the most studied catalytic systems in the LA esterification. By immobilization of LCAB onto surface functionalized SBA-15, meso-molding three-dimensional macroporous organosiclica or Immo-bead 150, a high yield of different LA esters at mild reaction temperature has been obtained (Badgujar and Bhanage 2015; Zhou *et al*., 2018; Salvi and Yadav, 2019). However, their main disadvantages are high cost of production, low stability and non-reusability, immobilization of lipase onto suitable support, etc. Additionally, LA esterification with shorter chain alcohols resulted in a lower conversion to LE because of the higher polarity which caused the inactivation of lipase.

The sulfated metal oxides (SMO) have received a great attention as promising acid catalysts. Sulfate groups onto metal oxides act as both Lewis and Brönsted sites and provide a strong acidity of these oxides even higher than pure sulfuric acid ("super acidity"). Among them, sulfated ZrO_2 and sulfated SnO_2 have the strongest acidity. Acidity of some SMO reported by Arata et al. is summarized in Table 1 (Arata *et al.*, 2003). It is worth noticing that due to the limitation of the standard pH scale, the acidity of SMO is expressed by the Hammett acidity function (H_0). H_0 can be used to describe the acidity of concentrated and non-aqueous strong acidic solutions. As can be seen from

Table 1, H_0 has negative values showing greater acid strength for lower H_0 values. On this scale, H_0 for the pure sulfuric acid is determined to be –12.

Table 1. Acidity of SMO reported by Arata et al. (Arata *et al*., 2003).

Sulfated metal oxide	Calcination *T*, °C[a]	Hammett acidity (H_0)[b]
SO_4-SnO_2	550	–18.0
SO_4-ZrO_2	650	–16.1
SO_4-TiO_2	525	–14.6
SO_4-Al_2O_3	650	–14.6
SO_4-Fe_2O_3	500	–13.0

[a] Calcination temperature represents the temperature required to generate the highest acidity of SMO; [b]The acid strengths of SMO were estimated by the color change of Hammett indicators and using the temperature-programmed desorption of pyridine as a basic probe.

The most common procedure for the preparation of the SMO includes the synthesis of amorphous metal oxide gels as precursors, treatment of the precursors with sulfate-containing solutions (usually solution of sulfuric acid or ammonium sulfate) and calcination of the sulfated materials in an air atmosphere (Matsuhashi *et al*., 2001; Moreno *et al*., 2011).

A number of studies have proved that the sulfation of metal oxides enriched their acidity providing high catalytic activity in various catalytic systems. The strong acidity of SMO originates from both Lewis (metal atoms) and Brönsted acid sites (protons on the surface hydroxyl groups) are shown in Figure 18 (Khder *et al*., 2008). Considering the reported data, the sulfation leads to the generation of the strong Lewis acidity probably due to the presence of a sulfate complex in which covalent S=O bond acts as electron-withdrawing species that increases the Lewis acid strength of metal cation (M^{n+}). Moreover, in the presence of water or surface hydroxyl groups, the Lewis acid sites can be converted to Brönsted acid sites *via* proton transfer.

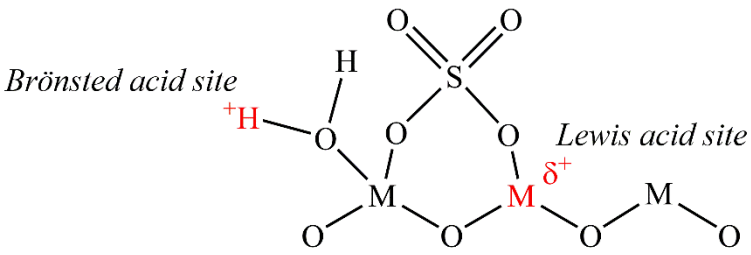

Figure 18. Lewis and Brönsted acid sites onto SMO (M represents the metal atoms such as Ti, Zr or Sn).

Owing to their strong acidity, SMO have been considered as potential catalysts for the LA esterification. Sulfated-ZrO_2, Nb_2O_5, TiO_2 and SnO_2 were applied in the synthesis of ELA reaching conversion rate up to 44% for sulfated-SnO_2 at 70 °C (Fernandes *et al*., 2012). Moreover, a higher yield of ELA (77%) was obtained using nanoparticles of sulfated-SnO_2 (Popova *et al*., 2018). In addition, ELA was obtained by sulfated TiO_2/ZrO_2 nano composites in a yield of 90% at 105 °C (Li *et al*., 2012).

Based on the reported results, it can be concluded that the main disadvantage of SMO is a low catalytic activity or/and low reusability (Khder *et al*., 2008; Matsuhashi *et al*., 2011; Fernandes *et al*., 2012). The low reusability of SMO is attributed to the leaching of sulfate species (even after the first catalytic test). In order to overcome these limitations, many studies have been performed to prevent leaching from SMO. One of the possible strategies is immobilization of SMO on the suitable supports. Immobilization prevents the agglomeration and contributes to better dispersion of acid active sites on SMO offering their better accessibility.

Catalytic performance of the sulfated-ZrO_2 supported on mesoporous silica KIL–2 was studied in the LA esterification with ethanol and *n*-butanol (Popova *et al*., 2016). A significant higher conversion rate of LA was obtained in the esterification to ELA in comparison to BLA (51 and 20% respectively). However, the LA conversion to ELA decreased to 47% after three reaction cycles.

ELA was also synthetized using sulfated Si-doped ZrO_2 catalysts (Kuwahara *et al*., 2014). However, the catalysts also suffered from the leaching of sulfate species causing a decrease in the conversion rate of LA to ELA from 66% to 13% after five repeated reaction cycles.

Zeolites, mainly synthetic ones, are also used as solid catalysts for the LA esterification with different alcohols. Their unique properties including hydrothermal stability, porosity and acidity are responsible for the LA conversion to LE (Maheria *et al*., 2013; Patil *et al*., 2014; Nandiwale *et al*., 2015). Selected literature data obtained for the LA esterification are summarized in Table 2. The catalytic activity of the studied zeolites seems to be correlated to the type of zeolites and reaction conditions such as reaction temperature and time, amount of catalyst etc. Contrary to non-zeolitic catalysts, the catalytic activity of zeolites is not highly related to their acidity but is mainly related to their porous structure (Maheria *et al*., 2013; Fernandes *et al.*, 2014). Namely, the microporous structure of zeolite restricts the diffusion of molecule of reactants leading to the low accessibility of active sites and thereby to decrease in catalytic activity. However, this can be overcome by the generation of mesoporous zeolites. As an example, mesoporous SBA-15 led to total conversion of LA to ELA which was explained to the combination of moderately strong acidity of SBA-15 and high surface hydrophobicity (Melero *et al*., 2013). However, catalytic activity of the SBA-15 decreases significantly after three reaction cycles.

Desilication has been applied as one of the highly effective methods for improvement of the catalytic performance of zeolites (Nandiwale *et al*., 2014). For instance, desilicated HZSM–5 showed significantly higher catalytic activity compared to parent HZSM–5 due to an increase of specific surface area, generation of mesoporosity, and thus improvement of accessibility to active sites (Nandiwale *et al*., 2014).

Table 2. Esterification of LA with different alcohol in the presence of different zeolites.

Catalyst	Alcohol	Reaction temp., °C	LA conversion, %	Reuse	Ref.
HUSY (5 wt.%)	Ethanol	70	8	n.r. [a]	Fernandes *et al.*, 2012
HBEA (5 wt.%)			5	n.r.	
HMOR (5 wt.%)			3	n.r.	
HZSM–5 (5 wt.%)			5	n.r.	
HMCM–22 (5 wt.%)			12	n.r.	
Bimodal micro-mesoporous HBEA (20 wt.%)	Ethanol	78	40	4	Patil *et al.*, 2014
HBEA (10 wt.%)	*n*–Buthanol	120	82.2	5	Maheria *et al.*, 2013
HMOR (10 wt.%)			29.5	n.r.	
HY (10 wt.%)			32.2	n.r.	
HZSM–5(10 wt.%)			30.6	n.r.	
DHZSM–5[b] (20 wt.%)	*n*–Buthanol	120	98	6	Nandiwale and Bokade, 2015
DHZSM–5 (20 wt.%)	Ethanol	120	95	6	Nandiwale *et al.*, 2014
DHZSM–5 (25.4 wt.%)	*n*-Octanol	120	99	7	Nandiwale *et al.*, 2014
DTPADHZSM–5[c] (25 wt.%)	Ethanol	78	94	4	Nandiwale *et al.*, 2013

[a] not reported; [b] Desilicated HZSM–5 and [c] Dodecatungstophosphoric acid (DTPA) on desilicated HZSM–5.

3. EXPERIMENTAL AND METHODS

3.1 Materials

Zeolites

Zeolitic tuffs with a high content of clinoptilolite (CLI) used in this study were obtained from two Serbian deposits: Zlatokop (area of Vranjska Banja) and Slanci (near Belgrade). The used samples were firstly sieved to obtain particles of 0.063–0.125 mm for which previous studies were shown that are optimal for experimental work (Rajic *et al*., 2009; Jevtic *et al*., 2014). Then samples were washed using deionized water for several times and dried overnight at 105 °C until a constant mass.

Soils

Soil samples were collected from Serbia (Varna, 44°40'24" N and 19°39'25" E), Norway (59°41'09" N and 10°46'37" E) and Bosnia and Herzegovina (Kakanj, 44°07'53" N and 18°06'27" E). To minimize heterogeneity, the samples were collected from the top layer (0–20 cm) from different locations within the field site. Prior to the experiments, the soil samples were homogenized at room temperature, air dried, sieved through a 2 mm sieve mesh and stored in polyethylene bags.

According to the World Reference Base (World reference base for soil resources 2014), the used soil samples are classified as sandy soil (soil from Norway, NW), silty loam (soil from Serbia, SRB) and silty clay (soil from Bosnia and Hercegovina, BH).

Chemicals

All chemicals used in this study were of analytical grade and used without purification:

- 1–Octanol ($C_8H_{18}O$, p.a., Sigma Aldrich)
- Ammonium acetate (CH_3COONH_4, p.a, Carlo Erba)
- Ammonium hydroxide (NH_4OH, 25 v/v%, Sigma Aldrich)
- Ammonium nitrate (NH_4NO_3, p.a. Fluka)
- Ammonium sulfate ($(NH_4)_2SO_4$, p.a. Fluka)
- D–(+)–Glucose ($C_6H_{12}O_6$, p.a. Sigma Aldrich)
- Ethanol absolute (C_2H_5OH, p.a. Sigma Aldrich)
- Glacial acetatic acid (CH_3COOH, p.a., Merck)

- Hydrochloric acid (HCl, 35 wt.%, Sigma Aldrich)
- Iron(III) chloride hexahydrate ($FeCl_3 \cdot 6H_2O$, p.a., Fluka)
- Levulinic acid ($C_5H_8O_3$, p.a. Sigma Aldrich)
- Magnesium chloride ($MgCl_2$, p.a., Sigma Aldrich)
- Manganese(II) chloride ($MnCl_2$, p.a., Sigma Aldrich)
- NitraVer5 Nitrate Reagent Powder Pillows (HACH)
- PhosVer3 Phospahte Reagent Powder Pillows (HACH)
- Potassium dihydrogen phospahete (KH_2PO_4, p.a. Carlo Erba)
- Potassium nitrate (KNO_3, p.a., Sigma Aldrich)
- Sodium acetate trihydrate ($CH_3COONa \cdot 3H_2O$, p.a., Fluka)
- Sodium carbonate (Na_2CO_3, p.a., Fluka)
- Sodium chloride (NaCl, p.a., Carlo Erba)
- Sodium hydroxyde (NaOH, p.a., Carlo Erba)
- Tin(II) chloride dihydrate ($SnCl_2 \cdot 2H_2O$, p.a. Sigma Aldrich)

3.2 Modification procedures

Preparation of H-containing clinoptilolite (HCLI)

A triple treatment of CLI with 1 mol dm^{-3} HCl at 100 °C for 4 h using a solid/liquid mass ratio of 1:70 was followed by treatment with 0.2 mol dm^{-3} NH_4OH at 65 °C for 0.5 h (solid/liquid ratio=1:30). The obtained HCLI was separated and dried at 80 °C until a constant mass.

Preparation of the manganese/magnesium-containing clinoptilolite (MnCLI and MgCLI)

The preparation of MnCLI and MgCLI was carried out by using a similar procedure reported by Camacho et al. (Camacho *et al.*, 2011). CLI (10 g) was suspended in a 10 cm^3 of $MnCl_2$ or $MgCl_2$ solution (conc. 2.5 mol dm^{-3}) and 1.0 cm^3 of 1 mol dm^{-3} NaOH and heated for 5 h at 150 °C. Then, the suspension was separated by centrifugation and the obtained solids were dried and calcined at 500 °C for 1 h. Finally, the calcined products (MnCLI and MgCLI) were washed several times with distilled water and dried to a constant mass at 105 °C.

Preparation of the iron-containing clinoptilolite (FeCLI)

FeCLI was prepared by using a slightly modified procedure described by Habuda-Stanić et al. (Habuda-Stanić *et al.*, 2008*).* 10 g of CLI was mixed with 50 cm^3 of 0.1 mol dm^{-3} $FeCl_3$ in an acetate buffer at pH 3.6, for 1 h at room temperature. Then 45 cm^3 of 4 % NaOH were added, the suspension was stirred for 1 h and finally mixed with 25 cm^3 of a 4 % NaCl solution. The suspension was then stirred for another hour at 50 °C. After filtering, the Fe-containing sample (FeCLI) was heated to dryness, calcined at 500 °C for 1 h, washed several times with distilled water and dried to a constant mass at 105 °C.

Preparation of SnO_2-containing clinoptilolite (SnHCLI)

Wet impregnation method:

SnHCLI samples with approx. 5–12 wt.% of Sn were prepared following a slightly modified method described by Matsuhashi et al. and Sowmiya et al. (Matsuhashi *et al*., 2001; Sowmiya *et al*., 2007). HCLI was suspended in deionized water using a solid/liquid mass ratio 1:100 and stirred for about 10 min. The pH of the suspension was adjusted to 10 by dropwise addition of a 25 wt. % NH_4OH. Then, an ethanolic solution of $SnCl_2 \cdot 2H_2O$ (C_0=2 g dm^{-3}) was added dropwise under stirring. The pH was kept constant. The added volumes of $SnCl_2 \cdot 2H_2O$ solution were varied from 100 to 250 cm^3 in order to obtain SnHCLI with different amounts of Sn. The suspensions were separated by centrifugation after 24 h of stirring, washed with 4 wt.% CH_3COONH_4 and then with deionized water until chloride free. SnHCLI samples were dried overnight at 120 °C and then calcined at 400 °C for 2 h. The samples were denoted as SnHCLI5, SnHCLI9 and SnHCLI12 where numbers refer different Sn contents: SnHCLI5 – 4.5 wt.%, SnHCLI9 – 9.2 and SnHCLI12 – 12.3.

Mechanochemical method:

SnHCLI samples (with approx. 5–12 wt.% of Sn) were also prepared by a mechanochemical method by using a similar procedure reported in the literature (Yang *et al.*, 2004; Chakravarty *et al.*, 2016). As a starting material, HCLI, anhydrous $SnCl_2$, Na_2CO_3 and $C_6H_{12}O_6$ were used. The molar ratio of $SnCl_2$:Na_2CO_3:$C_6H_{12}O_6$ was 1:1.25:1.5. Milling was carried out in a planetary ball mill (TENCAN, XQM–(2–16)A)) using alumina balls with 12 mm and 17 mm in diameter at room temperature. The ball

to powder mass ratio was 10:1, and powders were ground for 15 min at 350 rpm. After calcination at 600 °C in an air atmosphere for 3 h, the obtained products (MSnHCLI5, MSnHCLI9 and MSnHCLI12) were washed with deionized water and dried at 100 ºC for 24 h.

Preparation of sulfated SnO_2-containig clinoptilolite

SnHCLI samples obtained by both wet impregnation and mechanochemical method were further treated with $(NH_4)_2SO_4$ solution (conc. 1 or 3 mol dm^{-3}) by using a solid/liquid mass ratio of 1:50. The suspensions were stirred at room temperature for 24 h. Then, the solids were separated by centrifugation, washed and dried overnight at 120 °C to a constant mass. Samples obtained by wet impregnation were then calcined for 2 h at 400 °C. The products obtained by wet impregnation were denoted as SSnHCLI5, SSnHCLI9 and SSnHCLI12 whereas products obtained by mechanochemical method were denoted as MSSnHCLI5, MSSnHCLI9 and MSSnHCLI12.

3.3 Adsorption studies

3.3.1 Nitrate adsorption

The adsorption experiments were performed by a batch method. The adsorption capacity of MCLI toward nitrates (M–Fe, Mn or Mg) was investigated as a function of the adsorbent amount, temperature and the initial concentration of the nitrate solution. All nitrate solutions were prepared by dissolving KNO_3 in deionized water. The influence of different parameters on the adsorption efficiency was investigated as follows:

1) The effect of the adsorbent amount was investigated at 25 °C by shaking different amounts of MCLI (0.5, 1.0, 1.5 and 2.0 g) with 50.0 cm^3 of KNO_3 solution (C_0 = 100 mg dm^{-3}) for 24 h in a thermostated water bath (Memmert, WBE 22).
2) The effect of temperature was studied with 1.0 g of MCLI and 50.0 cm^3 of KNO_3 solution (C_0 = 100 mg dm^{-3}) at 25, 35 and 45 °C for 24 h.
3) The influence of the initial KNO_3 concentration (50, 100, 200 and 300 mg dm^{-3}) was studied by shaking the 1.0 g of MCLI with 50.0 cm^3 of the appropriate nitrate solution at 45 °C for 24 h.

3.3.2 Phosphate adsorption

Adsorption of phosphate was studied using FeCLI. The adsorption experiments were performed at 25 °C by a batch method. All solutions were prepared by dissolving an appropriate amount of KH_2PO_4 in deionized water. 1.0 g of FeCLI was suspended in 100 cm^3 of the appropriate concentration of KH_2PO_4 solution (50, 100, 200 and 300 mg PO_4^{3-} dm^{-3}) and left under shaking in a thermostated water bath at 25 °C (Memmert, WBE 22) for contact times up to 1440 min. Then, the suspensions were separated by filtration and the concentration of the phosphate in the solution was determined colorimetrically.

3.4 Kinetic studies

The adsorption kinetics of nitrate onto MCLI was studied by shaking 1.0 g of each adsorbent (FeCLI, MnCLI or MnCLI) with 50.0 cm^3 of an aqueous solution of nitrate (C_0 = 300 mg dm^{-3}) at 45 °C for a contact time from 30 to 1440 min in a thermostated water bath (Memmert, WBE 22). The kinetic adsorption of phosphate was studied only for FeCLI. The experiments were carried out at 25 °C by using solid:liquid ratio of 1:100 and different initial concentration of phosphate solution (50, 100, 200 and 300 mg PO_4^{3-} dm^{-3}) for a contact times up to 1440 min.

Kinetic results for both nitrate and phosphate adsorption were studied by using the most applied kinetic models in adsorption including Lagergren pseudo-first-order, Lagergren pseudo-second-order and Intra-particle diffusion (Weber-Morris) model.

Pseudo-first-order model

The non-linear form of the pseudo-first-order model given by the Lagergren (Lagergren, 1898) can be expressed as:

$$\frac{dq_t}{dt} = k_1(q_e - q_t) \qquad (1)$$

where q_t and q_e are the amount of adsorbate onto MCLI (mg g^{-1}) at time t and equilibrium, respectively and k_1 (min^{-1}) is the rate constant of the first-order adsorption. Integrating the equation (1) at boundary conditions t = 0 and q_t = 0 to t = t and q_t = q_t, the following linear form obtains:

$$\log(q_e - q_t) = \log q_e - \frac{k_1}{2.303} t \qquad (2)$$

The applicability of this kinetic model is determined by the plot of log(q_e – q_t) versus t which should yield a straight line if the experimental data conform to this kinetic model. The parameter q_e and k_1 could be calculated from the intercept and slope of the obtained plots, respectively. Moreover, the linear regression coefficient $R^2 \approx 1$ also indicates to conformity of this model.

Pseudo-second-order model

The pseudo-second-order model given by the Lagergren (Ho and McKay, 1998; Ho, 2006) is expressed as follows:

$$\frac{dq_t}{dt} = k_2(q_e - q_t)^2 \qquad (3)$$

where q_t and q_e are the amount of adsorbate onto MCLI (mg g^{-1}) at time t and equilibrium, respectively and k_2 (g mg^{-1} min^{-1}) is the rate constant of the pseudo-second-order adsorption.

Integration between the same limits ($t = 0$ and $q_t = 0$ to $t = t$ and $q_t = q_t$) yields the following expression:

$$\frac{t}{q_t} = \frac{1}{k_2 q_e^2} + \frac{1}{q_e} t \qquad (4)$$

The plot of t/q_t versus t will give a straight line showing that this kinetic model is applicable to the experimental data. The values of q_e and k_2 could be obtained from the slope and intercept of the plot, respectively.

Intra-particle diffusion model

The intra-particle diffusion model or Weber–Morris model is widely applied model to study the rate limiting step of adsorption (Weber and Morris, 1963). This model can be expressed by equation:

$$q_t = k_{int} t^{1/2} + C$$

where q_t is the amount of adsorbate onto MCLI (mg g^{-1}) at time t (h), k_{int} is the rate constant (mg g^{-1} $h^{-1/2}$) and C is the intraparticle diffusion constant (i.e. intercept of the line) (mg g^{-1}) that is directly proportional to the boundary layer thickness.

The values of the constants k_{int} and C can be calculated from the linear plot of the q_t versus the square root of time ($t^{1/2}$). If the line passes through the origin, intra-particle diffusion is the rate-controlling step of adsorption. However, very often, the line does not pass through the origin and it contains multiple linear sections suggesting that the intra-particle diffusion is not the only rate-limiting step. The adsorption can be also controlled by the mass transfer of adsorbate from the bulk liquid phase to the external surface of the adsorbent through a boundary layer (film diffusion), surface diffusion that includes slow movement of adsorbate from the boundary layer to the adsorbent surface or by movement of adsorbate to the pore system of the adsorbent (pore diffusion) (Tran *et al.*, 2017).

3.5 Adsorption isotherms

The equilibrium adsorption data were analyzed by three isotherm equations (Langmuir, Freundlich and Temkin isotherm models) that are commonly applied for description of adsorption equilibrium data.

Langmuir adsorption isotherm

The Langmuir adsorption isotherm assumes homogenous adsorbent surface where all the adsorption sites possess equal affinity toward adsorbate. Linear form of Langmuir isotherm can be expressed as follows (Langmuir, 1916):

$$\frac{C_e}{q_e} = \frac{1}{Q_0} C_e + \frac{1}{Q_0 b}$$

where C_e is the equilibrium concentration of adsorbate (mg dm^{-3}), q_e is the amount adsorbed at equilibrium (mg g^{-1}), Q_0 is the maximum amount of adsorbate per unit mass

of adsorbent (mg g^{-1}) and b is the Langmuir adsorption equilibrium constant related to adsorption energy (dm^3 mg^{-1}).

The Q_0 and b can be calculated from the slope and intercept, respectively, of the linear plot C_e/q_e versus C_e.

For predicting the favourability of the adsorption process, the Langmuir isotherm can also be expressed in terms of a dimensionless constant R_L (separation factor) which is defined as a follows:

$$R_L = \frac{1}{(1 + bC_0)}$$

where b is the Langmuir adsorption equilibrium constant related to adsorption energy (dm^3 mg^{-1}) and C_0 is the initial concentration of the adsorbate (mg dm^{-3}).

The value of R_L indicates the adsorption process to be favourable for $0<R_L<1$, unfavorable for $R_L>1$, linear for $R_L=1$ or irreversible for $R_L=0$.

Freundlich adsorption isotherm

Freundlich adsorption isotherm assumes that the surface of adsorbent is heterogenous with respect to the distribution of adsorption sites through the adsorbent surface. This isotherm can be used to describe multilayer adsorption with interaction between adsorbed ions. The Freundlich model can be represented as follows (Freundlich, 1906):

$$logq_e = logK_f + \frac{1}{n} logC_e$$

where C_e is the equilibrium concentration of adsorbate (mg dm^{-3}), q_e is the amount adsorbed at equilibrium (mg g^{-1}), K_f (dm^3 g^{-1}) and n (dimensionless) are Freundlich constants that are indicators of the adsorption capacity and adsorption intensity, respectively.

The values of K_f and n can be determined from the intercept and slope of the linear plot of the $\log q_e$ versus $\log C_e$, respectively. The value of Freundlich constant n below or equal to one indicates a chemisorptions process whereas the n values greater than one indicates that adsorption is physical process.

Temkin adsorption isotherm

The Temkin adsorption isotherm includes a factor which takes into account the interactions between adsorbent and adsorbate. This isotherm is based on assumption that: 1) the adsorption heat of all molecules decreases linearly with coverage of the adsorbent surface due to repulsions between adsorbate molecules (Temkin and Pyzhev, 1940; Kucherova *et al*., 2018) and 2) adsorption is characterized by a uniform distribution of binding energies (up to maximum binding energy). The Temkin isotherm can be described by linear equation (Temkin and Pyzhev, 1940):

$$q_e = BlnA + BlnC_e$$

where C_e is the equilibrium concentration of adsorbate (mg dm^{-3}), q_e is the amount of adsorbed at equilibrium (mg g^{-1}), A is the Temkin equilibrium binding constant (dm^3 g^{-1}), B is the Temkin isotherm constant related to heat of adsorption and $B=RT/b_T$ where R is the universal gas constant (8.314 J mol^{-1} K^{-1}), T is the absolute temperature (K) and b_T is the Temkin constant related to the heat of adsorption (kJ mol^{-1}).

The constant A and B can be calculated from the intercept and slope of the plot of a straight line of lnC_e versus q_e.

3.6 Leaching experiments

Leaching of potassium and nitrate ions from different soil types in the presence of CLI

The leaching experiments were performed at room temperature using column systems. Columns were organized in eight experimental systems with three replications of each (Table 3). KNO_3 was used as a source of potassium and nitrate ions. The amount of added KNO_3 corresponded to 10 mg N $(100\ g\ soil)^{-1}$ and 28 mg K $(100\ g\ soil)^{-1}$ which represents 200 kg N and 550 kg K ha^{-1} soil. The used N amount corresponded to the usually applied rate for grass (clover) production (Di and Cameron, 2002). However, the amount of K was high compared to the usual agricultural production but suitable for the leaching experiments in which a high amount of water was used for irrigation. The amounts of CLI (1 wt. %) and FeCLI (0.5 and 1 wt.%) corresponded to about 10 and 20

t zeolite ha^{-1}, respectively, which are suitable amounts to be used in the agricultural practice.

Table 3. Column systems used in K^+, NO_3^--leaching experiments.

System	Component
I	Soil
II	Soil + KNO_3
III	Soil + 1 wt.% CLI
IV	Soil + 1 wt.% CLI + KNO_3
V	Soil + 0.5 wt.% FeCLI
VI	Soil + 0.5 wt.% FeCLI + KNO_3
VII	Soil + 1 wt.% FeCLI
VIII	Soil + 1 wt.% FeCLI + KNO_3

Columns were made from plexiglass, with diameter= 24 mm and length= 30 cm. They were filled with soil or with homogenized mixture of soil and amendments (CLI/FeCLI or KNO_3). Homogenization of the mixtures was accomplished by a rotating shaker during 24 h using locked plastic beakers. In order to compress the fillings to the same height each column was finally carefully shaken. At the bottom of each column, a nylon filter covered with PVC balls (about 2 cm in height) was placed to prevent the loss of solid. In order to provide an effective distribution of water, the top of each column was covered with the PVC balls. The experimental setup used for the leaching experiments is shown in Figure 19.

For the leaching experiment, the filled columns were previously saturated with distilled water and then regularly irrigated homogenously with distilled water from the top of the column, at a flow rate of 1.3 cm^3 h^{-1}. The flow rate was chosen to correspond to 500 mm of precipitation during 7 days in order to study the effect of CLI and FeCLI addition on the leaching of K and (NO_3–N) through the heavy precipitation over a short period of time which is usual phenomenon. All experiments were performed in the absence of light to prevent possible growth of the plants which fragments or seeds are present in cultivated soils. The leachates (of about 30 cm^3) were collected at the column bottom

every day during seven days. The samples were stored in a refrigerator prior to the analysis.

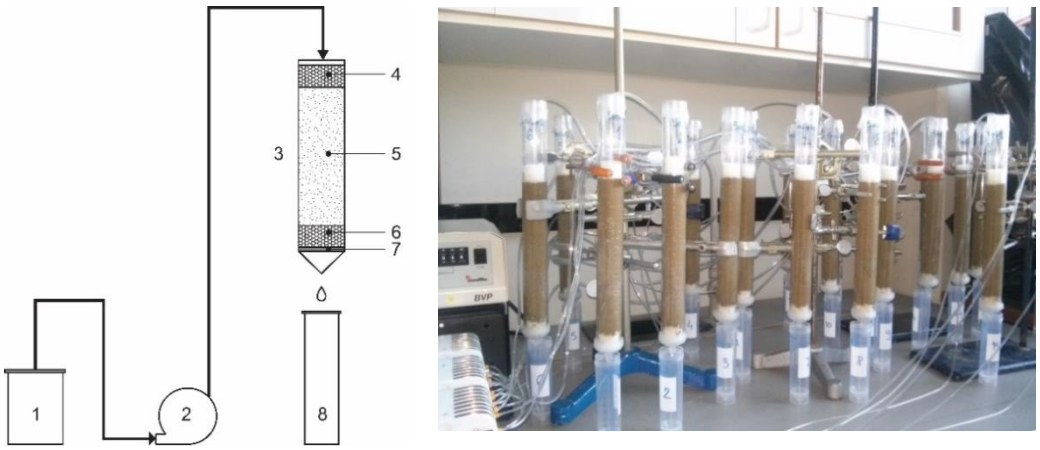

Figure 19. The experimental setup used for the leaching experiments: 1) water tank; 2) peristaltic pump; 3) plexiglass column; 4) PVC balls; 5) soil or soil/FeCLI mixture; 6) PVC balls; 7) PVC filter; 8) sample collector.

Leaching of phosphate ions from sandy soil in the presence of CLI

The leaching of phosphate was studied using columns system. The columns were organized in several groups with three replications of each (Table 4) and using the leaching procedure previously described.

Amounts of the added FeCLI corresponded to about 10 (0.5 wt.%), 30 (1.5 wt.%) and 50 (2.5 wt.%) t FeCLI ha^{-1}. As a source of phosphate, solid KH_2PO_4 was applied. Saturation and irrigation amount of distilled water was retained in the same value as in previously leaching experiments. However, in contrast to previously leaching experiments, the experiments were prolonged (twelve days instead of seven) since the very low and almost constant amount of phosphate was leached during the seven days.

Table 4. Column systems used in PO_4^{3-}-leaching experiments.

System	Component
I	Soil
II	Soil + KH_2PO_4
III	Soil + 0.5 wt.% FeCLI
IV	Soil + 0.5 wt.% FeCLI + KH_2PO_4
V	Soil + 1.5 wt.% FeCLI
VI	Soil + 1.5 wt.% FeCLI + KH_2PO_4
VII	Soil + 2.5 wt.% FeCLI
VIII	Soil + 2.5 wt.% FeCLI + KH_2PO_4

3.6.1 Leaching kinetic studies

Collected samples during leaching experiments were analyzed by several kinetic models including zero-order, first-order, second-order, Intra-particle diffusion model, Elovich and Avrami kinetic model.

Statistical data analysis was done by the Paired Samples T-Test using statistical software - Statistical Package for the Social Sciences (SPSS Ver. 22). The statistical significance was defined at $p < 0.05$.

Zero-order

The zero-order equation can be given as (House, 2007):

$$q_t = q_0 - k_0 t$$

where q_0 and q_t are the leached amount (mg g^{-1}) at time t=0 and time t, respectively and k_0 (min^{-1}) is the rate constant of the zero-order (mg kg^{-1} h^{-1}) and can be determined from the plot of q_t versus t.

First-order

The first-order equation can be represented as (House, 2007):

$$\ln(q_t) = \ln(q_0) - k_1 t$$

where q_0 and q_t are the leached amount (mg g^{-1}) at time *t=0* and time *t* respectively and k_1 (min^{-1}) is the first-order rate constant (h^{-1}) and can be calculated from the plot of ln(q_t) versus *t*.

Second-order

The second-order equation can be given as (House, 2007):

$$\frac{1}{q_t} = \frac{1}{q_0} - k_2 t$$

where q_0 and q_t are the leached amount (mg g^{-1}) at time *t*=0 and time *t*, respectively and k_2(min^{-1}) is the second-order rate constant (mg $kg^{-1})^{-1}$ and can be calculated from the plot of $1/q_t$ versus *t*.

Intra-particle diffusion model

The intra-particle diffusion model or (Weber and Morris model) is described in the previous kinetic section.

Elovich kinetic model

The Elovich equation mainly describes chemisorption kinetics and adsorption process at heterogeneous surfaces. The linear form of the Elovich model can be given by the following equation (Roginsky and Zeldovich, 1934):

$$q_t = \frac{1}{\beta}\ln(\alpha\beta) + \frac{1}{\beta}\ln(t)$$

where q_t is the amount of adsorbed (mg g^{-1}) at time *t* (h), α is the initial adsorption rate (mg g^{-1} h) and β is the desorption constant (g mg^{-1}).

The constants α and β can be determined from the slope and intercept of the linear plot of ln*t* versus q_t.

Avrami kinetic model

The Avrami kinetic model has been originally applied to describe the phase transitions and crystal growth of material and has recently been used to predict adsorption kinetic onto different solid adsorbents. Linearized equation of this kinetic model can be expressed as (Avrami, 1939; Songolzadeh *et al*., 2015):

$$\ln[-\ln(1-X)] = \ln(k_A) + n_A \ln(t)$$

where X is the percentage of the leached (%) at time t (h^{-1}), k_A – is the Avrami kinetic constant (h^{-1}) and n_A is the Avrami constant.

The values of the n_A and k_A can be calculated from the slope and intercept of the plot ln[–ln(1–X)] versus ln(t), respectively.

3.7 Catalytic experiments

Conversion of LA into OLA and ELA was carried out in a batch reactor with magnetic stirrer under reflux (Figure 20). Prior to the catalytic test, the catalysts were pre-treated *ex-situ* in oven for at 1 h at 200 °C, at static conditions. In a typical catalytic experiment, the reactor was charged with 1 g LA, 7 ml ethanol or octanol and 0.2 g powder catalyst while the LA/octanol (ethanol) weight ratio was maintained 1:7. The reactor was placed in an oil bath, heated under stirring with 200 rpm at the reaction temperature of 100 °C for 5 h. The thermocouple was positioned in the reaction mixture for accurate measurement of the reaction temperature. Samples were taken at chosen time intervals and analyzed. At the end of the reaction, the reactor was cooled to room temperature and the catalyst was recovered by centrifugation. The mass balance was made on the basis of carbon-containing products.

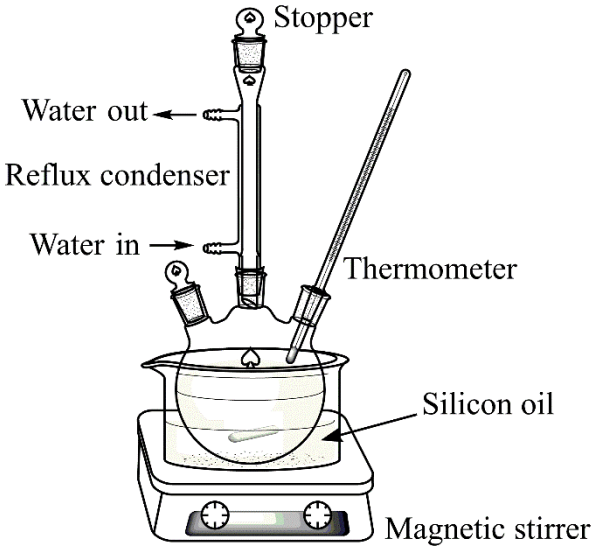

Figure 20. Experimental setup used in catalytic experiments.

Catalyst reusability

Reusability of the catalyst was tested in six reaction cycles (one with the fresh catalyst and five repeated cycles with the reused catalyst). After completion of the reaction in each cycle, the catalyst was separated by centrifugation, washed with acetone, dried at 60 ºC for 5 h and calcined at 400 ˚C in air for 3 h.

3.8 Material characterization

Determination of cation exchange capacity of the zeolitic tuff

Cation exchange capacity (CEC) of the used zeolitic tuffs was determined using a standard procedure based on the ion-exchange with 1.0 mol dm^{-3} ammonium acetate solution at room temperature for 24 h (Schollenberger and Simon, 1945). Concentration of Na^+, K^+, Ca^{2+} and Mg^{2+} was measured in filtrates and CEC value was expressed in mmol of M^+ per 100 g of CLI.

Determination of physicochemical properties of the soil samples

Soil pH was determined in distilled water with a soil to solution mass ratio of 1:2.5 using Orion SA 720 pH meter (Orion, Cambridge, MA, USA) (Thomas, 1996).

The soil organic matter (SOM) was analyzed by the combustion method at 550 °C (Nabertherm, LE 6/11/B150, Lilienthal, Germany) (Thomas, 1996).

Total nitrogen content (N_{TOT}) was measured by Dumas method (Bremner and Mulvaney, 1982). Samples were heated with CuO at a high temperature in a stream of purified CO_2. Then, the gases liberated were led over hot Cu to reduce nitrogen oxides to N_2 and then over CuO to convert CO to CO_2. The obtained mixture of N_2–CO_2 is collected in a nitrometer containing the concentrated alkali which absorbs CO_2 and the volume of N_2 gas is the measure. The analysis of N_{TOT} was performed at 1050 °C using LECO CHN 1000 analyzer (LECO Corporation, St. Joseph, MI, USA).

The concentration of the plant available K was determined by the Egners Al method (Egner *et al*., 1960). Soil samples were extracted with 0.1 mol dm^{-3} ammonium lactate solution and 0.4 mol dm^{-3} acetic acid (pH=3.7) with a soil to solution mass ratio of 1:20 for 90 min.

Atomic absorption spectroscopy (AAS)

The concentration of metal in the solution was measured using AAS (Varian SpectrAA, 55B). Measurement accuracy was ± 2%. All measurements were done in accordance with the manual recommendations.

UV/Visible spectroscopy (UV/VIS)

The concentration of nitrate and phosphate in the solution was determined by UV/VIS spectrophotometer (HACH DR2800). Cadmium reduction method (with NitraVer5 reagent) and ascorbic acid method (with PhosVer3 reagent) was used to measure the nitrate and phosphate concentration, respectively. Before analysis, solutions were filtered through 0.45 µm membrane filter. All measurements were done in accordance with the HACH manual recommendations.

The adsorbed amount (q_t) of nitrate and phosphate after time t was calculated according to the following formula:

$$q_t = \frac{C_0 - C_t}{m} \cdot V$$

where C_0 and C_t are concentrations of adsorbate (nitrate or phosphate) in the aqueous solution (mg dm^{-3}) before and after contact with the MCLI, respectively, V is the volume of the solution in dm^3 and m is mass of the MCLI in g.

Gas chromatography (GC)

GC analysis used to analyze samples obtained in the catalytic experiments. Analyses were performed using a flame ionization detector equipped with a WCOT FUSED SILICA 25m x 0.25mm COATING CP-SIL 43CB column. Nitrogen was used as a carrier gas with manual injection (the sample volume injected was 1 μl). The column temperature increased from 100 to 200 °C (20 °C min^{-1}) whereas the injector and detector temperature were 250 and 300 °C, respectively. The LA conversion rate was determined using the LA/OLA or LA/ELA area ratio.

Powder X-ray powder diffraction (PXRD)

PXRD was performed to determine the mineral composition of the zeolitic tuffs and to check crystallinity after the experiments. PXRD patterns of the samples were recorded using an APD2000 Ital Structure diffractometer with CuKα radiation (λ=0.15418 nm) generated at 38 kV and 28 mA. Scans were performed in the 2θ range 5–50° with a step of 0.02° per 1 s. Semi-quantitative PXRD analysis was conducted using the Rietveld refinement and the Topas-Academic v.4 software package (Coelho, 2007).

Mineral composition of the soil samples was also determined by PXRD analysis using a Philips PW 1710 (Philips, Almelo, The Netherlands) diffractometer with the CuKα radiation (λ=0.15418 nm) in the 2θ range 2–70° with a 2θ step of 0.02°. Detailed informations on the clay minerals present in the soil samples were obtained by pretreatment of the samples prior to the PXRD analysis. Pretreatment included: a) air-drying, b) saturation with ethylene glycol and c) heating at 300 or at 550 °C (Moore and Reynolds, 1997). Qualitative analysis was established according to Brown (Brown and Brindley, 1980). A semi-quantitative analysis of minerals was performed by measuring the peak intensities calculated from the PXRD patterns and by comparing them to the peak intensities of pure minerals (Pederstad and Jørgensen, 1985). Pipette method was used for determination of the content of sand, silt and clay fractions in the soils (Elonen, 1971).

Scanning Electron Microscopy (SEM) coupled with energy dispersive X-ray spectroscopy (EDS)

Surface morphology and elemental composition of the CLI and CLI-modified samples were studied by the SEM equipped with EDS analysis. SEM images were collected using a Carl Zeiss Supra™ 3VP field-emission gun scanning electron microscope (FEG-SEM) equipped with EDS detector (Oxford Analysis) with INCA Energy system for quantification of elements. Before analysis, the samples were carefully prepared in order to make them conductive. The procedure included the embedding grains in an epoxy film, polishing the crystallites, cutting them with a fine-grid diamond cutter and coating them with carbon. An intersection view of the crystallite grains was obtained that enabled detailed EDS analysis of the major mineral phases. The Inca scanning software was used to study the data analysis.

Thermal analysis (TG/DTG)

Thermal analysis was applied to study the thermal behavior of the samples. The measurements were performed using a SDT Q-600 instrument (TA Instruments). About 10 mg of samples were heated in opened alumina cups (90 µl) from room temperature to 800 °C at a heating rate of 10 °C min^{-1} under synthetic air (100 ml min^{-1}). Results were evaluated with TA-Universal Analysis software.

X-ray photoelectron spectroscopy (XPS)

XPS analyses were carried out on a PHI–TFA XPS spectrometer (Physical Electronics Inc). Powders were on carbon adhesion tape used for SEM microscopy and introduced in ultra-HV spectrometer. During the XPS analyses, the vacuum was in the range of 10–9 mbar. The analyzed area was 0.4 mm in diameter whereas the analyzed depth was about 3–5 nm. X-ray radiation from monochromatic Al source at photon energy of 1486.6 eV was applied for excitation of the sample surfaces. The survey wide-energy spectra were taken over an energy range of 0–1200 eV with pass energy of analyzer of 187 eV in order to identify and quantify present elements on the surface. The high-energy resolution spectra were acquired with energy analyzer operating at resolution of about 0.6 eV and pass energy of 29 eV. During data processing, the spectra were aligned by setting the C 1s peak at 284.8 eV, characteristic for C–C/C–H bonds. The accuracy

of binding energies was about ±0.3 eV. Quantification of the surface composition was performed from XPS peak intensities taking into account the relative sensitivity factors provided by instrument manufacturer (Moulder *et al*., 1995). MultiPak software was used to analyze the obtained XPS spectra. High resolution spectra were fitted with Gauss-Lorentz functions and Shirley function was used for background removal. In order to analyze the in-depth distribution of elements in the sub-surface region up to 25 nm deep, the XPS depth profiling was performed in combination with ion sputtering. The Ar ions of energy 4 keV were used. The velocity of the ion sputtering was estimated to be 1.0 nm min^{-1} calibrated on the Ni/Cr multilayer structure of the known thickness.

UV/Visible diffuse reflectance spectroscopy (DRS)

DRS analysis was used to investigate the presence of oxide species onto CLI-modified samples. Spectra were recorded using an UV/VIS spectrophotometer (V–650, JASCO) equipped with a photomultiplier tube detector. The powder sample was put into a cell and measured in the range from 200 to 800 nm at room temperature.

Solid-state nuclear magnetic resonance (NMR)

NMR analyses were carried out on a 600 MHz Varian NMR system equipped with a 3.2 mm Varian HX CPMAS probe. Larmor frequencies for ^{27}Al and ^{29}Si nuclei were 156.20 MHz and 119.09 MHz, respectively. For ^{27}Al magic-angle spinning (MAS) measurements excitation pulse of 0.8 µs was used, number of scans was 3000 and repetition delay between scans was 1 s. Sample rotation frequency was 16 kHz. For ^{29}Si MAS measurements excitation pulse was 2.8 µs, repetition delay was 60 s, and number of repetitions was 2400.

Textural properties

Textural properties of samples were determined by nitrogen physisorption at –196 °C using a Micromeritics Instrument (ASAP 2020). Before analysis, all the samples were degassed at 200 °C for 4 h under high vacuum. The specific surface area (S_{BET}) was calculated using the Brunauer, Emmett, Teller (BET) method up to relative pressures p/p_0=0.15. The total pore volume (V_{tot}) was assessed at p/p_0=0.99. Pore size distribution

was analyzed according to the Barrett, Joyner and Halenda method (BJH) from the adsorption isotherms.

Fourier transform infrared spectroscopy (FTIR)

FTIR analysis was used to study the structural features of the samples. FTIR spectra were collected at room temperature on a Digilab-FTS 80 interferometer by using KBr pellets method. The spectra were recorded in the range of 400–4000 cm^{-1}, at a resolution of 4 cm^{-1} and 100 scans.

FTIR was also applied to study surface acidity of the samples used in the catalytic experiments. FTIR spectra were collected by applying a self-supported wafer technique with pyridine (Py) as the probe molecule. FTIR spectra were recorded by using a Nicolet Impact Type 400 spectrometer at room temperature averaging 32 scans at a resolution of 2 cm^{-1}. Spectra were normalized to a wafer thickness of 5 mg cm^{-2}. Before the Py adsorption, the samples were evacuated in a high vacuum (HV,$<10^{-6}$ mbar) for 1 h at 400°C. Then, samples were treated with Py at 50 mbar and degassed in HV for 0.5 h at 100 °C, 200 °C, 300 °C and 400 °C. After evacuation, spectra were collected at room temperature.

4. RESULTS AND DISCUSSION

4.1 Physico-chemical characterization

Soils

Mineral composition of the soil samples was determined by PXRD analysis (Figure 21). The shown diffractograms displayed presence of different mineral phases in the samples. Nonclay minerals such as quartz and feldspar were present in all three samples. Quartz was dominant in the NW sample which is evident by diffractions at 2θ=20.81 and 26.63°. Diffractions at 2θ=13.90, 22.1, 23.6, 24.3, 28.1 and 30.2° correspond to feldspars which were an abundant mineral group in the NW sample (Oumabady, 2014). The diffraction at 2θ=29.6° corresponds to calcite and it is present only in the BH sample. To identify all clay minerals, the PXRD analysis was performed after each of the four soil treatments (1,2 -heating at 550 and 300 ºC, respectively, 3 -saturation with ethylene glycol and 4 - air–drying treatment) (Figure 21). The NW soil displayed weak reflections related to clay minerals, confirming the low clay content. Kaolinite was present in the BH and SRB samples displaying diffractions at 2θ=12.4, 20.1, 25.7 and 35.1°. Saturation with ethylene glycol and heating at 300 °C did not affect the kaolinite crystallinity which structure however collapsed after heating at 550 °C (Haque *et al*., 2013; Szymański *et al*., 2014). The diffraction at 2θ=12.4° which was present in the pattern of the NW sample most likely belonging to a second order reflection of vermiculite and chlorite which has its first order reflection at 2θ=6.5°. The NW soil is less than 10,000 years old, which is reflected in the presence of less weathered clay minerals as illite, vermiculate and chlorite (Øgaard and Krogstad, 2005). The diffraction at 2θ=9.07° was found in all three patterns and it corresponds to illite. The diffraction was unaffected by treatments with ethylene glycol and heating. An additional diffraction of illite at 2θ=18.0° was evident only in the patterns of the BH and SRB samples.

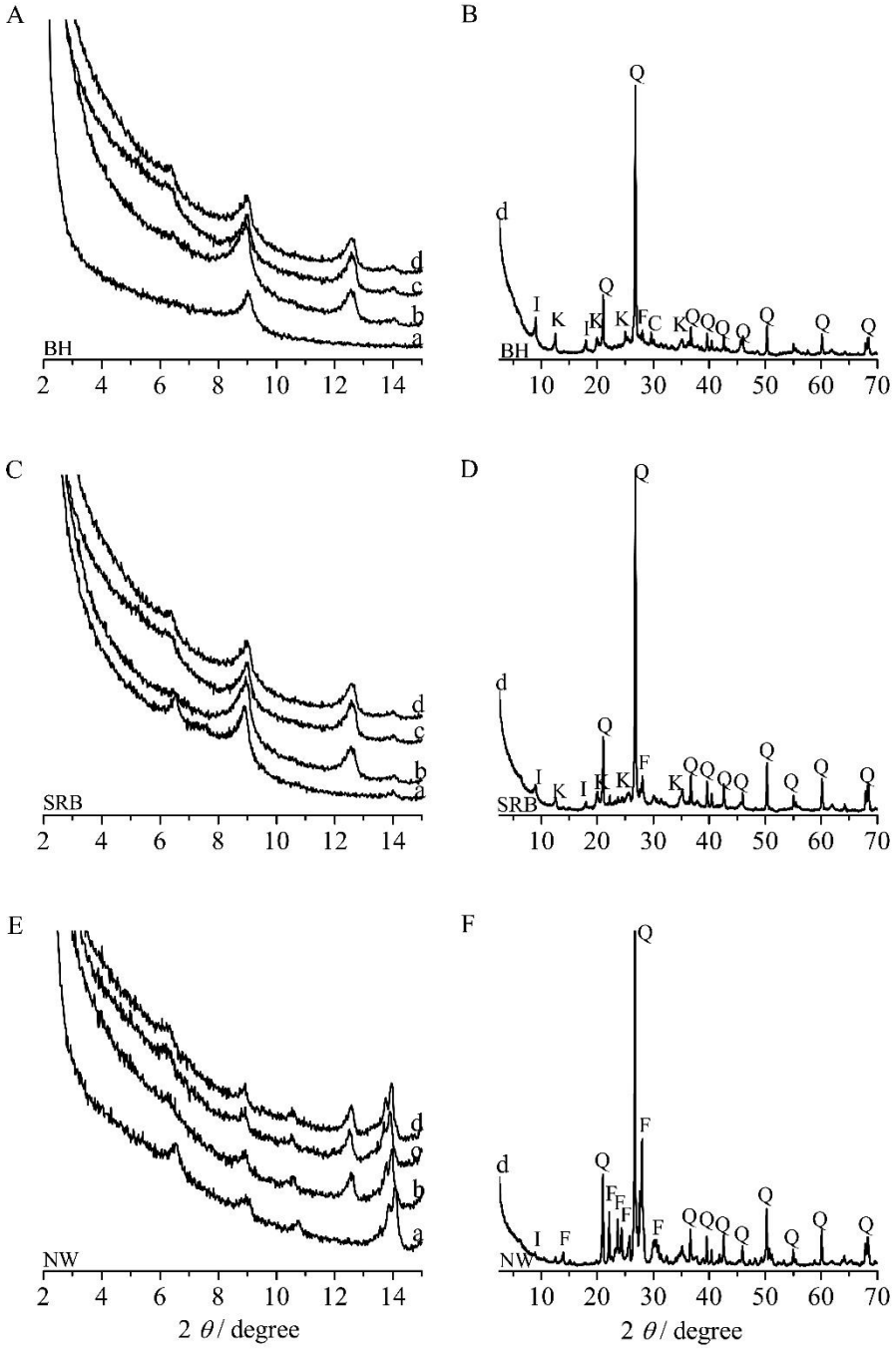

Figure 21. PXRD patterns of the soil samples (A, B – BH soil; C, D – SRB soil and E, F – NW soil. Soil treatments are marked as: a – heating at 550 ºC; b – heating at 300 ºC; c – saturation with ethylene glycol; d – air-drying treatment. Minerals are marked as: Q – quartz, F – feldspar, C – calcite, K – kaolinite and I – illite.

The selected physicochemical properties of the soil samples are given in Table 5. According to the content of sand, silt and clay phase, the used soil samples are classified as sandy soil (NW), silty loam (SRB) and silty clay (BH). As can be seen, sandy (NW) and silty loam (SRB) soils are acidic (pH= 5.1 and 5.7, respectively) whereas the silty clay (BH) is slightly alkaline (pH=7.5). The BH and SRB soils are old cultivated grassland and pasture possessing a higher content of organic matter (OM) which resulted in a higher amount of total nitrogen (N_{TOT}) in comparison to NW. K-containing clay mineral illite is present in all soils samples. It is evident from the concentration of plant available potassium (K–Al). It is also evident that BH sample has the highest clay content and higher K content than the NW and SRB samples.

Table 5. Selected physicochemical properties of the studied soil samples.

Sample	Sand	Silt	Clay	OM[a]	N_{TOT}[b]	pH	K-Al[c], mg kg^{-1}
	wt.%						
NW	94	3	3	1.3	0.01	5.1	10
SRB	4	73	23	4.3	0.16	5.7	115
BH	8	50	42	11.5	0.47	7.5	286

[a]OM-organic matter; [b]N_{TOT}-total nitrogen; [c]concentration of the plant available K;

Zeolitic tuffs

Mineral composition of the zeolitic tuffs was studied by PXRD analysis. The obtained PXRD diffraction patterns are presented in Figure 22. In both zeolitic tuffs, from Vranjska Banja deposit (VBCLI) and Slanci deposit (SCLI), zeolite – clinoptilolite is the major mineral phase. The diffraction peaks at 2θ= 9.8; 11.7; 12.8; 17.2; 19.1; 22.4; 26.0; 29.9 and 32.3° correspond to the clinoptilolite (Treacy and Higgins, 2001). The PXRD patterns also showed that both tuffs contain a slight amount of albite (2θ= 22.0; 24.5 and 27.8°) and quartz (2θ=20.8 and 26.7°).

Results of a quantitative analysis performed by the Rietveld method is given in Table 6. Both tuffs have a high content of clinoptilolite which is slightly higher in SCLI (81 wt.%) in comparison to VBCLI (73 wt.%).

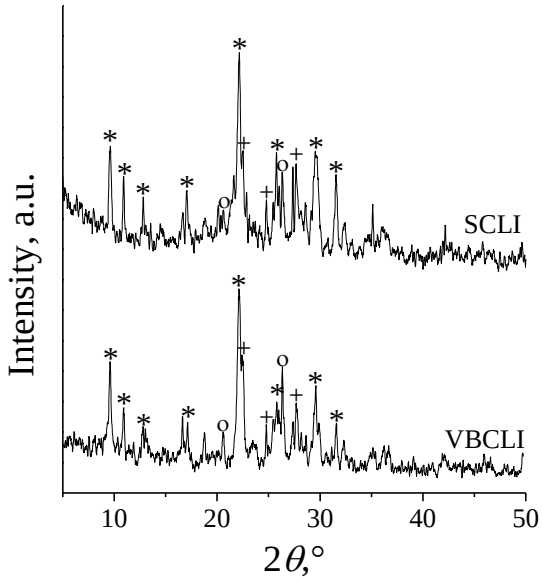

Figure 22. PXRD patterns of the zeolitic tuffs (*clinoptilolite; °quartz and +albite).

Table 6. Mineral composition of the used zeolitic tuffs.

Zeolitic tuff	Clinoptilolite	Quartz	Albite
		wt.%	
VBCLI	72.6	12.8	14.6
SCLI	80.9	4.4	14.7

VBCLI-zeolitic tuff from the Zlatokop (area of Vranjska Banja) and SCLI-zeolitic tuff from the Slanci (near Belgrade) deposit.

The surface morphology and elemental composition of the tuffs were studied using SEM coupled with EDS analysis. The shape and color contrast evident in SEM images (Figure 23) confirmed the presence of different mineral phases. The clinoptilolite phase with the Si/Al about 4.8 is found for VBCLI and 4.9 for SCLI (Table 7). The Si/Al molar ratio for feldspars is lower being in the range of 2.5–2.7 (Godelitsas and Armbruster, 2003).

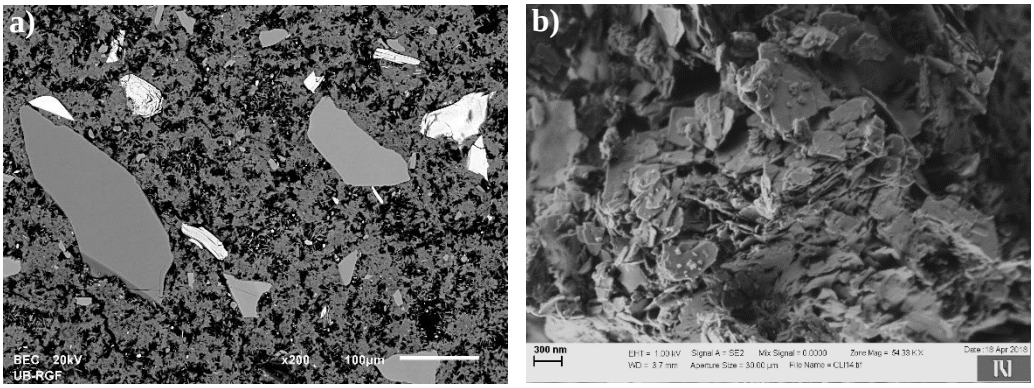

Figure 23. Representative SEM images of the used zeolitic tuffs.

Table 7. Average elemental composition of the CLI phase in the zeolitic tuffs obtained by EDS analysis.

Zeolitic tuff	Si	Al	O	Na	K	Ca	Mg	Fe
	at.%							
VBCLI	23.02	4.76	68.60	0.38	0.71	1.23	0.70	0.69
SCLI	22.90	4.65	69.85	0.17	0.49	1.21	0.69	0.04

Cation exchange capacity (CEC) of the zeolitic tuffs is given in Table 8. The CEC value is similar for both tuffs. However, the chemical nature of the exchangeable cations differs: VBCLI contains higher amounts of Na and K whereas the SCLI contains Ca, and Mg in higher concentrations. This shows that different origins of tuffs influence the chemical composition of the zeolite phase.

Table 8. Cation exchange capacity (CEC) of the used zeolitic tuffs.

Zeolitic tuff	Na^+	K^+	Ca^{2+}	Mg^{2+}	Σ
	Concentration (mmol M^+/100g)				
VBCLI	18.1	16.0	89.6	27.2	150.9
SCLI	5.2	13.3	117.6	32.8	168.9

Thermal behavior of the zeolitic tuffs was studied by TG/DTG. Figure 24 shows that the total weight loss in the temperature range up to 800 °C was 8.0 wt.% for VBCLI and

11.2 wt.% for SCLI. The loss corresponds to dehydration process which occurs discontinuously suggesting that water molecules leave the zeolite lattice from different crystallographic sites.

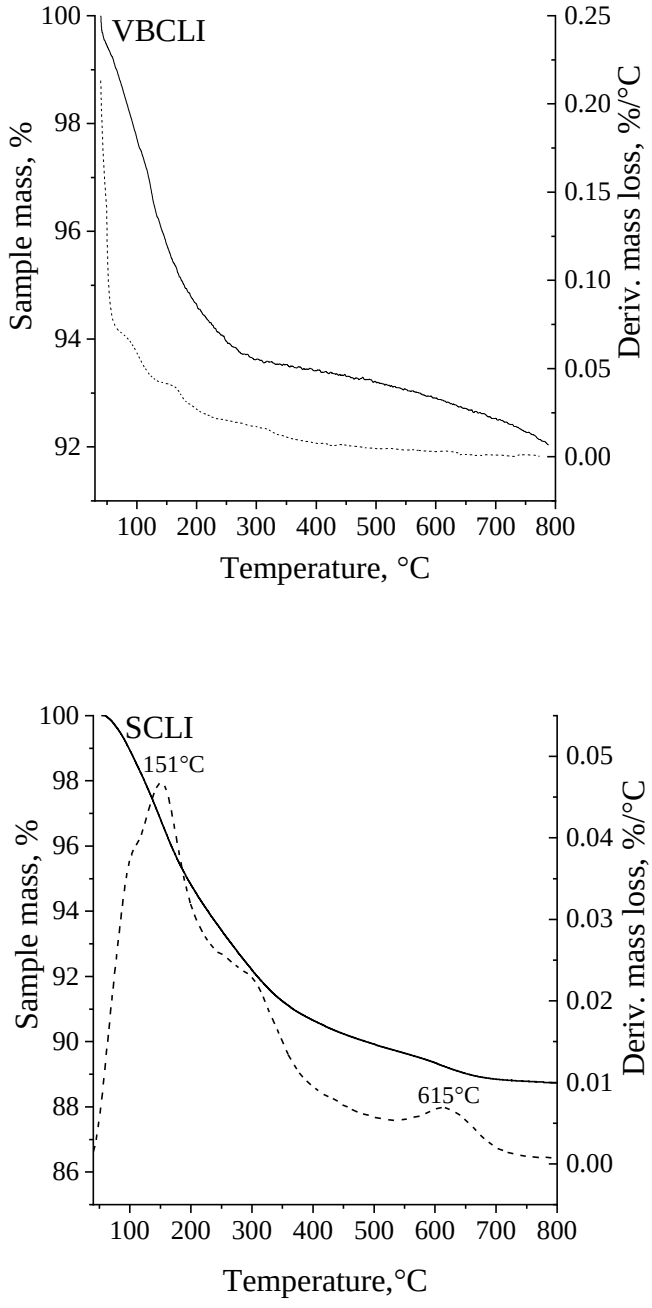

Figure 24. TG– (solid line) and DTG– (dashed line) curves of the used zeolitic tuffs.

Modified clinoptilolite samples

PXRD patterns of the CLI samples enriched with Mn, Fe, Mg or Sn are presented in Figure 25. The results showed that the crystallinity of the CLI lattice remained preserved during the modification of CLI to MCLI. A new diffraction peak appeared in the patterns of FeCLI and MnCLI indicating formation of novel crystalline phases after the modification. In the PXRD pattern of MnCLI, a new diffraction is observed at 2θ=32.9° which is associated to the Mn_2O_3 crystal phase (Ahmadi *et al*., 2017). Diffraction peak at 2θ=35.7° in the PXRD pattern of FeCLI indicates the presence of Fe_2O_3 onto CLI (Zieliński *et al*., 2010; Lassoued *et al*., 2017; Arabpour and Nezamzadeh-Ejhieh, 2015; Nairat *et al*., 2015). In the PXRD patterns of MgCLI and SnHCLI only diffractions corresponded to clinoptilolite are evident.

However, PXRD patterns of the SnHCLI as well as SO_4-SnHCLI (SSnHCLI) obtained by mechanochemical method showed a significantly loss in the CLI crystallinity Therefore, these samples were not used in further experimental work.

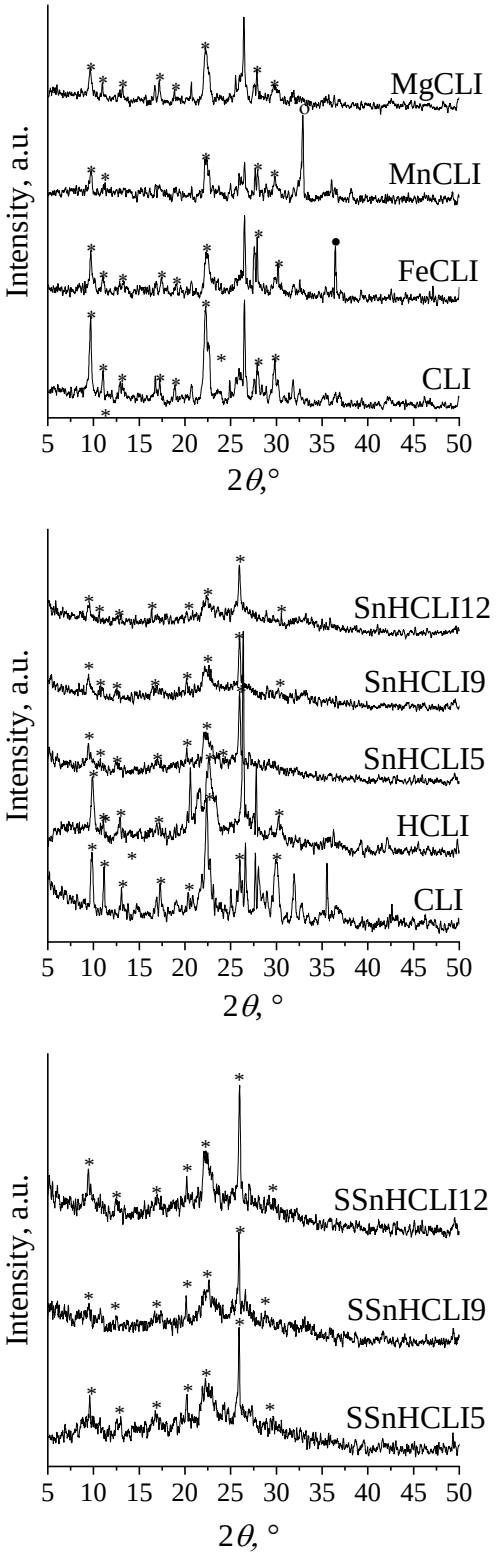

Figure 25. PXRD patterns of the CLI-modified samples obtained by wet impregnation. Diffractions of CLI are marked by asterix (*).

The surface morphology of MCLI samples was studied by SEM analysis. The analyses showed that the formation of oxide species such as Fe_2O_3, Mn_2O_3, MgO and SnO_2 have not changed the morphology of the clinoptilolite phase. Representative SEM images of SnHCLI sample are given in Figure 26.

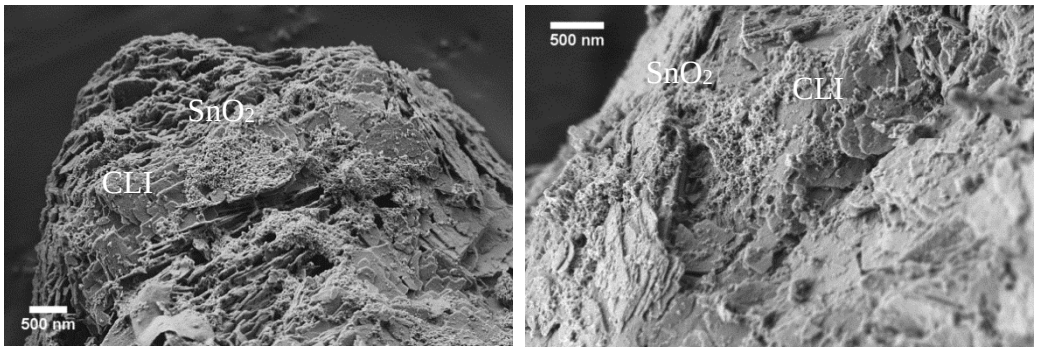

Figure 26. Representative SEM images of the SnHCLI sample.

Average chemical compositions of the CLI phase in all modified samples obtained by EDS are summarized in Table 9. The results clearly showed that the modification of CLI to MgCLI, MnCLI and FeCLI did not proceed only *via* an ion-exchange process. Namely, the content of exchangeable cations in CLI remained almost constant although the increase in the Mg, Mn and Fe content was evident. Since the modification occurred in an alkaline medium, it seems likely that some metal complex hydroxo species were adsorbed at the CLI surface and during the calcination converted to the oxides. These results are consistent with the literature results showing a modification of CLI with different metal oxide species (Jiménez-Cedillo *et al.,* 2011; Kragović *et al.,* 2013). In addition, the Si/Al molar ratio of these samples was not noticeably changed confirming also that the CLI lattice was not influenced by the modification.

In contrast, the conversion of CLI to HCLI causes a partial dealumination of the CLI lattice which is confirmed by an increase of the Si/Al molar ratio. Also, the content of Na decreased significantly and K, Ca and Mg were not detected after the formation of HCLI. As can be seen from Table 9, the conversion of HCLI to SnHCLI resulted in the enrichment of HCLI with Sn in different amounts. These samples were sulfated in further procedure which causes a partial leaching of Sn. The leaching extent varies from 43% (SnHCLI5), 13% (SnHCLI9) to 25% (SnHCLI12).

The molar ratio of S/Sn in SSnCLI samples showed that partial sulfation of SnHCLI was achieved and the S/Sn molar ratio decreases with the increase of Sn content (SnHCLI5=0.8<SnHCLI9=0.4<SnHCLI12=0.2). A similar phenomenon was reported for the sulfated ZrO_2-containing KIL–2 material (Popova *et al.*, 2016). The lowest S/Zr molar ratio was found for the highest amount of the loaded Zr. The lowest sulfation extent in the SnHCLI samples with the highest Sn content could be explained by different accessibility of Sn within the CLI lattice. It seems likely that all Sn crystallographical sites are not available for the sulfation.

Table 9. Average chemical compositions of CLI phase obtained by EDS for the MCLI samples.

Sample	Si	Al	O	Na	K	Ca	Mg	Fe	Mn	Sn	S	Si/Al
	at.%											
HCLI	37.8	5.4	56.8	0.04	–	–	–	–	–	–	–	7.0
MnCLI	24.4	4.7	66.6	0.4	0.5	1.1	0.4	–	1.9	–	–	5.2
MgCLI	23.6	4.7	64.2	0.5	0.8	1.2	4.7	0.3	–	–	–	5.0
FeCLI	22.4	4.4	63.2	0.8	0.8	1.1	0.6	6.7	–	–	–	5.1
SnHCLI5	31.5	4.4	63.3	0.1	–	–	–	–	–	0.7	–	7.2
SSnHCLI5	23.5	3.2	72.5	0.1	–	–	–	–	–	0.4	0.3	7.3
SnHCLI9	21.9	2.8	73.7	–	–	–	–	–	–	1.6	–	7.8
SSnHCLI9	20.2	2.8	75.1	–	–	–	–	–	–	1.4	0.5	7.2
SnHCLI12	20.4	2.7	74.4	0.1	–	–	–	–	–	2.4	–	7.6
SSnHCLI12	18.9	2.5	76.1	–	–	–	–	–	–	1.8	0.7	7.6

Thermal analysis of CLI-modified samples was performed before the calcination step in order to examine the formation of oxide phase during heating. The obtained results are presented in Figure 27. It is evident that TG/DTG curves of the modified samples displayed novel maxima and the corresponding weight losses differed from those present in the thermogram of the parent CLI sample.

The changes were most conspicuous in the thermogram of the MgCLI. The total mass loss of up to 800 °C was 21 %. DTG curve displayed three strong maxima centered at about 172, 238 and 441 °C. The first DTG maximum could be assigned to the loss of

physically adsorbed water (7.2 %) whereas the second one to loss of the coordinated water molecules strongly bound to CLI lattice (4.1.%). The last DTG maximum could be attributed to the transformation of the hydrous magnesium species to magnesium oxide. Crystallization of different oxide species in the CLI matrix at this temperature range has already been reported (Rajić *et al*., 2013).

For the MnCLI and FeCLI, the total mass loss up to 800 °C was 17 and 12 %, respectively. For both samples, differences were more pronounced below 300 °C. DTG curve of MnCLI displays maxima at about 137 (loss of about 4.8 %) and 211 °C (loss of about 2.2 %) whereas DTG curve of FeCLI exhibits maxima at about 79 (loss of about 4.3 %) and 140 °C (loss of about 6.0 %). The maxima displayed below 140 °C could be assigned to the release of water molecules whereas further mass loss and corresponding DTG maxima could be attributed to the dehydration of hydroxo species and formation of the corresponding oxides onto CLI.

From Figure 27, it is also evident that the total mass loss of SnCLI samples increases with the Sn content onto CLI from 12.3 (SnHCLI5) to 13.8 % (SnHCLI12). DTG curves of each SnHCLI sample display maximum centered at about 60 °C which corresponded to the mass loss from 6.5 (SnHCLI5) to 7.3 % (SnHCLI12). This can be assigned to the loss of physically adsorbed water. In the temperature range 200–400 °C weight loss was from 3.6 (SnHCLI5) to 4.3 % (SnHCLI12) and can be attributed to the dihydroxylation of the SnHCLI samples. The last event with DTG maxima at about 500 °C (loss of about 2.2 %) can be ascribed by the formation of the Sn oxide species in the CLI matrix.

The total mass loss of the SnHCLI samples after sulfation (Figure 27) also increases with the Sn content onto CLI showing the loss from 11.0 (SSnHCLI5) to 12.3 % (SSnHCLI12). The first DTG maximum (at about 60 °C) corresponded to mass loss from 5.3 (SSnHCLI5) to 5.7 % (SSnHCLI12). In addition, DTG curves displayed two resolved maxima in temperature range 200–400 °C with mass loss from 2.9 (SSnHCLI5) to 3.7 % (SSnHCLI12). This can be ascribed to the presence of coordinated water molecules strongly bound to sulfate groups. DTG maxima in the 400–600 °C temperature range can be ascribed to the decomposition of sulfate to SOx species. The corresponding mass loss increased with the increase of the Sn content being 2.9 % for SSnHCLI5 and 3.5 % for SSnHCLI12. Similar observations have been reported suggesting the decomposition of a more weakly bound sulfate species at lower

temperature and more strongly bound sulfate at the higher temperature (Gutiérez-Báez *et al*., 2004; Noda *et al*., 2005; Shi and Li, 2013; Popova *et al*., 2018).

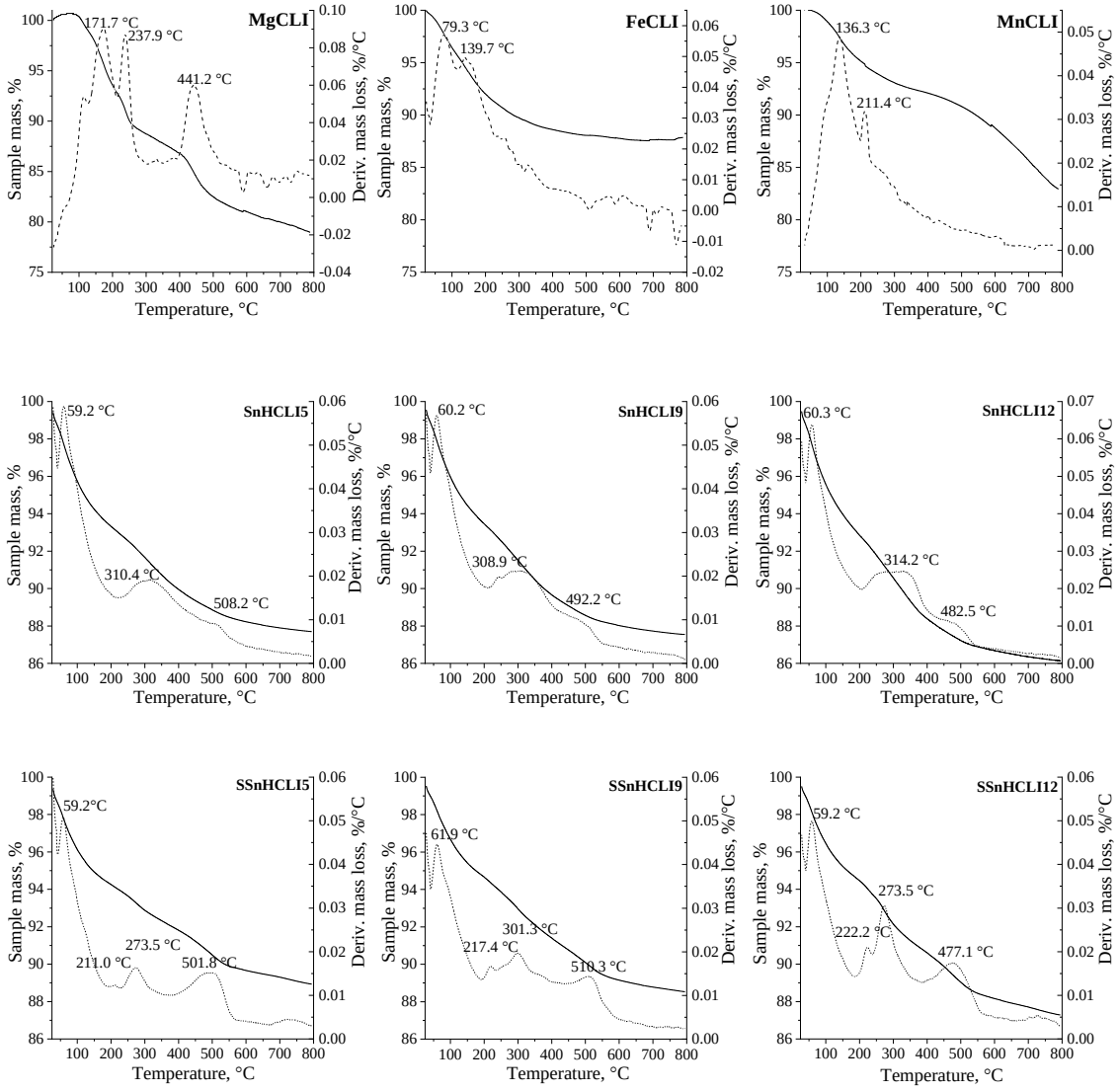

Figure 27. TG– (solid line) and DTG– (dashed line) curves of the CLI-modified samples.

Textural properties were studied by the N_2 adsorption/desorption isotherms and the relating results are given in Table 10. The specific surface area (S_{BET}) of parent CLI is 24 $m^2 g^{-1}$ which is in agreement with the literature data (Garcia-Basabe *et al*., 2010). As can be seen, the modification affects the porous structure of CLI.

The decrease in the S_{BET} value was most pronounced for MnCLI, for which specific surface area decreased to 17.5 $m^2 g^{-1}$. The effect has been reported for MnCLI and was explained by the formation of MnO_2 (Camacho *et al.*, 2011). Decrease of S_{BET} was found also for MgCLI (24.4 $m^2 g^{-1}$) and FeCLI (28.1 $m^2 g^{-1}$). This could be attributed to the formation of oxide particles at the surface of the CLI. It seems likely that oxide species partially blocked the CLI pore system and accordingly decrease specific surface area. A similar phenomenon was reported for Zn-, Cu- and Fe-containing CLI (Ates *et al.*, 2011; Nezamzadeh-Ejhieh and Khodabakhshi-Chermahini, 2014; Amiri and Nazamzadeh-Ejhieh, 2015).

For HCLI specific surface area slightly increased. The increase can be explained by a partial dealumination of the aluminosilicate lattice resulting in the opening of the pores and thereby in an increase of S_{BET}. In addition, almost complete replacement of the metal cations by H^+ also contributes to the more available space within the CLI (Farías *et al.*, 2009; Garcia-Basabe *et al.*, 2010).

SnHCLI obtained by conversion of HCLI showed an increasing trend of S_{BET}: increase of S_{BET} increases with the Sn content. This could be explained by modification procedure which caused additional dealumination at higher Sn content.

Conversion of SnHCLI to SSnHCLI led to a small decrease of S_{BET}. This can be due to a partial pore blockage of pore system caused by sulfate groups. The decrease varies with Sn content from 3% for SSnHCLI5 to about 20% for SSnHCLI9.

Based on the IUPAC classification, all clinoptilolite samples exhibit the adsorption isotherm of type IV (Figure 28) that are typical for zeolitic materials containing both micropores due to structural features of the framework, and mesopores introduced by modification (Sing *et al.*, 1985). In addition, the isotherms exhibit a hysteresis loop of type H3 (in the range p/p_0=0.5–1) that is characteristic for the clinoptilolite structure and could arise from multilayer adsorption and capillary condensation either in mesopores of impurities (feldspars, quartz) or in the space between the zeolite crystallites.

Table 10. Textural properties of the CLI and CLI-modified samples.

Sample	S_{BET}[a], $m^2\ g^{-1}$	S_{ext}[b], $m^2\ g^{-1}$	V_{mic}[c], $cm^3\ g^{-1}$	V_t[d], $m^3\ g^{-1}$	d[e], nmÅ
CLI	30.9	28.9	0.0008	0.0988	15.0
MgCLI	24.4	20.9	0.0293	0.0700	13.7
MnCLI	17.5	16.7	0.0883	0.0891	18.7
FeCLI	28.1	29.3	0.1409	0.1424	16.8
HCLI	31.6	24.5	0.0023	0.1204	29.6
SnHCLI5	39.7	27.3	0.0048	0.1307	17.0
SSnHCLI5	38.4	30.0	0.0044	0.0738	22.4
SnHCLI9	41.6	24.3	0.0073	0.0760	23.0
SSnHCLI9	33.2	17.7	0.0095	0.1208	31.5
SnHCLI12	79.8	64.9	0.0069	0.0929	15.0
SSnHCLI12	67.9	52.3	0.0086	0.0880	14.6

[a]Specific surface area based on BET theory determined in the p/p_0 range corresponding to the increasing trend of Rouquerol plot; [b]external surface area $S_{BET} - S_{mic}$; [c]micropore volume based on *t*-plot analysis; [d]total pore volume based on BJH adsorption analysis; [e]average pore size based on BJH desorption analysis.

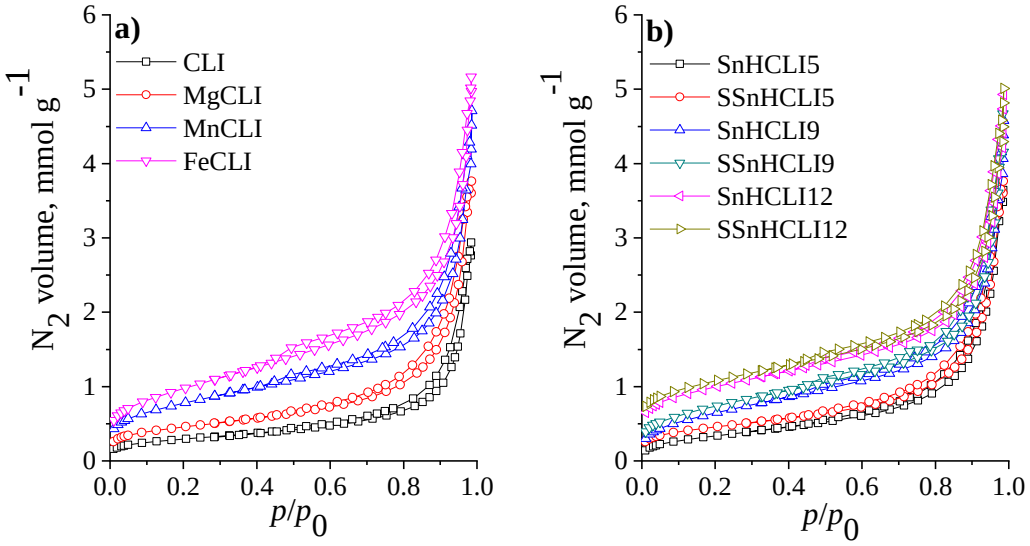

Figure 28. Adsorption/desorption isotherms of nitrogen at –196 °C of CLI and CLI-modified samples.

SnHCLI and SSnHCLI samples were further characterized by XPS method in order to obtain a deeper insight into the concentration profile of Sn inside the samples. Figure 29 shows XPS survey spectra for the HCLI, SSnHCLI5 and SSnHCLI9 samples. The peaks corresponding to the CLI framework elements (O, Si and Al) are present in all spectra. Also, C 1s peak is visible in the spectra resulting from the contamination layer due to sample handling in air. The peak at 284 eV demonstrates that the C 1s peak does

not belong from carbonate which shows peaks in the range from 290 to 291 eV (Cerjan Stefanovic *et al.,* 2007; Rajic *et al*., 2009). This is also confirmed from the XPS depth profile of the C (Figure 30). Namely, a drastic decrease of the C 1s signal after the 2 min of the sputtering time is additional evidence that the C originates from the contamination layer rather than from carbonate species often contained in the zeolitic tuff.

The spectra of Sn-containng CLI samples exhibit new peaks originating from the Sn. Figure 31 shows the spectra of SSnHCLI5 and SSnHCLI9 as well as the Sn depth profile. Two peaks located at 487.4 and 495.8 eV for SSnHCLI5, and 487.5 and 496.0 eV for SSnHCLI9 are evident and can be assigned to Sn $3d_{5/2}$ and Sn $3d_{3/2}$, respectively. The peaks are in accordance with the literature data (Mallesham *et al.,* 2013; Rajalakshmi *et al*., 2015) which suggested the presence of the SnO_2 species in the zeolite matrix.

Moreover, the Sn XPS depth profile of SSnHCLI5 shows a small accumulation of Sn at the surface and decrease of the Sn concentration from top to bottom. More pronounced Sn accumulation is evident in the sample with a higher Sn content (SSnHCLI9). However, the spectrum also indicates the presence of Sn inside the lattice which was unexpected since this shows that the Sn species are not present only onto the surface of the CLI but also inside its lattice. A similar phenomenon was reported for the Sn(IV)-containing zeolite β (Dijkmans *et al*., 2015; Guan *et al.,* 2018). It was concluded that the two-step modification which includes: 1) dealumination and 2) impregnation with $SnCl_4$ resulted in the creation of holes inside the zeolite lattice. The Sn(IV) species are located in holes forming covalent Si–O–Sn bonds with the zeolite lattice.

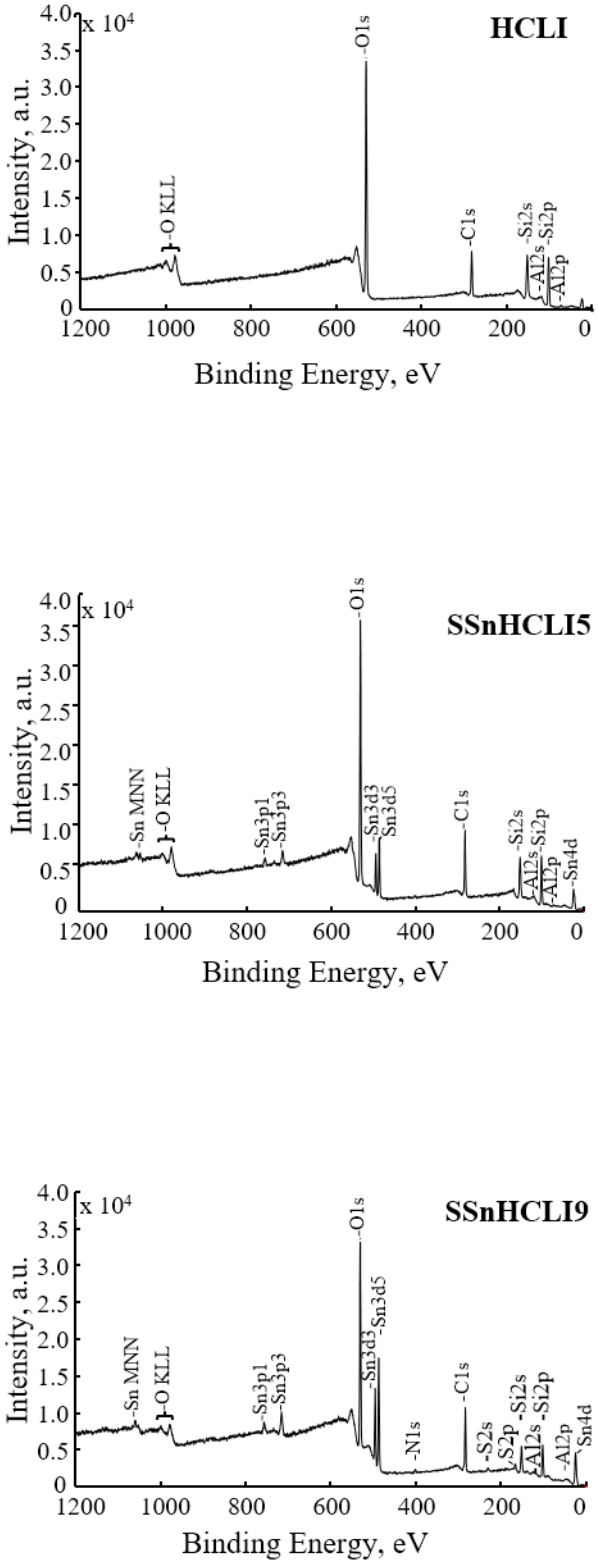

Figure 29. XPS survey spectra from the surface of HCLI, SSnHCLI5 and SSnHCLI9.

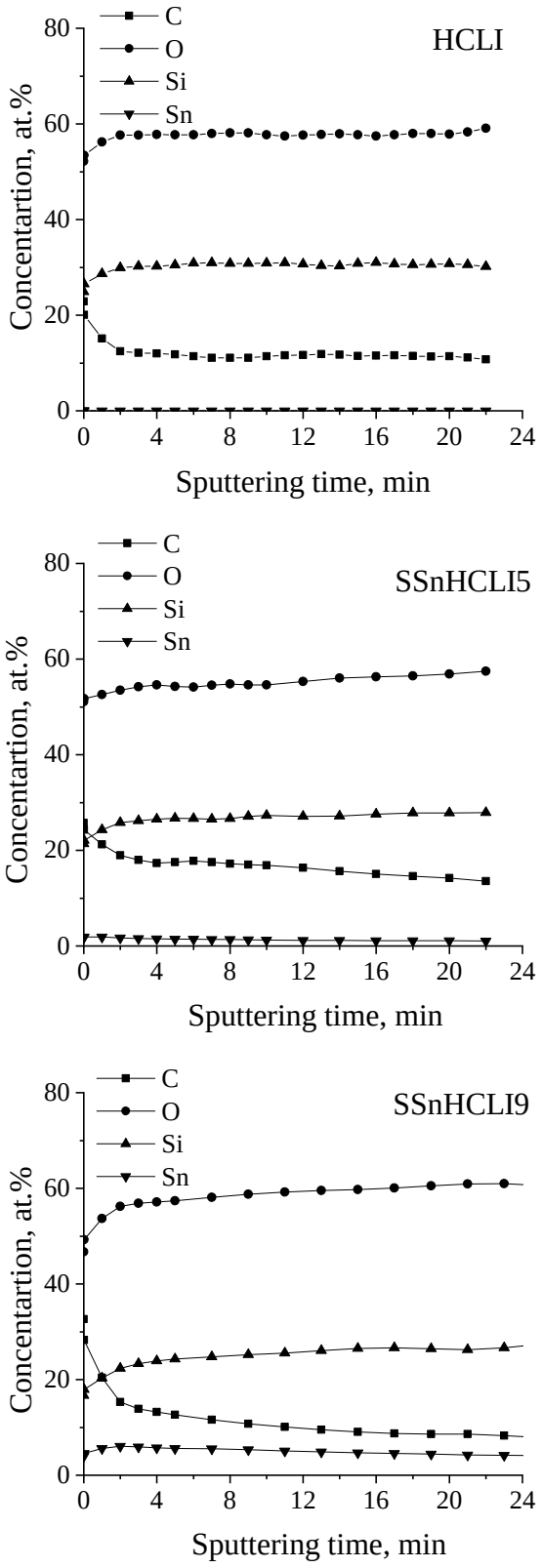

Figure 30. XPS depth concentration profiles of Sn, Si, O and C inside the HCLI, SSnHCLI5 and SSnHCLI9.

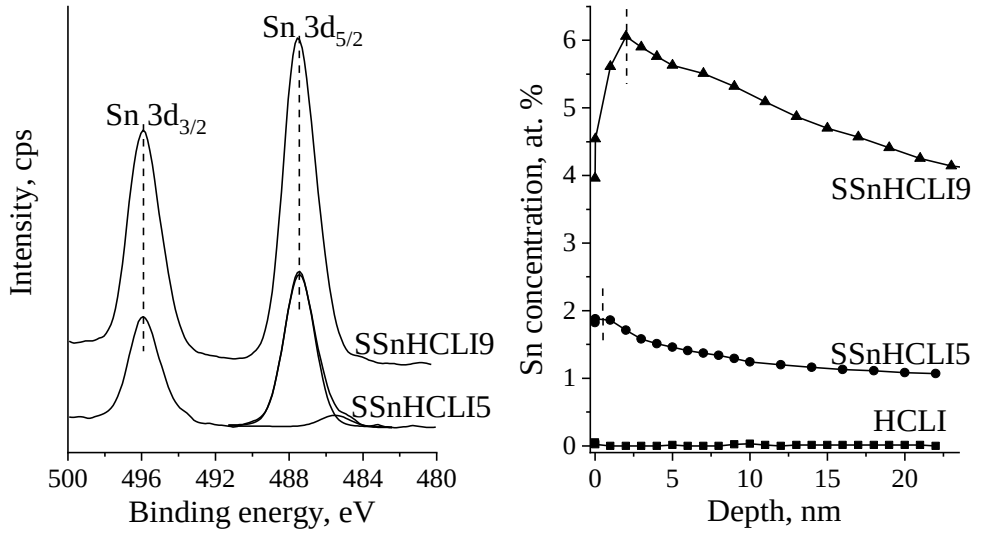

Figure 31. XPS spectra of Sn (left) and Sn XPS depth profile (right).

The presence of SnO_2 onto HCLI surface was examined by DRS spectroscopy in near UV region. Namely, in this region pure SnO_2 displays a strong peak centered at about 263 nm (Figure 32).

This peak is found in all Sn-containing CLI samples. Also, an increase in the absorption intensities with the increase of Sn content is evident. This strongly supports the fact that SnO_2 is present in all Sn-containing samples.

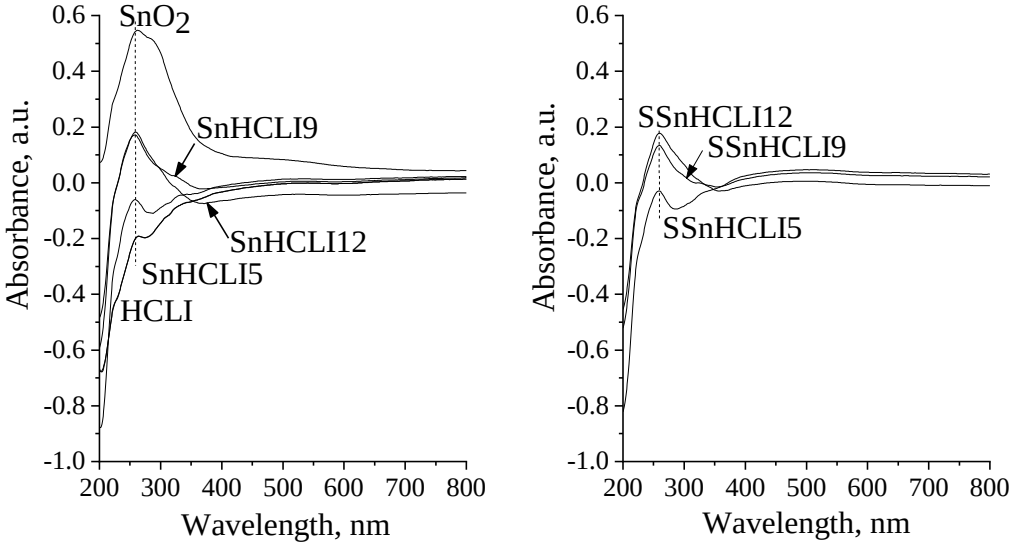

Figure 32. Diffuse reflectance spectra of SnO_2 and SnO_2-containing samples.

The fact that Sn-containing samples contain oxide species not only at the surface of the clinoptilolite lattice but also into lattice itself, as well as the fact that the textural properties were changed after modification of CLI to SnHCLI, required a deeper insight into the structural changes. This was studied by solid state NMR analysis.

^{27}Al MAS NMR spectra of the representative samples (HCLI, SnHCLI9 and SSnHCLI9) given in Figure 33a show three broad peaks at around 55, 30 and 0 ppm. The peak at 55 ppm is characteristic for tetrahedrally coordinated Al atoms belonging to structural AlO_4. The other two peaks do not appear in the ^{27}Al MAS NMR spectrum of clinoptilolite (Farías *et al.,* 2009; Garcia-Basabe *et al.,* 2010).

The peak at 0 ppm is explained by the presence of octahedrally coordinated extra-framework Al species (AlO_6 structural units). Their formation occurred during the conversion of CLI to HCLI which caused a partial dealumination of the aluminosilicate lattice (Lippmaa *et al.,* 1986; Farías *et al.,* 2009; Garcia-Basabe *et al.,* 2010). The second peak at around 30 ppm was ascribed to the extra-framework five-coordinated Al also formed by the dealumination.

Spectrum of SnHCLI9 displayed an additional peak appears at around 15 ppm. This peak was ascribed to the hexa-coordinated aluminum species surrounded by SiO species (Lippmaa *et al.,* 1986; Zhang *et al.,* 2010). All this suggests that the conversion of CLI to HCLI led to the formation of extra-framework Al–O–Si species in the SnHCLI9. These species contribute to Lewis acidity of the sample.

The ^{29}Si MAS NMR spectra are for all samples are very similar (Figure 33b) showing the presence of Si atoms with different environments. Deconvolution of the ^{29}Si NMR spectrum displayed three resonances at about –110, –101 and –92 ppm. The resonances at –101 ppm and –92 ppm are notably enhanced compared to the signal at –110 ppm, indicating that the former peaks can be assigned to the Si atoms that have H atoms in vicinity (Q^3 and Q^2 sites, $(OSi)_3Si(OH)$ and $(OSi)_2Si(OH)_2$, respectively), whereas the latter peak belongs to Q^4 $[Si(OSi)_4]$**.**

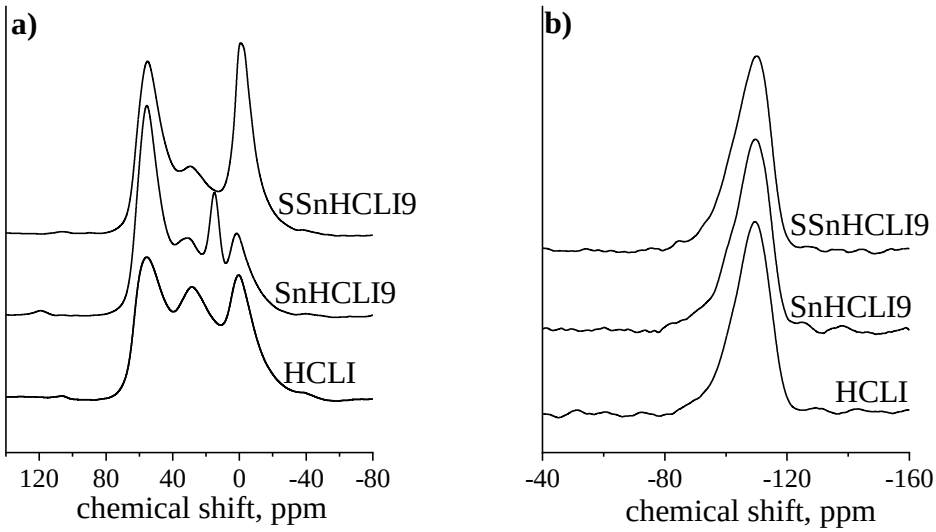

Figure 33. a) ^{27}Al and b) ^{28}Si MAS NMR spectra of the catalysts**.**

Interaction of nitrate and phosphate ions with MCLI samples (M=Mn, Fe, Mg) was studied by FTIR analysis. The FTIR spectra are given in Figure 34. All FTIR spectra exhibit vibrations characteristic for a zeolite lattice.

The strong vibration band around 1069 cm^{-1} corresponds to asymmetric stretching of T–O (T= Si or Al) of the tetrahedra building blocks (Breck, 1974). A vibration band at around 467 cm^{-1} arises from the T–O bending vibrations while the vibration band around 607 cm^{-1} belongs to the stretching bonds between tetrahedral units. A broad vibration band in the region between 3500 and 3700 cm^{-1} originates from the stretching vibrations of the hydroxyl groups (Mozgawa *et al.* 2011) whereas the band at 1634 cm^{-1} is due to the presence of water molecules. A vibration band observed around 1380 cm^{-1} appearing only in the spectra of the nitrate-containing MCLI corresponds to asymmetric stretching vibrations of nitrate ions (Islam and Patel, 2009). This band is confirmation that oxide particles (MgO, Fe_2O_3 and Mn_3O_4) onto surface of CLI make CLI available to negatively charged nitrate ions. Vibration band around 1054 cm^{-1} corresponding to asymmetric stretching of P–O of phosphate groups is not shown in the FTIR spectrum of phosphate-containing samples, probably due to overlapping of this band with the strong band of zeolite lattice (Shi *et al.*, 2019). There is only weak band around 539 cm^{-1} which corresponds to bending vibration of O–P–O.

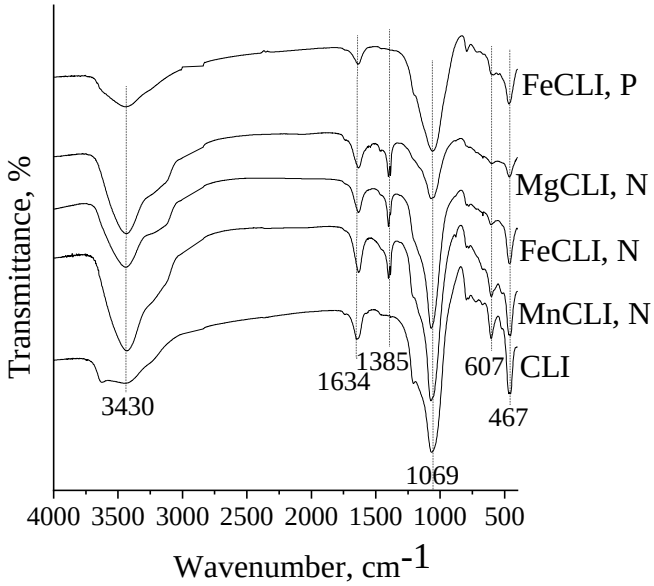

Figure 34. FTIR spectra of the CLI and MCLI samples after nitrate (referred as N) and phosphate (referred as P) loading.

Acidity of HCLI and Sn-containing samples were also studied by FTIR analysis. The spectra were recorded after pyridine (Py) adsorption which was used as a probe molecule.

The spectra are shown in Figure 35. The vibrations at 1615 and 1452 cm^{-1} are due to the ring vibrations of coordinatively bound Py and can be ascribed to the Lewis acid sites (LPy). The vibrations at 1638 and 1550 cm^{-1} arise from the protonated Py formed from an interaction of Py with protons belonging to hydroxyl groups (Brönsted acid sites, BPy) (Karge *et al.*, 2003).

FTIR spectra of both nonsulfated and sulfated samples displayed bands showing the presence of both Lewis and Brönsted acid sites.

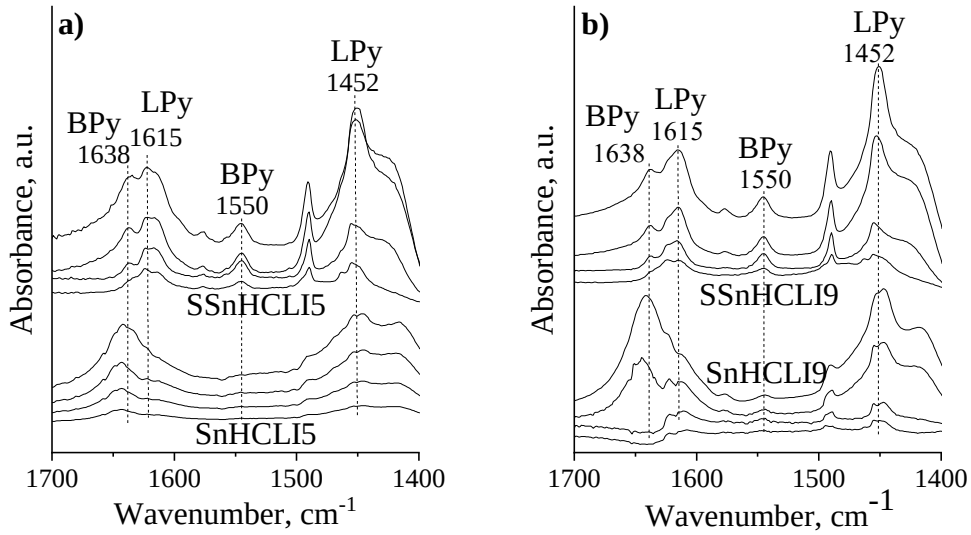

Figure 35. FTIR spectra of adsorbed pyridine (Py) for: a) SnHCLI5/SSnHCLI5 and b) SnHCLI9/SSnHCLI9. Spectra were collected after Py desorption at temperature of 100, 200, 300 and 400 °C (shown from top to bottom for each sample). Lewis- and Brönsted acid sites are marked by LPy and BPy, respectively.

Concentration of the Lewis and Brönsted acid sites was calculated by integration of absorption band at 1550 and 1452 cm^{-1} using molar extinction coefficients of 1.67 and 2.22 cm μmol^{-1}, respectively (Emeis *et al.*, 1993). The obtained results are summarized in Table 11. It is evident that the amount of Lewis acid sites of SnHCLI is higher than the amount of Brönsted acid sites. This can be explained by the presence of the coordinatively unsaturated Sn ions in the CLI lattice (Platero *et al.*, 1996; Popova *et al.*, 2016). It has been also reported that incorporation of metal ions such as Sn^{4+}, Zr^{4+} or Ti^{4+} into the zeolite lattice can create Lewis acid sites (Guan *et al.*, 2018). For instance, the presence of two types of Lewis acid sites are found in Sn-containing zeolite *β*: the first one corresponds to the Sn atoms completely coordinated by lattice oxygen, Sn(–Si–O–)$_4$, whereas the second one belongs to partially hydrolyzed framework Sn atoms, (–Si–O–)$_3$Sn–OH (Boronat *et al.*, 2005). Moreover, the results from Table 11 show that a higher amount of Sn in HCLI led to an increase in the amount of Lewis acid sites, whereas Brönsted acid sites remain unaffected.

For SSnHCLI the amounts of acid sites are significantly higher than for SnHCLI. These suggest that sulfate species act as Lewis acid sites and also increase Brönsted acidity. A

similar effect has been reported for sulfated ZrO_2/KIL-2 and sulfated nano-SnO_2 (Popova *et al.*, 2016; Popova *et al*., 2018). According to the model proposed by Khder and coworkers (Khder *et al*., 2008), the presence of sulfate groups at the surface of the solid may lead to the generation of strong Lewis acidity. The sulfate groups act as electron withdrawing species, causing an inductive effect which contributes to the Lewis acid strength. In addition, presence of water leads to convertion of the Lewis acid sites to Brönsted acid sites *via* proton transfer.

Table 11. Acidity of the samples calculated from the FTIR spectra.

Sample	Brönsted sites, μmol g^{-1}	Lewis acid sites, μmol g^{-1}
SnHCLI5	0	55.5
SSnHCLI5	117.4	240.0
SnHCLI9	3.8	164.5
SSnHCLI9	143.7	236.4

4.2 Modified clinoptilolite as a soil supplement

Since the clinoptilolite has been found as a good carrier for nitrate and phosphate ions and the clinoptilolite lattice contains movable cations which are plant nutrients, one of the aims of this doctoral thesis was the develop a novel, environmentally friendly and cost-effective soil supplement using clinoptilolite. To achieve these, batch and column experiments were carried out. In batch experiments, nitrate and phosphate adsorption onto clinoptilolite were studied whereas leaching experiments were performed only using column system in order to make the leaching conditions similar to environmental ones.

4.2.1 Batch experiments

4.2.1.1 Nitrate adsorption

Effect of zeolite amount on the nitrate adsorption capacity

The effect was studied by varying the amount of FeCLI, MgCLI and MnCLI from 0.5 to 2.0 g using the initial nitrate concentration of 100 mg dm^{-3}. As shown in Figure 36, the increase of the zeolite amount led to an increase of nitrate adsorption efficiency. For all samples, the nitrate adsorption initially increases sharply with increasing adsorbent

mass up to 1.0 g. Then, a negligible increase of adsorbed nitrate occurred with higher amount of zeolite. Thus, double increase of zeolite mass leads to only 10% increase of the nitrate adsorption. The decrease of adsorption efficiency has been explained by the two phenomena: 1) decrease in the adsorption per unit mass of adsorbent due to the unsaturation of the adsorption sites and 2) reduction of the effective surface area due to particle aggregation (Islam and Patel; 2009). Taking this into account a ratio of 1.0 g of zeolite and 50 cm^3 of liquid phase (nitrate solution) was chosen as the optimal solid/liquid ratio in further experiments.

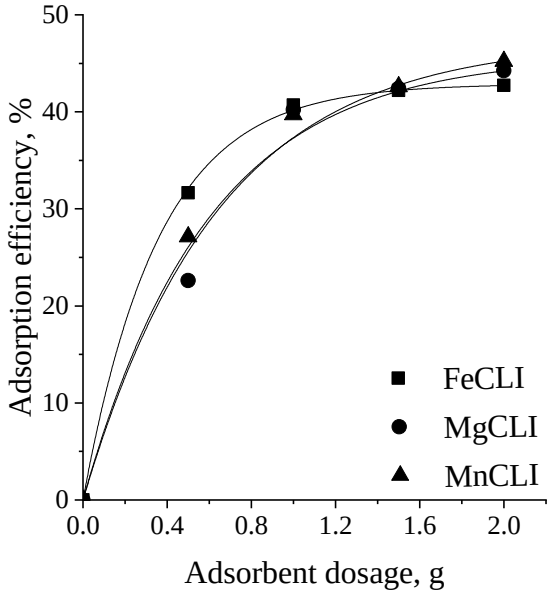

Figure 36. Effect of the zeolite amount on the nitrate adsorption onto MCLI samples.

Effect of temperature

The effect of temperature was studied at 25, 35 and 45 °C. The results are shown in Figure 37. The results showed that temperature increasing enhances the adsorption efficiency for all studied MCLI indicating that the adsorption process was endothermic. This increase could be explained by better diffusion of nitrate inside CLI lattice and accordingly, by better accessing of adsorption sites. Since the adsorbed amount of nitrate at zeolite surface (q_t) was highest at the highest temperature, effect of initial concentration on nitrate adsorption was investigated at 45 °C.

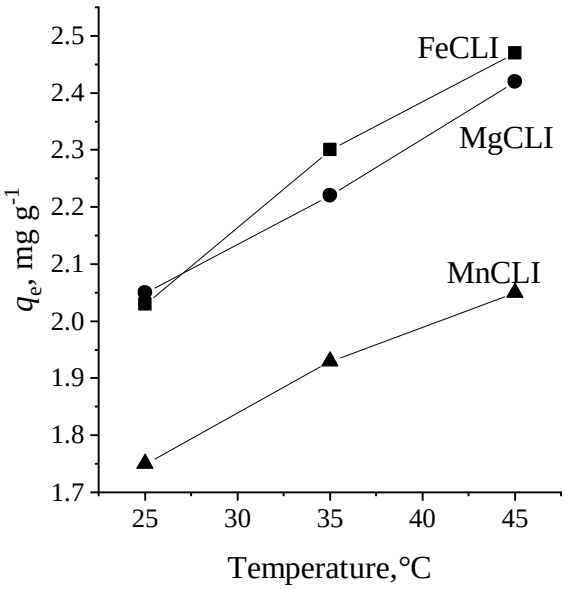

Figure 37. Effect of the temperature on the nitrate adsorption onto MCLI samples (initial NO_3^- concentration is 100 mg dm^{-3}).

Effect of the initial concentration on nitrate adsorption

The effect of initial nitrate concentration was studied for the concentration range 50–300 mg dm^{-3}. Figure 38 shows change of the amount of adsorbed nitrate on MCLI (q_t) at 45 °C. The increase of q_t with initial nitrate concentration is evident for all MCLI. Moreover, the results indicate that the adsorption did not reach saturation in the studied concentration range for 24 h. The most pronounced adsorption effect is observed for the FeCLI showing that the q_t on FeCLI increased from 1.5 (C_0= 50 mg dm^{-3}) to 5.6 mg g^{-1} (C_0= 300 mg dm^{-3}). The presented results indicate that the adsorption is influenced by the oxides present on the CLI surface suggesting that FeCLI is the most perspective adsorbent for the nitrate adsorption.

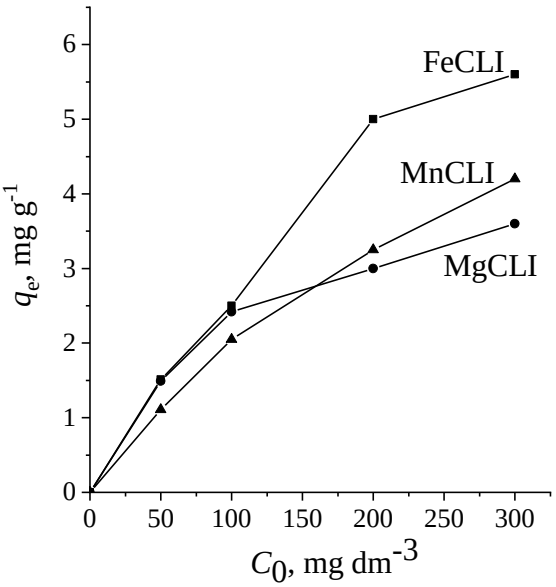

Figure 38. Effect of the initial NO_3^- concentration on the adsorption efficiency of MCLI samples.

Adsorption kinetics

In order to study mechanism of the adsorption process, adsorption kinetic experiments were carried out. The experiments were performed at 45 °C using the initial nitrate concentration of 300 mg dm^{-3}. The obtained results are shown in Figure 39. It can be seen that the q_t onto MCLI increased with the contact time. The adsorption is initially relatively fast which can be attributed to larger number of available active sites at the surface of MCLI at the beginning. After about 400 min, the adsorption slowed down due to the saturation of MCLI.

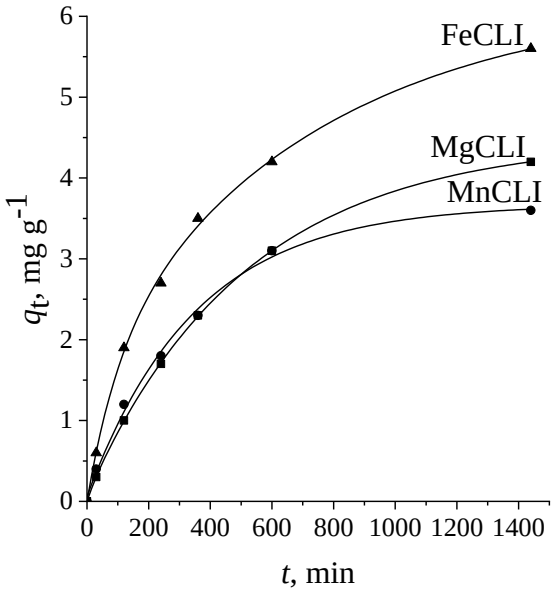

Figure 39. Nitrate adsorption kinetics onto MCLI samples.

Furthermore, the kinetic results were analyzed by three kinetic models (Lagergren pseudo-first-order, Lagergren pseudo-second-order and Intra particle diffusion model or Weber–Morris) that are the most applied models for studying the adsorption by zeolite from aqueous media. The obtained kinetic parameters for all studied MCLI samples are summarized in Table 12. The values of the correlation coefficient (R^2) indicate that the Lagergren pseudo-second-order model best describes the adsorption kinetics for all studied MCLI samples (Figure 40). Also, experimental q_e values are in good agreement with the estimated data. This indicates that during nitrate removal chemisorption occurred. The most probable mechanism includes formation of "donor-acceptor" bonds between nitrate ions and metal cations onto MCLI. Similar observations have been found for the adsorption of nitrate and phosphate onto oxide-modified zeolites (Teimouri *et al*., 2016; Kaplanec *et al*., 2017). Additionally, the kinetics data were also tested by the Weber–Morris model in order to examine whether the intra-particle diffusion is involved in the adsorption process. The straight line was obtained indicating that diffusion is involved into adsorption but it is not the rate controlling step of since the lines did not pass through the origin (Weber and Morris, 1963; Aravindhan *et al*., 2009). It can be concluded that the kinetic results are in agreement with Lagergren pseudo-second-order model. This model is acceptable for a variety of adsorbents

including different type of zeolites, nano-sized alumina, activated carbon, sepiolite, chitosan hydrogel beads (Özcan *et al*., 2005; Chatterjee and Woo, 2009; Bhatnagar *et al*., 2010).

Table 12. Kinetic parameters for the nitrate adsorption onto MCLI.

Kinetic model	**Kinetic parameters**		
LPFO	q_e, mg g^{-1}	k_1, h^{-1}	R^2
FeCLI	4.99	0.1323	0.9811
MgCLI	4.19	0.1332	0.9895
MnCLI	3.68	0.1919	0.9839
LPSO	q_e, mg g^{-1}	k_2, g mg^{-1} h^{-1}	R^2
FeCLI	5.89	0.0179	0.9982
MgCLI	4.42	0.0431	0.9950
MnCLI	3.84	0.0259	0.9961
Weber-Morris	C	k_{int}, mg g^{-1} h$^{-1/2}$	R^2
FeCLI	0.2235	1.1726	0.9521
MgCLI	0.2247	0.9532	0.9713
MnCLI	0.1698	0.7778	0.9065

LPFO – Lagergren pseudo-first-order; LPSO – Lagergren pseudo-second-order; q_e – the nitrate amount adsorbed at equilibrium, k_1 – the rate constant of the first-order kinetic model; k_2 – the rate constant of the second-order kinetic model; C – the intraparticle diffusion constant that is directly proportional to the boundary layer thickness; k_{int} – the intraparticle diffusion rate constant, R^2 – correlation coefficient.

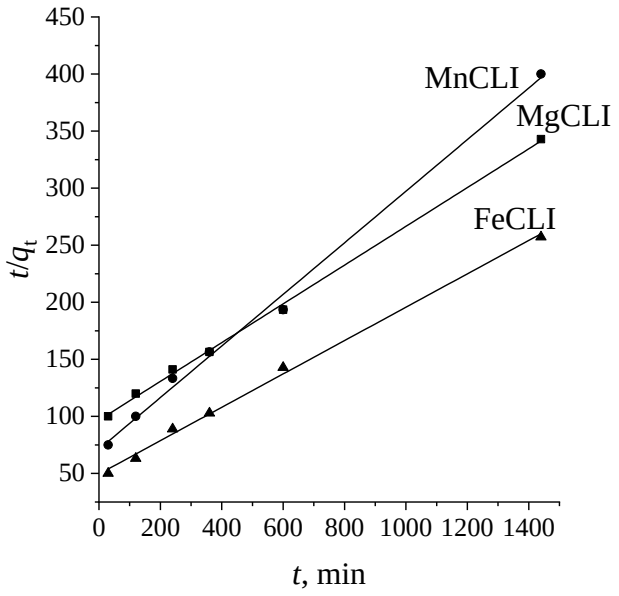

Figure 40. Pseudo-second-order kinetic model for the adsorption of nitrate onto MCLI.

Adsorption isotherms

The equilibrium adsorption data were analyzed using three common isotherms: Langmuir, Freundlich and Temkin isotherm models. The results are given in Table 13 showing that experimental results are in good agreement with the Langmuir isotherm (R^2= 0.9961).

The important features of the Langmuir isotherm can be expressed in terms of a dimensionless constant R_L (separation factor) which is used to express the favourability of the adsorption process. The calculated values of R_L at studied initial nitrate concentrations are shown in the Figure 41. These values indicate favourable adsorption process of nitrate onto MCLI. Moreover, lower values of R_L at higher initial concentrations demonstrated that nitrate adsorption is also favourable at higher concentrations. The favourability of the adsorption process can be also predicted from the Freundlich constant *n*. The obtained *n* values are greater than 1 indicating the nitrate adsorption on MCLI is a favourable process. However, correlation coefficient (R^2) values for Freundlich isotherm are slightly lower than for Langmuir. In addition, the lowest values for the correlation coefficient (R^2) were obtained for the Temkin isotherm model (Table 13).

Table 13. Isotherm parameters of the nitrate adsorption on MCLI at 45 °C.

Isotherm	**Isotherm parameters**		
Langmuir	Q_0**, mg g^{-1}**	b**, dm^3 mg^{-1}**	R^2
FeCLI	8.46	0.011	0.9654
MgCLI	4.16	0.021	0.9667
MnCLI	7.58	0.006	0.9961
Freundlich	K_f**, dm^3 g^{-1}**	n	R^2
FeCLI	0.26	1.66	0.9512
MgCLI	0.48	2.71	0.9275
MnCLI	0.11	1.48	0.9904
Temkin	A**, dm^3 mg^{-1}**	b_T**, kJ mol^{-1}**	R^2
FeCLI	0.10	1.35	0.9060
MgCLI	0.24	3.07	0.9014
MnCLI	0.06	1.69	0.9132

Q_0 – maximum amount of nitrate per unit mass of MCLI; b – Langmuir adsorption equilibrium constant related to adsorption energy; K_f, n – Freundlich constants; A – Temkin equilibrium binding constant; b_T – Temkin constant related to the heat of adsorption (kJ mol^{-1}).

Range of enthalpy change (i.e. change of heat of adsorption) can give an indication for the physical or chemical nature of the adsorption. Thus, the values of parameter b_T in the Temkin isotherm give an insight into bonding energy showing type of interaction between adsorbent and adsorbate (Kiran and Kaushik, 2008; Liu and Zhang, 2015). The obtained values of b_T for all studied adsorbents (Table 13) indicate that interactions between all MCLI and nitrate ions do not include either ion-exchange or physisorption. According to Monazam and Omotude (Monzam *et al*., 2012; Omotude *et al*., 2018) higher values of b_T indicate an ion-exchange process whereas lower ones indicate physisorption (electrostatic interactions between charged molecules). Typical range of bonding energy for ion-exchange mechanism is reported to be 8–16 kJ/mol. Values up to −20 kJ/mol indicate the physisorption whereas the values less than −40 kJ/mol are ascribed to chemisorption.

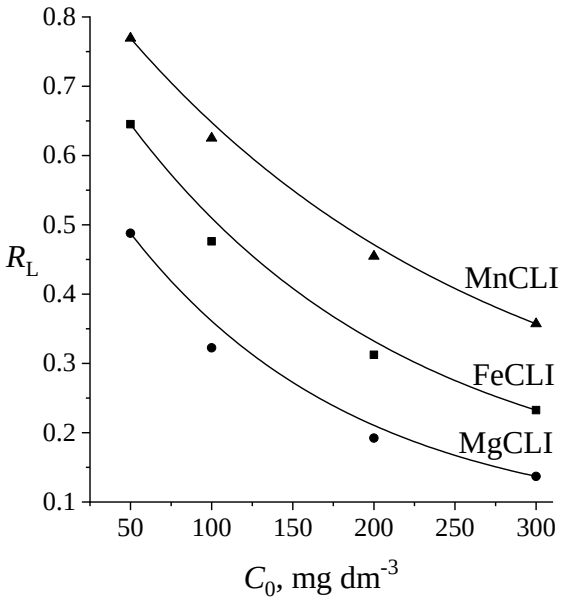

Figure 41. Separation factor (R_L) obtained from the Langmuir isotherm model as a function of initial nitrate concentrations.

It should be stressed that the obtained results are difficult to compare with literature ones due to differences in experimental conditions including different initial concentrations, pH, liquid/solid ratio, reaction temperature and contact time. Langmuir isotherm model has been applied to describe the nitrate adsorption onto various adsorbents. For instance, for initial nitrate concentration range 1–100 mg dm^{-3}, nano-alumina removed about 4.0 mg g^{-1} at 25 °C and pH=4.4 (Bhatnagar *et al*., 2010). The adsorption capacity of the composite chitosan/zeolite/ZrO_2 was reported to be 23.58 mg g^{-1} for initial nitrate concentrations from 5 to 80 mg dm^{-3} at 35 °C and at pH=3 (Teimouri *et al.*, 2016). For initial nitrate concentration of 100 mg dm^{-3} and pH=6, at 50 °C the adsorption capacity of hydroxyapatite was 21 mg g^{-1} (Islam *et al*., 2010). Moreover, Freundlich isotherm model has been also applied to describe the nitrate adsorption. Accordingly, the adsorption capacity of modified steel slag was found to be 6.2 mg g^{-1} for initial concentrations of 20–300 mg dm^{-3} at 25 °C and at pH=6 (Yang *et al*., 2017). The adsorption capacity of the modified wheat residue was 2.08 mmol g^{-1} at initial concentration range 100–800 mg dm^{-3} at 23 °C and pH=6.8 (Wang *et al*., 2007). Freundlich isotherm model has been also applied to describe the nitrate adsorption onto biochar from microwave pyrolysis of different biomass feedstocks (Chintala *et al*.,

2013). Depending of the type of feedstock the adsorption capacity was in the range from 3.5 to 15.2 mg g^{-1} at room temperature and at pH=4 (for initial nitrate concentrations up to 0.8 mmol dm^{-3}).

According to the literature data (Yang *et al*., 2017), electrostatic interactions between negatively charged nitrate anions and positively charged M–OH_2^+ groups may be responsible for nitrate adsorption onto metal-hydroxo-containing adsorbents. These M–OH_2^+ groups are formed mainly at lower pH as a result of the reaction between the H^+ from the solution and surface hydroxyl groups present on the adsorbent. Additionally, nitrate adsorption can also occur by an ion-exchange reaction between nitrate and surface hydroxyl groups present at the surface of the adsorbents.

4.2.1.2 Phosphate adsorption

Adsorption of phosphate ions from an aqueous medium was studied using FeCLI. The initial concentrations were in the range of 50–300 mg dm^{-3}. The obtained results are shown in Figure 42. It is evident that q_t increases with initial concentration reaching the amount of 24.9 mg g^{-1} for the phosphate concentration of 300 mg dm^{-3}. In addition, the adsorption at lower initial concentrations (50 and 100 mg dm^{-3}) occurred fast accomplishing the equilibrium for less than 60 min. At higher initial concentrations (200 and 300 mg dm^{-3}) the equilibrium is reached for approx. 240 min. For all initial concentrations, rapid adsorption of phosphate occurs at the initial stage suggesting the presence of a large number of available adsorption sites. Then, the adsorption is slower most probably due to steric factors – presence of the remaining adsorption sites at less available position.

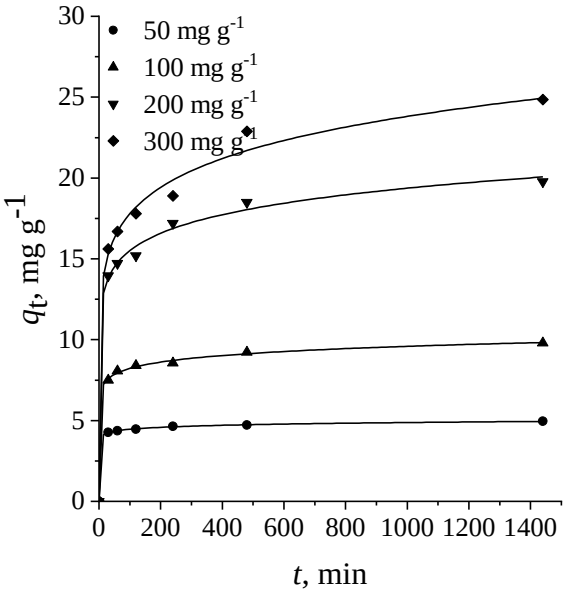

Figure 42. Adsorption kinetics for different initial phosphate concentrations.

The data shown in Figure 42 were analyzed using three kinetic models (Lagergren pseudo-first-order, Lagergren pseudo-second-order and Intra-particle diffusion model or Weber–Morris). The obtained kinetic parameters are given in Table 14. It can be seen that the experimental results agree well with the Lagergren pseudo-second-order model (Figure 43): R^2 values are very close to 1 and values of parameter q_e agree well with the experimentally obtained values. This suggests that chemisorption occurs during phosphate adsorption. Moreover, the values of rate constant k_2 decrease with the increase of initial concentration indicating that more time is required to reach equilibrium conditions at higher initial concentrations. The similar observation was found for the adsorption of phosphate on clinoptilolite treated with $Ca(OH)_2$ (Mitrogiannis *et al.*, 2017) as well as for the phosphate adsorption on different materials including oxides, chitosan, zeolites and MOFs (Liu and Zhang, 2015; Lalley *et al.*, 2016; Liu *et al.*, 2018).

Table 14. Kinetic parameters for the phosphate adsorption onto FeCLI.

Kinetic model	**Kinetic parameters**		
LPFO C_0**, mg dm^{-3}**	q_e**, mg g^{-1}**	k_1**, h^{-1}**	R^2
50	0.66	0.1492	0.9105
100	2.21	0.1658	0.9439
200	6.38	0.2045	0.9869
300	9.21	0.1076	0.9800
LPSO C_0**, mg dm^{-3}**	q_e**, mg g^{-1}**	k_2**, g mg^{-1} h^{-1}**	R^2
50	4.98	0.9267	0.9999
100	9.91	0.2685	0.9998
200	20.12	0.0987	0.9998
300	25.52	0.0503	0.9991
Weber-Morris C_0**, mg dm^{-3}**	C	k_{int}**, mg g^{-1} h$^{-1/2}$**	R^2
50	4.23	0.1572	0.9100
100	7.50	0.5074	0.8954
200	13.53	1.4146	0.8755
300	14.51	2.1548	0.9910

LPFO – Lagergren pseudo-first-order; LPSO – Lagergren pseudo-second-order; q_e – the phosphate amount adsorbed at equilibrium, k_1 – the rate constant of the first-order kinetic model; k_2 – the rate constant of the second-order kinetic model; C – the intraparticle diffusion constant that is directly proportional to the boundary layer thickness; k_{int} – the intraparticle diffusion rate constant, R^2 – correlation coefficient.

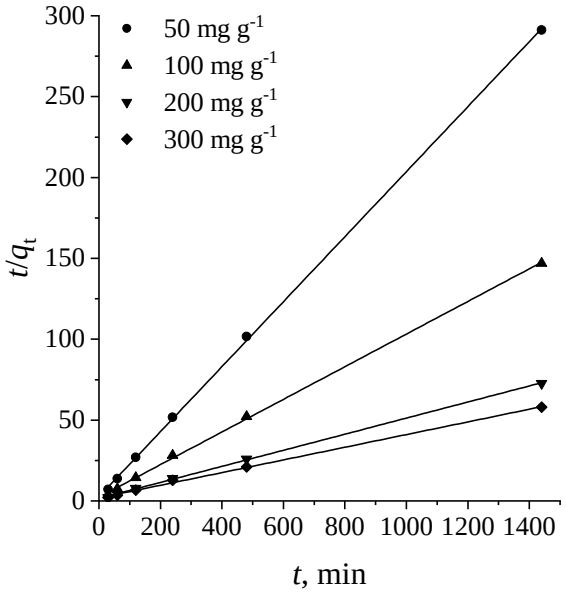

Figure 43. Lagergren pseudo-second-order kinetic model for the phosphate adsorption.

In order to study the extent to which diffusion participates in the adsorption of phosphate, the adsorption data were also analyzed by intra-particle diffusion model or Weber Morris model. The values of *C* (Table 14) indicate that the lines did not pass through the origin suggesting that the intra-particle diffusion is not the rate-controlling step.

Adsorption isotherms

The adsorption equilibrium data were further analyzed by Langmuir, Freundlich and Temkin adsorption isotherm models. The Langmuir isotherm model shows the best agreement with the experimentally obtained results (Table 15): R^2 is close to 1 and the maximum adsorption capacity (Q_0) calculated from the model (26.11 mg g^{-1}) is similar to the experimentally obtained value (24.85 mg g^{-1}). The values of dimensionless constant R_L (Figure 44) as another important parameter in the Langmuir model indicating that the adsorption is favourable process (R_L is in the range 0–1).

Table 15. Isotherm parameters of the phosphate adsorption onto FeCLI at 25 °C.

Isotherm	**Isotherm parameters**		
Langmuir	Q_0, mg g^{-1}	b, dm^3 mg^{-1}	R^2
	26.11	0.33	0.9973
Freundlich	K_f, dm^3 g^{-1}	n	R^2
	8.52	3.64	0.9834
Temkin	A, dm^3 mg^{-1}	b_T, kJ mol^{-1}	R^2
	46.33	0.85	0.8944

Q_0 – maximum amount of phosphate per unit mass of FeCLI; b – Langmuir adsorption equilibrium constant related to adsorption energy; K_f, n – Freundlich constants; A – Temkin equilibrium binding constant; b_T – Temkin constant related to the heat of adsorption (kJ mol^{-1}).

Based on the assumptions from Langmuir isotherm model, the adsorption occurs as a monolayer process. These results well agree with the literature data for the phosphate adsorption onto chitosan, different oxides as well as modified clinoptilolite (Huo *et al*., 2012; Liu and Zhang, 2015; Lalley *et al*., 2016). The value of the Freundlich constant *n* was higher than 1 indicating also that the phosphate adsorption was favourable. Temkin isotherm model gave the lowest value for the correlation coefficients (R^2). The obtained value of b_T suggests that interactions between the FeCLI and phosphate ions includes not only ion-exchange but also physisorption. A very similar value of b_T was reported

for phosphate adsorption onto adsorbents such as chitosan, magnetite or iron-zirconium modified activated carbon nanofibers (Liu and Zhang, 2015; Xiong *et al*., 2017; Hou *et al*., 2020). For these adsorbents, both chemisorption and physisorption were reported to be involved in the phosphate adsorption.

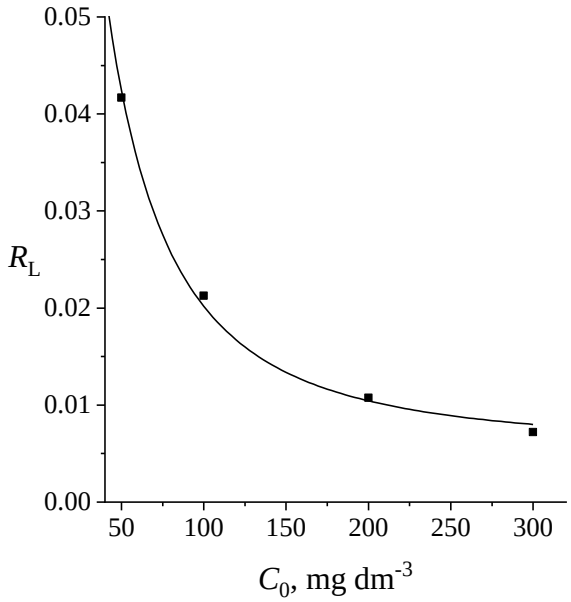

Figure 44. Separation factor (R_L) obtained from the Langmuir isotherm model as a function of initial phosphate concentrations.

In summary, the obtained results demonstrated a strong affinity oft the FeCLI toward phosphate anions. The mechanism of phosphate adsorption on adsorbents containing Fe(III) oxide particles has been widely studied. Considering literature data formation of both inner-sphere and outer-sphere complexes are involved in the adsorption process (Kim *et al*., 2011; Guaya *et al*., 2016; Li *et al*., 2016). Outer-sphere complexes (physisorbed phosphate) arise from the electrostatic interactions between negatively charged phosphate anions and $Fe–OH_2^+$ groups whereas inner-sphere complexes (monodentate and bidentate) form *via* ligand exchange reactions resulting in the formation of covalent Fe–O–P bonds.

Moreover, the adsorption mechanism can include also surface precipitation through the formation of slight soluble Ca, Zn, Al, or Mg phosphates (Li *et al*., 2016).

4.2.2 Leaching experiments

Leaching experiments were performed in order to study desorption of nitrate and phosphate into water media taking into account the application of nitrate- and phosphate-containing clinoptilolite as soil supplements.

The experiments were performed using a column system and three different types of soil: sandy soil from Norway, NW; silty loam soil from Serbia, SRB and silty clay soil from Bosnia and Hercegovina, BH.

Also, using leaching experiments, the retention of potassium (K^+) in the soils was studied.

Clinoptilolite as nitrate carrier

The results of the leaching experiments expressed as the amount of NO_3–N leached per kg of soil with time *t* are given in Figure 45.

The presented results showed that the amount of leached NO_3–N obtained from the system I (control system, only soil) varied with different soil samples: from 0.9 mg kg^{-1} (NW), 4.9 mg kg^{-1} (SRB) to 21.9 mg kg^{-1} (BH). The addition of both CLI and FeCLI to SRB and BH resulted in the lower leaching rate of NO_3–N. Thus, addition of 1 wt.% of CLI (systems III) decreased NO_3–N leaching to 2.7 for SRB and 16.3 mg kg^{-1} for BH. The effect of the FeCLI was more visible and depended on its amount. A higher amount of FeCLI led to higher NO_3–N retention in these soils. The results from the system VII (with 1.0 wt.% of FeCLI) showed that leached amount of NO_3–N was 1.9 mg kg^{-1} for the SRB and 7.3 mg kg^{-1} for the BH soil. However, the addition of both CLI and FeCLI exerted negative effect on the NO_3–N leaching from the NW sample (a slight increase in the leached NO_3–N was observed) which was also evident in all other systems.

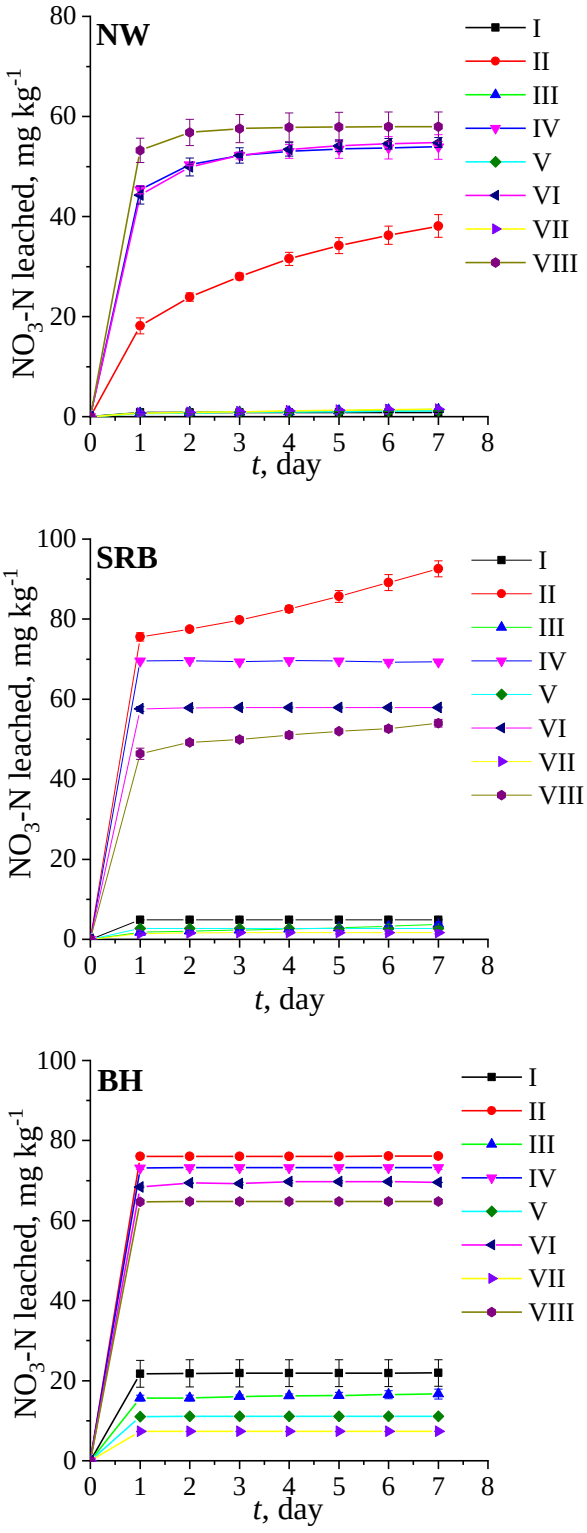

Figure 45. Amount of the leached NO_3–N over time (*t*) from the studied soils (systems: I – soil; II – soil + KNO_3; III – soil + CLI; IV – soil + CLI + KNO_3; V – soil + FeCLI 0.5 wt.%; VI – soil + FeCLI 0.5 wt.% + KNO_3; VII – soil + FeCLI 1 wt.%; VIII – soil + FeCLI 1wt.% + KNO_3).

As expected, much higher amount of NO_3–N was leached from the systems II that contained KNO_3 as typical mineral fertilizer. A positive effect of zeolite (CLI and FeCLI) addition was also observed in these systems (systems IV, VI and VIII) for SRB and BH soils. For the SRB soil, addition of 1 wt.% of CLI (system IV) reduced leaching of NO_3–N from 94.0 to about 69.4 mg kg^{-1} whereas the addition of the same amount of FeCLI (system VIII) reduced NO_3–N leaching to about 55.0 mg kg^{-1}. For the BH soil, the effect of zeolite addition was lower in comparison to SRB soil. The amount of leached NO_3–N was slightly reduced after CLI addition (system IV), from 77.0 to about 73.0 mg kg^{-1}. Addition of FeCLI decreased NO_3–N leaching to 69.5 (0.5 wt.% FeCLI, system VI) and 64.6 mg kg^{-1} (1 wt.% FeCLI, system VIII).

Different effects of the zeolite addition on the NO_3–N retention in the SRB and BH soil could be attributted mainly to the differences in physico-chemical properties of these two soils. SRB is acidic soil in contrast to BH which is alkaline soil. Therefore, it can be assumed that in the BH soil there is competition between nitrate and hydroxyl ions for the adsorption sites on the zeolite.

Irrespective of the soil types or treatments, the highest amount of NO_3–N leached out during the first day of experiment and then the leaching proceeded slowly until the end of the experiment. This could be attributed not only to a high amount of irrigation water but also to high solubility of nitrate. High leaching rate of nitrate at the beginning of the leaching experiments was also observed for silty clay and sandy soils ameded with Italian chabazite (Colombani *et al*., 2015). It was assumed that saturation of the columns by pumping synthetic rainwater from the inlet lead to dissolution of the salt (that was used as a source of nitrate) and move of nitrate by the water phase to bottom of the column. Therefore, a high concentration of nitrate was near the bottom of the column and leached at the begging of the irrigation.

Clinoptilolite as phosphate carrier

The use of FeCLI as a soil supplement in order to retain phosphate ions in the sandy (NW) soil was studied. The results of the leaching experiments are presented in Figure 46 as a relationship between the leached amount of phosphate from the soil (mg P per kg soil) over time *t*.

The obtained results showed that leaching of phosphate from the NW soil was occurred in a small extent during the period of 7 days. Therefore, leaching experiments were prolonged up to 12 days. During this period, an increase in the phosphate leaching was observed (Figure 46). As expected, a higher amount of phosphate was leached from the systems which contained KH_2PO_4 as a phosphate fertilizer. Leaching rate of phosphate from the NW soil was reduced by addition of FeCLI in systems without as well as in the systems contained KH_2PO_4. The higher retention of phosphate was observed for the systems with a higher amount of FeCLI.

However, taking into account a very small concentration of leached amount of phosphate from all the studied systems, it is ungrateful to discuss in detail to which extent (giving the retention efficiency of FeCLI in the percentage) FeCLI influence the retention of phosphate. Moreover, a visible and statistically significant improvement of phosphate retention was observed for all the systems with FeCLI (Figure 46).

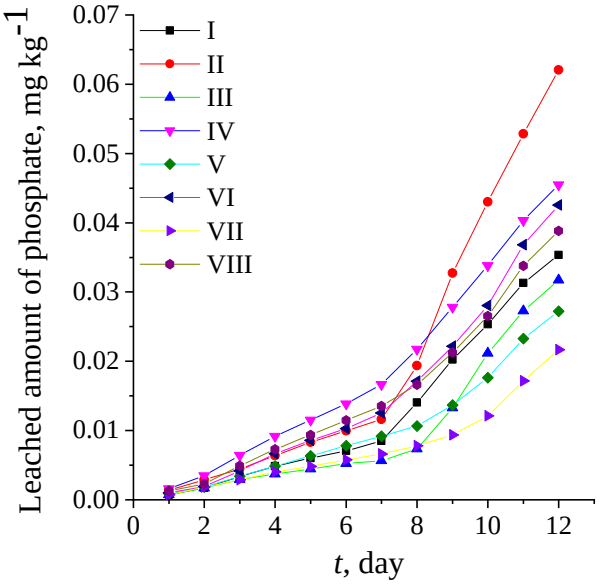

Figure 46. Amount of the leached phosphate for the studied systems over time (*t*) from NW soil (systems: I – soil; II – soil + KH_2PO_4; III – soil + FeCLI 0.5 wt.%; IV – soil + FeCLI 0.5 wt.% + KH_2PO_4; V – soil + FeCLI 1.5 wt.%; VI – soil + FeCLI 1.5 wt.% + KH_2PO_4; VII – soil + FeCLI 2.5 wt.%; VIII – soil + FeCLI 2.5 wt.% + KH_2PO_4).

The effect of FeCLI on the phosphate retention in the examined sandy soil could be ascribed to a high affinity of FeCLI toward phosphate ions due to the presence of iron oxide particles onto CLI. Decrease in the phosphate leaching by addition of Fe-containing clay minerals such as kaolinite, calcite, bentonite and zeolite has also been observed for the sandy soil (Mohorami and Jalali, 2014).

A small leaching rate of phosphate from the studied sandy (NW) soil can be ascribed by a high affinity of phosphate toward soil particles present in the sandy soils. Namely, retention of phosphate in this type of soil can be attributed to the adsorption and precipitation reactions. In acidic soils, such as NW soil used in this study, oxides and hydroxide minerals of Al and Fe are primarily included in the phosphate adsorption (Brady and Weil, 2004).

Clinoptilolite as Potassium carrier

Retention of potassium (K^+) in the NW, SRB and BH soils were studied in the presence of the CLI and FeCLI. The obtained leaching results shown in Figure 47 are expressed as a percentage of the leached K^+ amount (X) from the studied soil over time (t). The X values were calculated as the ratio of the K^+ amount (mg K^+ per kg soil) leached from the soil after time t and the total K^+ amount calculated as a sum of the plant available K^+ and the K^+ added by KNO_3 (mg K^+ per kg soil). The calculated amount underestimates the real total K amount in the soils but probably represents the leaching potential for the experimental period of seven days.

For all studied systems, K^+ leaching from the NW sample was higher than from the SRB and BH samples. In the system I (control system, only soil), 18.6% of K^+ was leached from the NW, 5.4% from BH and 4.4% from SRB soils during the 7 days. The obtained results indicated that the addition of both forms of zeolites (CLI and FeCLI) to NW soil reduces K^+ leaching. Addition of CLI (1 wt.%, system III) reduces K^+ leaching to 16.4%. However, FeCLI in comparison to CLI reduced the K leaching to a higher extent. Addition of the same amount of FeCLI (1 wt.%, system VII) reduces K^+ leaching to 6%. In addition, K^+ leaching from the system V that contained 0.5 wt.% of FeCLI was reduced to 7%.

A slightly visible but statistically significant reduction in the K^+ leaching ($p < 0.05$) was also evident for the SRB and BH samples after the addition of both zeolites CLI and FeCLI.

The system II included the presence of solid KNO_3 as a typical mineral fertilizer to the soil. The influence of the zeolite addition on the K^+ leaching amounts and the kinetics was studied in the systems IV, VI and VIII. For the NW soil the addition of CLI reduced the K^+ leaching from 44.6 to 27.0% whereas FeCLI reduced the K^+ leaching depending on the zeolite amount as follows: to 26.0 % (0.5 wt. % FeCLI, the system VI) and to 12.0 % (1.0 wt. % FeCLI, the system VIII). The results clearly showed that the addition of FeCLI can improve retention of K^+ retention in the sandy soil.

The K^+ leaching from SRB and BH samples in the system II was significantly smaller (8.3 and 6.3%, respectively) than from the NW sample. This can be attributed to the fact that clayey soils such as SRB and BH have a higher ability to retain K^+ than sandy ones. For these two samples, the addition of both forms of zeolite had a positive effect on the K^+ retention. Addition of 1.0 wt.% of FeCLI reduced the K^+ leaching from the SRB sample to 3.3% and to 4.2% for the BH sample.

The obtained results (Figure 47) clearly show that the leaching of K^+ is highly dependent on the soil type. As expected, the K^+ leaching is the most pronounced for the NW sample confirming high mobility of K^+ from sandy soils. These soils have limited ability to bind plant nutrients such as K^+ due to the low content of clay. NW soil contained much less clay (only 3%) in comparison to SRB (23%) and BH (42%). The content of silt was also very low (3%) in NW whereas SRB and BH soils contained a much higher amount of silt 73% and 50%, respectively. Since that clays are strongly negatively charged, positively charged cations such as K^+, Ca^{2+} or Mg^{2+} are easily bind in these soils, and thus the leaching of K^+ occurs to a smaller extent.

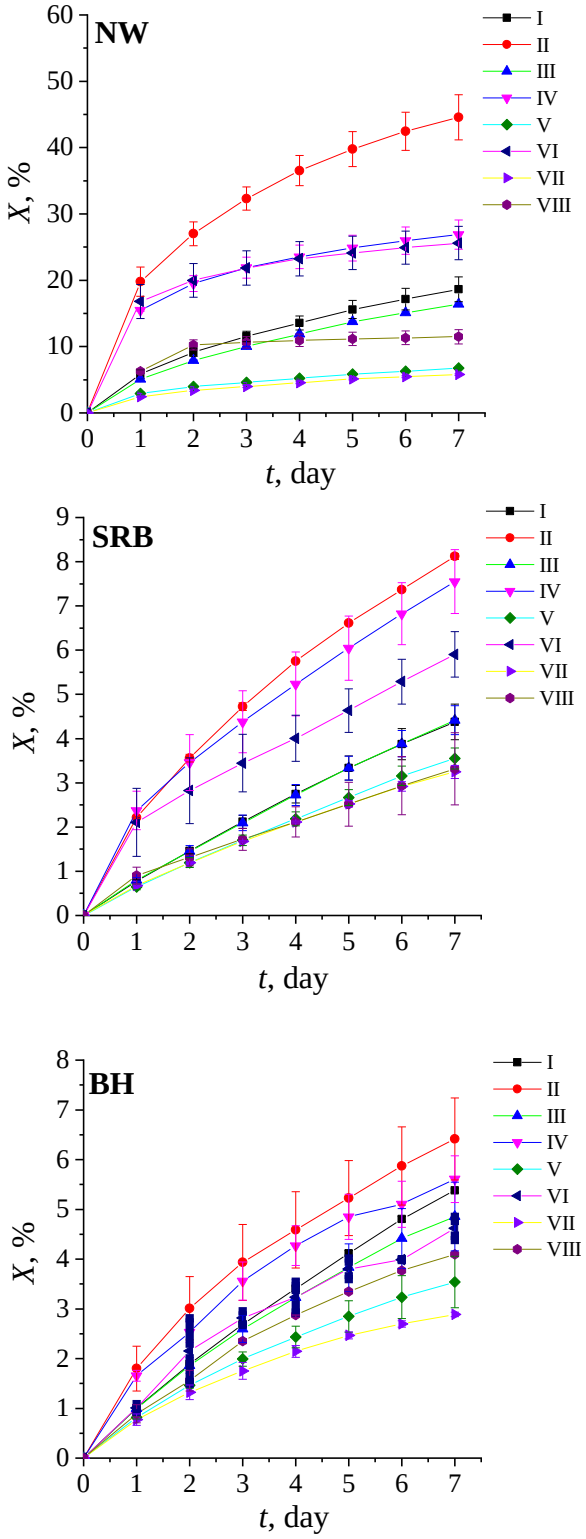

Figure 47. Percentage of leached potassium (*X*) over time (*t*) from the studied soils (systems: I – soil; II – soil + KNO_3; III – soil + CLI; IV – soil + CLI + KNO_3; V – soil + FeCLI 0.5 wt.%; VI – soil + FeCLI 0.5 wt.% + KNO_3; VII – soil + FeCLI 1 wt.%; VIII – soil + FeCLI 1 wt.% + KNO_3).

Both CLI and FeCLI improve the K^+ retention which is evident in the control system as well as in the systems containing KNO_3. The better efficiency of FeCLI than of CLI could be explained by a better adsorption ability of FeCLI towards K^+ than that of parent CLI. The FeCLI contains particles of Fe_2O_3 at the surface of the CLI phase, which enhances the adsorption ability of the zeolite towards different cations (Kragović *et al*., 2013). Moreover, the K^+ adsorption mechanism for CLI proceeds by ion-exchange, whereas for FeCLI physisorption can be also included. Previously studies also indicated that the retention of K^+ can be enhanced in sandy soils by the addition of CLI. The findings show that leaching of K^+ can be significantly decreased even from sandy soil amended with municipal compost (Moraetis *et al*., 2015). Very recently, it has been reported that K-saturated CLI applied to sandy soil and sandy soil amended with chemical fertilizers can be used in preventing the K^+ loss from soil (Eslami *et al*., 2018). In contrast to the sandy NW soil, the CLI addition has a very low reduction effect on the SRB and BH samples, which are silty loam and silty clay, respectively. The presence of FeCLI has a somewhat higher effect, which could be attributed to its better adsorption ability toward K^+. These soils are capable to retain K^+ to a high extent and therefore the effect of both form of zeolites (CLI and FeCLI) is poorly visible for the observed systems.

Leaching kinetics of potassium from the studied soils

The kinetic data obtained from the leaching experiments were analyzed by the different kinetic models given in Table 16. The best agreement ($R^2 \approx 1$) was found for the Avrami kinetic model. The values of n (Avrami constant) and $\ln k_A$ (k – Avrami rate constant of the K^+ leaching) were calculated from the slope and the intercept of the obtained plot $\ln[-\ln(1-X)]$ *versus* $\ln t$, respectively. The obtained values of the parameters and coefficients of determination (R^2) are shown in Table 16. According to the Avrami model, the parameter n describes the mechanism of the leaching process: the initial rate of reaction approaches zero for $n > 1$, being infinite and decreases with time for $n < 1$ or being finite for $n = 1$. It is evident that the Avrami parameter n for all the studied systems suggests that the initial rate of K^+ leaching is high and decreases with time ($n < 1$). The Avrami kinetic model has been applied to describe the kinetic data obtained from the batch and dynamic (column) systems of different processes including

adsorption, dissolution and leaching (Demirkiran and Künkül, 2007; Vargas *et al*., 2011; Zheng and Chen, 2014; Songolzadeh *et al*., 2015).

Table 16. Kinetic models used in studying of the K^+-leaching.

Kinetic model	R^2	**Mean**
Zero-order	0.5954 – 0.9999	0.96
First-order	0.6007 – 0.9999	0.97
Second-order	0.6060 – 0.9999	0.97
Parabolic-diffusion	0.7063 – 0.9998	0.98
Elovich	0.8165 – 1	0.96
Avrami	0.8823 – 1	0.99

Kinetic parameters of the K leaching obtained by Avrami model

System	**NW**			**SRB**			**BH**		
	n	$\ln k_A$	R^2	n	$\ln k_A$	R^2	n	$\ln k_A$	R^2
I	0.6313	-4.8042	0.9997	0.9051	-7.7212	0.9998	0.8770	-7.3682	0.9997
II	0.5111	-3.1322	0.9997	0.6430	-5.7606	0.9994	0.5633	-5.6299	0.9904
III	0.6367	-4.9709	0.9998	0.8941	-7.6740	0.9999	0.8232	-7.1861	0.9991
IV	0.2430	-2.4508	0.9979	0.6099	-5.6914	0.9990	0.4702	-5.5571	0.9942
V	0.4566	-5.1479	0.9993	0.8882	-7.8628	1	0.7639	-7.2289	0.9988
VI	0.3176	-2.7720	0.9977	0.5391	-5.6109	0.9940	0.6856	-6.2227	0.9980
VII	0.4396	-4.9191	0.9993	0.8185	-7.5899	0.9999	0.7589	-7.1802	0.9988
VIII	0.2875	-3.4967	0.8823	0.6793	-6.9145	0.9962	0.7759	-7.1196	0.9999

k_A – Avrami rate constant; n – Avrami constant.

4.3 Application of modified clinoptilolite in catalytic esterification of levulinic acid

In these experiments, CLI was loaded with SnO_2 (SnHCLI) and then sulfated to convert SnHCLI to SO_4-SnHCLI (SSnHCLI). The catalysts were prepared by two methods: 1) wet impregnation and 2) mechanochemical treatment. Catalytic tests were performed in a batch system under mild conditions, atmospheric pressure and at 100 °C.

1) Catalytic activity of the catalysts obtained by wet impregnation

Esterification of levulinic acid with octanol

The obtained catalytic results indicated that both studied samples nonsulfated (SnHCLI) and sulfated (SSnHCLI), were catalytically active in the esterification reaction in contrast to non-modified HCLI which showed very low catalytic activity (less than 10% after 5 h) with both alcohols octanol (Oc) and ethanol (Et). In addition, the esters of LA were only carbon products (selectivity of 100%) from the esterification reactions.

Figure 48 shows the results of the esterification LA into OLA in the presence of SnHCLI and SSnHCLI. For all SnHCLI samples, the LA conversion to OLA was about 55% after 5 h. This indicates that Sn concentration does not affect the catalytic activity of SnHCLI samples. It seems likely that modification by more than 4.5 wt.% Sn leads to the Sn deposition inside the pores or on the zeolite walls where the Sn species are not accessible for the reaction. According to the XPS depth profiles, deposition of the Sn species occurs not only at the surface but also inside the lattice of CLI.

Relatively high catalytic activity of the SnHCLI could be attributed to the presence of relatively high amounts of Lewis acid sites. However, although the amounts of Lewis acid sites increased by increasing the Sn content the LA conversion rate did not increase indicating that all acid sites are not available for the esterification of LA.

The presented results (Figure 48) show also that the sulfation treatment of the SnHCLI samples leads to a significant increase in the conversion rate of LA to OLA. The catalysts obtained by sulfation with 3 mol dm^{-3} $NH_4(SO_4)_2$ solution exhibit total conversion of LA to OLA while slightly lower conversion rate (95–99%) was achieved for the catalysts obtained by using 1 mol dm^{-3} $NH_4(SO_4)_2$ solution.

Total conversion of LA into OLA in the presence of SSnHCLI samples indicates that all SSnHCLI samples have similar acidity which is supported by FTIR measurements.

Significantly higher LA conversion was obtained for SSnHCLI than for SnHCLI which can be explained by the significantly higher amounts of both acid sites (Lewis and Brönsted) on SSnHCLI samples. As a comparison, the sulfated ZrO_2/KIL–2 showed higher conversion of LA into ELA and BLA compared to the non-sulfated samples which was attributed to higher acidity (Popova *et al*., 2016). It has been also reported that the sulfation of the SnO_2 leads to increase of catalytic activity and accordingly increase of the LA conversion to ELA. It can be explained by a synergetic action of Lewis and Brönsted acid sites (Popova *et al*., 2018).

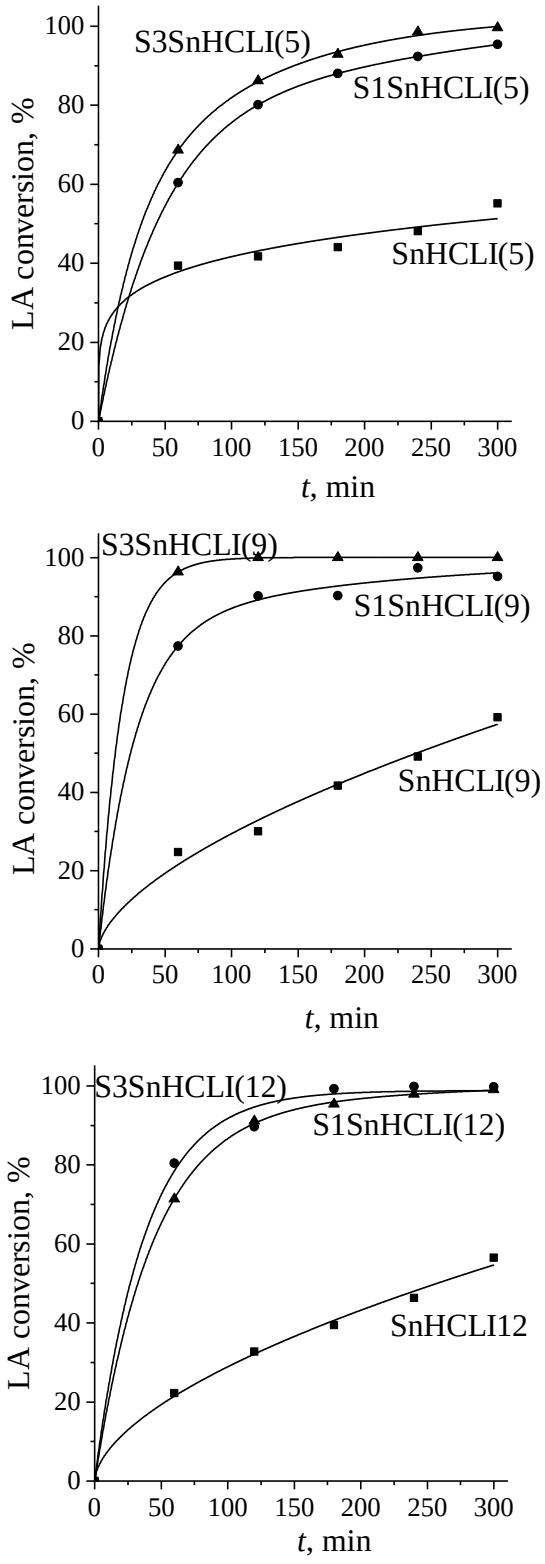

Figure 48. Esterification of LA with octanol (reaction conditions: *T*=100 °C, LA:Octanol ratio=1:7, *t*=5 h). S1 and S3 refers the concentration (1 or 3 mol dm^{-3}, respectively) of the used $NH_4(SO_4)_2$ solution.

Esterification of levulinic acid with ethanol

The results obtained for the conversion of LA to ELA in the presence of both SnHCLI and SSnHCLI are given in Figure 49. It can be seen that activity of SnHCLI in the conversion LA to ELA was significantly lower than in the LA conversion to OLA. However, in contrast to esterification with Oc the influence of the Sn content on the catalytic activity is evident. LA conversion to ELA increases from 9% for SnHCLI5 to 22% for SnHCLI12. This could be explained by the fact that catalytic active acid sites inside the pores of SnHCLI become more accessible to smaller ethanol molecules.

The presented results (Figure 49) also show that the conversion rate of LA to ELA increases after sulfation treatment confirming again that sulfate species play an important role in the esterification reaction. Treatment with lower concentration of $NH_4(SO_4)_2$ (1 mol dm^{-3}) increases conversion as follows: S1SnHCLI5 (13%)<S1SnHCLI9 (43%)<S1SnHCLI12 (72%). Additionally, the conversion to ELA is significantly higher for SSnHCLI obtained by treatment with 3 mol dm^{-3} solution showing LA conversion rate from 78% for S3SnHCLI5 to total conversion for S3SnHCLI12. Significantly higher conversion rate of sulfated catalysts could be ascribed to the presence of both Brönsted and Lewis acid sites. These results confirm suggestion that the presence of sulfate groups significantly influences the conversion of LA into ELA (Popova *et al.*, 2016; Popova *et al.*, 2018).

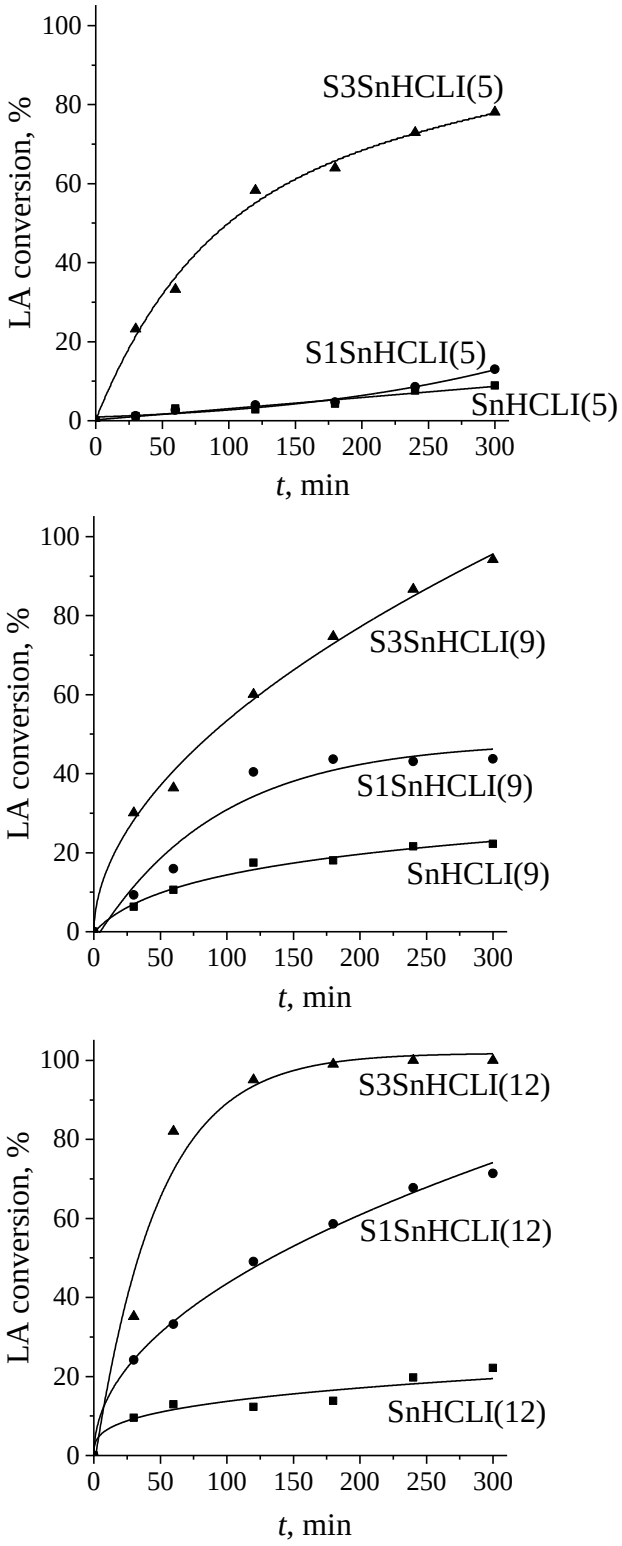

Figure 49. Esterification of LA with ethanol (reaction conditions: *T*=100 °C, LA:Ethanol ratio=1:7, *t*=5 h). S1 and S3 refers the concentration (1 or 3 mol dm^{-3}, respectively) of the used $NH_4(SO_4)_2$ solution.

Mechanism of LA esterification

Mechanism of the LA esterification with different alcohol over the sulfated catalysts has been discussed by several authors (Pasquale *et al.*, 2012; Popova *et al.*, 2018). All the reported results demonstrate the importance of acidity i.e. the presence of both Lewis and Brönsted acid sites on sulfated catalyst generated by sulfation treatment.

Based on the reported results, the esterification involves the participation of both acid sites (Lewis and Brönsted) in the esterification of LA with different alcohols. The proposed reaction mechanism consists of several steps:

- adsorption of LA on the acid sites (Lewis and Brönsted) which are present on the sulfated catalyst,
- formation of a protonated LA intermediate,
- nucleophilic attack of the oxygen atom from the alcohol on the carbonyl carbon which leads to the formation of anoxonium ion,
- loss of a water molecule from the oxonium ion and subsequent deprotonation which results in the formation of levulinate ester and the regeneration of the acid sites onto catalyst.

The proposed reaction mechanism is given in the Figure 50.

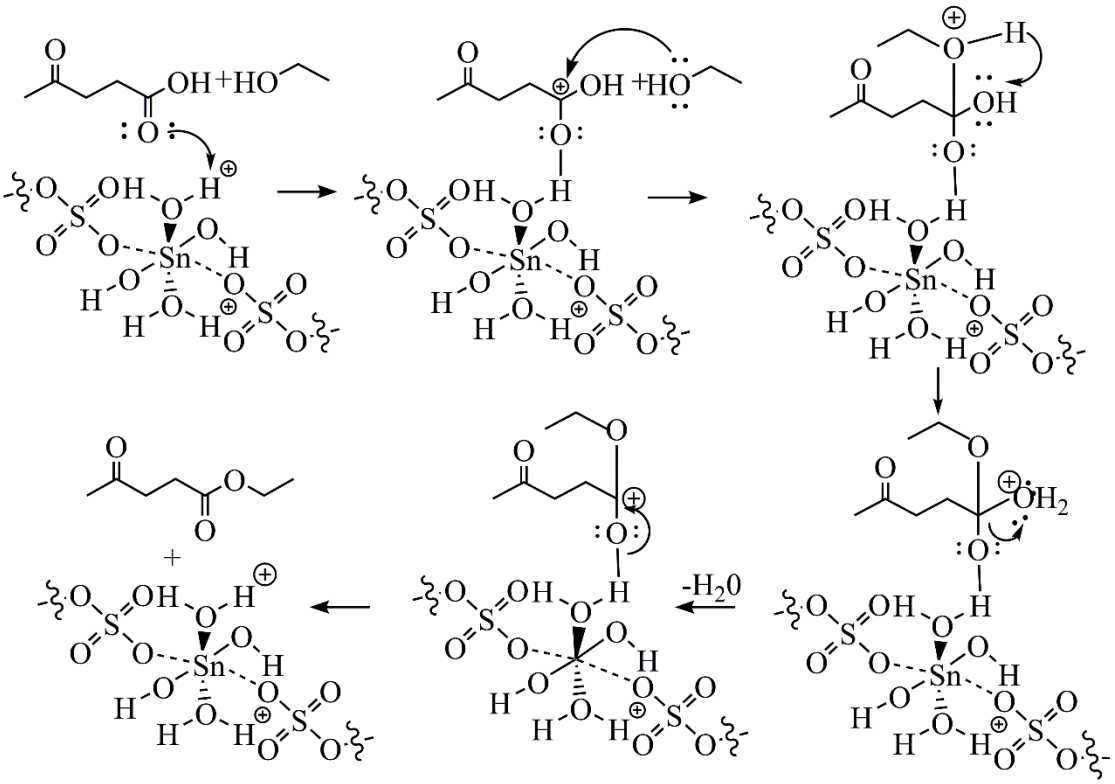

Figure 50. Reaction mechanism of the LA esterification (Popova *et al.*, 2018).

Reusability of the catalysts

Reusability tests were performed using the SSnHCLI9 catalyst. The obtained results are shown in Figure 51.

As can be seen, the catalytic activity of the catalyst as well as LA conversion rate decreased in the repeated reaction cycles in both reactions. Conversion rate of LA to OLA decreased from 100% (fresh catalyst) to 86% after next five reaction cycles. In contrast, the conversion rate of LA to ELA decreased from 94% (fresh catalyst) to about 68% after the first cycle and is stabilized at 66% in the next five cycles (Figure 51).

The decrease of the catalytic activity can be attributed to partial leaching of sulfate groups as reflected in the decrease of the S/Sn molar ratio (from 0.4 to 0.2). However, there was no further leaching of sulfate after the second cycle, suggesting that further desulfation is most probably prevented by structural features of the partially dealuminated CLI lattice. Crystallinity of the spent catalysts was checked by PXRD analysis. The obtained data confirmed that the catalyst remained crystallographically unchanged during the esterification reaction.

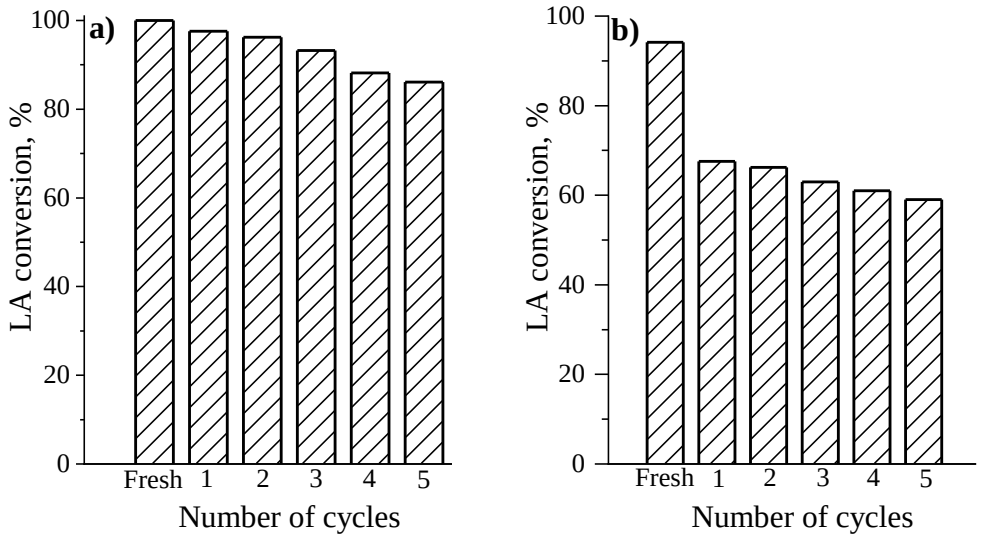

Figure 51. Reusability of the catalyst SSnHCLI9 in LA esterification with a) octanol and b) ethanol at the 100 °C, LA:Octanol/Ethanol ratio=1:7 and reaction time of 5 h.

Catalytic but also reusability results suggest that LA conversion to OLA and ELA proceeds in a different manner. It seems that esterification reaction with octanol mainly

occurs at the external surface of the catalysts. Octanol is long chain alcohol and molecules of octanol can not penetrate the pore system of the CLI-based catalyst. Moreover, conversion curves obtained in the esterification with octanol suggest that the reaction is faster than the reaction with ethanol. In contrast, the esterification of LA with ethanol may occur not only on the external surface of the catalyst but also in the pores. Ethanol is short chain alcohol and due to the appropriate sizes LA and ethanol molecules can penetrate in the pores. However, the formation of intermediate products and ELA is blocked in the pores and their diffusion out is limited which most probably lead to the coke formation and decreasing of catalytic activity. This suggestion was also supported by thermal analysis. Thermal analysis of the spent catalysts indicated that the residue after the OLA production is significantly lower (14 wt.%) than after production of ELA (26 wt.%). This suggests that lower catalytic activity of the catalyst in the repeated reaction cycles with Et can be ascribed by the higher coke formation during the esterification of LA.

A decrease of the catalytic activity of the sulfated catalysts in the esterification of LA was also observed for other catalytic systems. The literature results indicate that the reusability of the sulfated catalysts is limited since the catalysts suffer from the leaching of sulfate (active) species even after the first reaction cycles. Considerable decrease in catalytic activity and thus in LA conversion (from 40 to 14%) after the first reaction cycle was reported for sulfated SnO_2 (Fernandes *et al*., 2012). Also, a significant decrease in catalytic activity was observed for sulfated ZrO_2 (60% loss) and sulfated Si-doped ZrO_2 (80% loss) after five reaction cycles in the LA esterification with Et at 100 °C due to the partial leaching of sulfate species (Kuwahara *et al*., 2014). In addition, decrease in catalytic activity was also reported for sulfated ZrO_2/KIL-2 for which the LA conversion into ELA was 51% in the first run and 47% after three cycles (Popova *et al*., 2016).

Deactivation mechanism of the sulfated catalysts in the esterification reactions is still the subject of many investigations. According to the reported data, a decrease in catalytic activity can be explained by different reasons including acidity reduction, coke formation or phase transformation (from catalytically active to catalytically inactive metal oxide species) (Shi and Li, 2013). Deactivation mechanism proposed by Shi and Li suggests that some active sulfate groups may be lost, poisoned or turned to less

catalytic or even non catalytic sulfur species (Shi and Li, 2013). It has been assumed that the water molecules produced from the esterification reactions play an important role in the deactivation of the catalysts. It seems that hydrolysis of some strong Lewis acid sites (which arise from the metal cations) by water molecules occur which indirectly promotes their alcoholysis. This leads to a gradual acidity reduction of the catalyst and thus to the decrease in their catalytic activity.

2) Catalytic activity of the catalysts obtained by mechanochemical method

The results obtained for the conversion of LA to ELA in the presence of SSnHCLI, prepared by a mechanochemical method are given in Figure 52. Conversion of LA to ELA was higher for the catalyst prepared by using more concentrated $NH_4(SO_4)_2$ solution. Also, it can be seen that the highest LA conversion to ELA was obtained for the catalyst with medium content of Sn, MS1SnHCLI9 and MS3SnHCLI9. The conversion rate was about 26% and 43% after 5 h of reaction, respectively. The obtained results also indicated that an increase of Sn content onto HCLI leads to a decrease in LA conversion rate. The same observation has also been reported for the sulfated ZrO_2 KIL-2 composite (Popova *et al.*, 2016). The phenomenon was ascribed to the significant decrease of dispersion of ZrO_2 and the structure deterioration of the catalyst. Similarly, a decrease in catalytic activity by increase of ZrO_2 content was observed also for the sulfated ZrO_2 supported on SBA-15 (Barbera *et al.,* 2015). It has been reported that Zr-nanoparticles were located predominately outside the mesoporous channels for the lower content of ZrO_2. In contrast, an increase of ZrO_2 content results in the formation of Zr-nanoparticles predominantly inside the mesoporous channels. Moreover, it has been observed that this causes differences in the acidity of the catalysts and thus in the catalytic activity. Finally, it was assumed that the formation of Zr-nanoparticles inside the channels of the catalyst offers the catalytic active sites that are not accessible for the reactant molecules.

The results presented in the Figure 52 show that the catalytic activity of all sulfated catalysts, as well as the conversion rate of LA to ELA, was significantly lower than for the catalysts prepared by wet impregnation method. This suggests that preparation method significantly affects the catalytic activity in the esterification of LA.

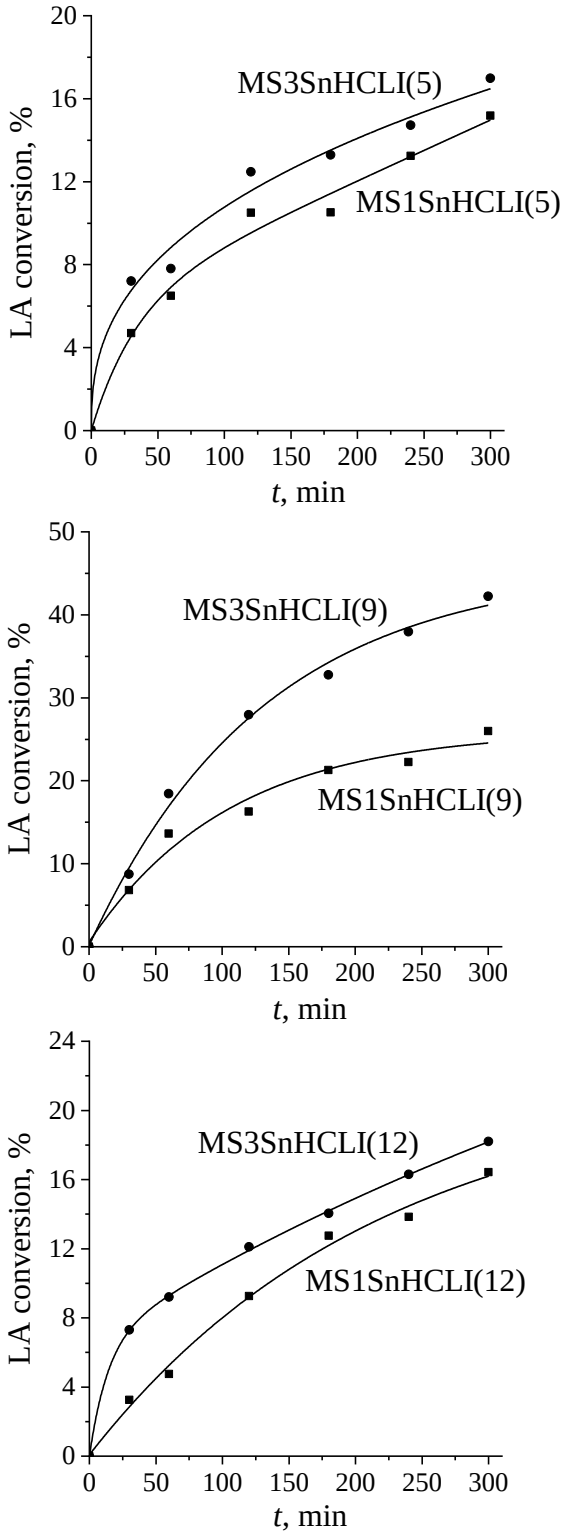

Figure 52. Esterification of LA with ethanol (reaction conditions: *T*=100 °C, LA:Ethanol ratio=1:7, *t*=5 h). S1 and S3 refers the concentration (1 or 3 mol dm^{-3}, respectively) of the used $NH_4(SO_4)_2$ solution.

5. CONCLUSIONS

The results obtained in this doctoral thesis strongly support the fact that the natural zeolite (clinoptilolite) from Serbian deposits can be effectively modified into environmentally friendly and cost-efficient adsorbents that can be further applied as soil supplement as well as to catalytically active and reusable catalysts for the esterification of levulinic acid.

Modification procedure is simple, with low energy consumption and consists of two relatively simple steps: a) treatment of the clinoptilolite in an alkaline solution of Mg, Mn(II), Fe(III) or Sn(IV) and b) calcination of the metal-enriched clinoptilolite.

Based on the detail characterization, the modification yielded MgO, Mn_2O_3, Fe_2O_3 and SnO_2 well dispersed particles onto clinoptilolite surface.

Considering all performed adsorption experiments it can be concluded that:

a) Adsorption using the prepared adsorbents is an endothermic process.
b) Concentration of nitrate on the adsorbents increased with increasing of initial nitrate concentration in water media.
c) 1:50 was found as an optimal mass/volume ratio for nitrate adsorption.
d) Nitrate adsorption capacity is affected by chemical nature of oxide presents onto clinoptilolite surface. Fe(III)–containing clinoptilolite shows the best adsorption capacity.
e) Nitrate adsorption can be described by Langmuir isotherm model whereas the adsorption kinetics follows the pseudo-second-order kinetic model.
f) Phosphate adsorption onto Fe(III)–containing clinoptilolite also follows the Langmuir isotherm model and the adsorption kinetics follows the pseudo-second-order kinetic model.
g) Mechanism of phosphate adsorption is complex including electrostatic interaction and formation of donor-acceptor bonds between phosphate ions and Fe(III).

From the leaching experiments it can be concluded that:

a) The retention efficiency of clinoptilolite and Fe(III)–containing clinoptilolite depends on the soil type.
b) The nitrate retention can be increased by the clinoptilolite and Fe(III)–containing clinoptilolite addition for the silty loam and silty clay soils. Fe(III)–containing clinoptilolite exerts a better retention effect than parent clinoptilolite.
c) Potassium retention increases in the following order: silty loam < silty clay << sandy soil. The Fe(III)–containing clinoptilolite has a higher retention effect than clinoptilolite.
d) Potassium leaching kinetics from all soil types follows the Avrami kinetic model.
e) Phosphate leaching from sandy soil proceeds in a small extent but addition of Fe(III)–containing clinoptilolite shows retention effect.

In catalytic experiments, the esterification of levulinic acid into ethyl and octyl esters was studied. The catalytic activity of SnO_2- and sulfated SnO_2-containing clinoptilolite was investigated in the esterification. From the obtained results the following conclusions can be reached:

a) Catalysts prepared by wet impregnation method show a higher catalytic activity with respect to catalysts prepared by mechanochemical method.
b) Non sulfated catalysts showed high activity in the conversion of levulinic acid to octyl levulinate. Conversion rate is around 55% for all the studied catalysts indicating that their catalytic activity is not affected by the Sn content. The effect is explained by hindered access of long chain of octanol to all acid sites especially that present inside the pores of clinoptilolite lattice.
c) Catalytic activity of non sulfated catalysts is significantly lower especially in the conversion of levulinic acid to ethyl levulinate. By increasing of the Sn content, the conversion rate increases (up to 22%) which is explained by the fact that catalytic active sites on the catalysts become more accessible to smaller ethanol molecules.

d) Sulfated catalysts exhibit total conversion of levulinic acid to both octyl- and ethyl levulinate which is attributed to the presence of a high amount of Brönsted and Lewis acid sites.
e) The conversion rate of levulinic acid decreased to 86% for octyl levulinate and to 66% for ethyl levulinate after five repeated reaction cycles. The decrease is explained by a partial leaching of sulfate groups. Higher catalytic activity in the conversion to octyl levulinate is ascribed to higher coke formation in the esterification to ethyl levulinate.

All presented results clearly demonstrate benefits of the use of natural clinoptilolite. It is highly perspective mineral for production of soil supplements for the retention of nitrate, phosphate and potassium ions. This is important not only for the agricultural practice but also for preservation of water bodies.

Clinoptilolite can also be the starting material for the preparation of catalysts applied for production of levulinate esters. Considering the fact that levulinic acid is one of twelve platform chemicals that can be obtained from biomass as well as that its esters have versatile application, the obtained results are important for use of clinoptilolite in design of environmentally friendly and cost effective catalysts.

6. REFERENCES

A European strategy for smart, sustainable and inclusive growth, Communication from the commission Europe 2020, Brussels, 3.3.2010 COM(2010) 2020.

Ahmadi M., Haghighi M., Kahforoushan D., Influence of active phase composition (Mn, Ni, Mn_xNi_{10-x}) on catalytic properties and performance of clinoptilolite supported nanocatalysts synthetized using ultrasound energy toward abatement of toluene from polluted air, *Process Saf. Environ.* **106** (2017) 294–308.

Akgül M. and Karabakan A., Selective synthesis of monoolein with clinoptilolite, *Micropor. Mesopor. Mat.* **131** (2010) 238–244.

Akgül M., Özyağcı B., Karabakan A., Evaluation of Fe- and Cr-containing clinoptilolite catalysts for the production of camphene from α-pinene, *J. Ind. Eng. Chem.*, **19** (2013) 240–249.

Alfaro M.A., Jarvis S.C., Gregory P.J., Factors affecting potassium leaching in different soils, *Soil Use Manage.* **20** (2004) 182–189.

Amiri A. and Nezamzadeh-Ejhieh A., Improvement of the photocatalytic activity of cupric oxide by deposition onto a natural clinoptilolite substrate, *Mat. Sci. Semicon. Proc.* **31** (2015) 501–508.

Andronikashvili T., Zautashvili M., Eprikashvili L., Burkiashvili N., Pirtskhalava N., Natural zeolite-one of the possibilities of transition from chemical to biological agronomy, *Bulletin of the Georgian National Academy of Sciences*, **6** (2012) 111–118.

Arabpour N. and Nezamzadeh-Ejhieh A., Modification of clinoptilolite nano-particles with iron oxide: Increased composite catalytic activity for photodegradation of cotrimaxazole in aqueous suspension, *Mat. Sci. Semicon. Proc.* **31** (2015) 684–692.

Arata K., Matsuhashi H., Hino M., Nakamura H., Synthesis of solid superacids and their activities for reactions of alkanes, *Catal. Today* **81** (2003) 17–30.

Aravindhan R., Raghava Rao J., Unni Nair B., Preparation and characterization of activated carbon from marine macro-algal biomass, *J. Hazard. Mater.* **162** (2009) 688–694.

Arora M., Eddy N.K., Mumford K.A., Baba Y., Perera J.M., Stevens G.W., Surface modification of natural zeolite by chitosan and its use for nitrate removal in cold regions, *Cold Reg. Sci. Technol.* **62** (2010) 92–97.

Ates A., Effect of alkali-treatment on the characteristics of natural zeolites with different compositions, *J. Colloid Interf. Sci.* **523** (2018) 266–281.

Ates A., Reitzmann A., Hardacre C., Yalcin H., Abatement of nitrous oxide over natural and iron modified natural zeolites, *Appl. Catal. A-Gen.* **407** (2011) 67–75.

Avrami M., Kinetics of Phase change I General Theory, *J. Chem. Phys.* **7** (1939) 1103–1112.

Badgujar K.C. and Bhanage B.M., Thermo-chemical energy assessment for production of energy-rich fuel additive compounds by using levulinic acid and immobilized lipase, *Fuel Process. Technol.* **138** (2015) 139–146.

Badgujar K.C., Badgujar V.C., Bhanage B.M., A review on catalytic synthesis of energy rich fuel additive levulinate compounds from biomass derived levulinic acid, *Fuel Process. Technol.* **197** (2020) 106213 (DOI: 10.1016/j.fuproc.2019.106213).

Barbera K., Lanzafame P., Pistone A., Millesi S., Malandrino G., Gulino A., Perathoner S., Centi G., The role of oxide location in HMF etherification with ethanol over sulfated ZrO_2 supported on SBA-15, *J. Catal.* **323** (2015) 19–32.

Bhatnagar A., Kumar E., Sillanpää M., Nitrate removal from water by nano-alumina: Characterization and sorption studies, *Chem. Ing. J.* **163** (2010) 317–323.

Bojic S., Martinov M., Brcanov d., Djatkov Dj., Georgijevic M., Location problem of lignocellulosic bioethanol plant - Case study of Serbia, *J. Clean. Prod.* **172** (2018) 971–979.

Boronat M., Concepción P., Corma A., Renz M., Valencia S., Determination of the catalytically active oxidation Lewis acid sites in Sn-beta zeolites, and their optimisation by the combination of theoretical and experimental studies, *J. Catal*. **234** (2005) 111–118.

Bozell J.J., Moens L., Elliott D.C., Wang Y., Neuenscwander G.G., Fitzpatrick S.W., Bilski R.J., Jarnefeld J.L., Production of levulinic acid and use as a platform chemical for derived products, *Resources Conserv. Recycl.* **28** (2000) 227–239.

Brady N.C. and Weil R.R., Elements of the nature and properties of soils, Pearson Education, Third Edition, 2009, pp.433–439.

Breck D.W., Zeolite molecular sieve structure, chemistry and use, Wiley-Interscience, New York, 1974.

Bremner J.M. and Mulvaney C.S., Methods of Soil Analysis Part 2 Agronomy 9, American Society of Agronomy, INC., Madison, WI, 1982, pp. 595–624.

Brown G. and Brindley G.W., Crystal structures of clay minerals and X-ray identification, Mineralogical Society, London, 1980, pp. 205–360.

Čađo S., Đurković A., Novaković B., Denić Lj., Dopuđa Glišić T., Veljković N., Stojanović Z., Sezonska dinamika fitoplanktona akumulacionog jezera Ćelije, Zbornik radova "VODA 2017".

Camacho I.M., Parra R.R., Deng S., Arsenic removal from groundwater by MnO_2-modified natural clinoptilolite zeolite: Effects of pH and initial feed concentration, *J. Hazard. Mater.* **189** (2011) 286–293.

Cerjan Stefanović Š., Zabukovec Logar N., Margeta K., Novak Tušar N., Arčon I., Maver K., Kovač J., Kaučić V., Structural investigation of Zn^{2+} sorption on clinoptilolite tuff from the Vranjska Banja deposit in Serbia, *Micropor. Mesopor. Mat.* **105** (2007) 251–259.

Chakravarty R., Chakraborty S., Shukla R., Bahadur J., Ram R., Mazumder S., Dev Sarma H., Kumar Tyagi A., Dash A., Mechanochemical synthesis of mesoporous tin oxide: a new generation nanosorbent for $^{68}Ge/^{68}Ga$ generator technology, *Dalton T.* **45** (2016) 13361–13372.

Chang C., Cen P, Ma X., Levulinic acid production from wheat straw, *Bioresource Technol.* **98** (2007) 1448–1453.

Chatterjee S. and Woo H., The removal of nitrate from aqueous solutions by chitosan hydrogel beads**,** *J. Hazard. Mat.* **164** (2009) 1012–1018.

Chen B., Li F., Huang Z., Yuan G., Hydrogen-transfer conversion of furfural into levulinate esters as potential biofuel feedstock, *J. Energy Chem.* **25** (2016) 888–894.

Chen H., Ruan H., Lu X., Fu J., Langrish T., Lu X., Catalytic conversion of furfural to methyl levulinate in a single-step route over Zr/SBA-15 in near-critical methanol, *Chem. Eng. J.* **333** (2018) 434–442.

Chintala R., Mollinedo J., Schumacher T.E., Papiernik S.K., Malo D.D., Clay D.E., Kumar S., Gulbrandson D.W., Nitrate sorption and desorption in biochars from fast pyrolysis, *Micropor. Mesopor. Mat.* **179** (2013) 250–257.

Christensen E., Williams A., Paul S., Burton S., McCormick R.L., Properties and performance of levulinate esters as diesel blend components, *Energ. Fuel* **25** (2011) 5422–5428.

Chutia P., Kato S., Kojima T., Satokawa S., Adsorption of As(V) on surfactant-modified natural zeolites, *J. Hazard. Mater.* **162** (2009) 204–211.

Cirujano F.G., Corma A., Liabrés i Xamena F.X., Conversion of levulinic acid into chemicals: Synthesis of biomass derived levulinate esters over Zr-containing MOFs, *Chem. Eng. Sci.* **124** (2015) 52–60.

Coelho A., TOPAS Academic 4.1 Coelho Software, Brisbane, Australia, 2007.

Colombani N., Mastrocicco M., Di Giuseppe D., Faccini B., Coltorti M., Batch and column experiments on nutrient leaching in soils amendedwith Italian natural zeolitites, *Catena* **127** (2015) 64–71.

Çoruh S., The removal of zinc ions by natural and conditioned clinoptilolites, *Desalination* **225** (2008) 41–57.

Đeković V., Anđelković A., Bošnjaković A., Janić M., Analiza kvaliteta vode u akumulaciji „Vrutci", Šumarstvo, (2017) 175–188.

Demirkiran N. and Künkül A., Dissolution kinetics of ulexite in perchloric acid solutions, *Int. J. Miner. Process.* **83** (2007) 76–80.

Devic G., Djordjevic D., Sakan S, Natural and anthropogenic factors affecting the groundwater quality in Serbia, *Sci. Total Environ.* **468–469** (2014) 933–942.

Dharne S. and Bokade V.V., Esterification of levulinic acid to *n*-butyl levulinate over heteropolyacid supported on acid-treated clay, *J. Nat. Gas Chem.* **20** (2011) 18–24.

Di H.J. and Cameron K.C, Nitrate leaching in temperate agroecosystems: sources, factors and mitigating strategies, *Nutr. Cycl. Agroecosys.* **46** (2002) 237–256.

Dijkmans J., Demol J., Houthoofd K., Huang S., Pontikes Y., Sels B., Post-synthesis Snβ: An exploration of synthesis parameters and catalysis, *J. Catal*. **330** (2015) 545–557.

Ding D., Wang J., Xi J., Liu X., Lu G., Wang Y., High-yield production of levulinic acid from cellulose and its upgrading to *γ*-valerolactone, *Green Chem.* **16** (2014) 3846–3853.

Dodić S.N., Zekić V. N., Rodić V.O., Tica N.Lj., Dodić J.M., Popov S.D., Situation and perspectives of waste biomass application as energy source in Serbia, *Renew. Sust. Energ. Rev.* **14** (2010) 3171–3177.

Doula M.K. and Ioannou A., The effect of electrolyte anion on Cu adsorption–desorption by clinoptilolite, *Micropor. Mesopor. Mat.* **58** (2003) 115–130.

Doula M.K., Synthesis of a clinoptilolite–Fe system with high Cu sorption capacity, *Chemosphere* **67** (2007) 731–740.

Du G., Li Z., Liao L., Hanson R., Leick S., Hoeppner N., Jiang W.T., Cr(VI) retention and transport through Fe(III)-coated natural zeolite, *J. Hazard Mater*., **221–222** (2012) 118–123.

Dziedzicka A., Sulikowski B., Ruggiero-Mikolajczyk M., Catalytic and physicochemical properties of modified natural clinoptilolite, *Catal. Today* **259** (2016) 50–58.

Egner H., Riehm H., Domingo W.R., Untersuchungen uber die chemische Bodenanalyse als Grundlage fur die Beurteilung des Nährstoffzustandes der Böden. II. Chemische Extraktionsmethoden zur Phosphor- und Kaliumbestimmung. Kungliga Lantbrukshügskolans Annaler **26** (1960) 199–215.

El Sharkawi H.M., Tojo S., Chosa T., Malhat F.M., Youssef A.M., Biochar-ammonium phosphate as an uncoated-slow release fertilizer in sandy soil, *Biomass Bioenerg.* **117** (2018) 154–160.

Elonen P., Particle size analysis of soil, *Acta Agral. Fenn.* **112** (1971) 1–122.

Emeis C.A., Determination of integrated molar extinction coefficients for Infrared absorption bands of pyridine adsorbed on solid acid catalysts, *J. Catal.* **141** (1993) 347–354.

Eslami M., Khorassani R., Coltorti M., Malferrari D., Faccini B., Ferretti G., Di Giuseppe D., Fotovat A., Halajnia A., Leaching behaviour of a sandy soil amended with natural and NH_4^+ and K^+ saturated clinoptilolite and chabazite, *Arch. Agron. Soil Sci.* **64** (2018) 1142–1151.

Farías T., Ruiz-Salvador A.R., Velazco L., de Ménorval L.C., Rivera A., Preparation of natural zeolitic supports for potential biomedical applications, *Mater. Chem. Phys.* **118** (2009) 322–328.

Fateminia F.S. and Falamaki C., Zero valent nano-sized iron/clinoptilolite modified with zero valent copper for reductive nitrate removal, *Process. Saf. Environ.* **91** (2013) 304–310.

Fernandes D.R., Rocha A.S., Mai E.F., Mota C.J.A., Teixeira da Silva V., Levulinic acid esterification with ethanol to ethyl levulinate production over solid acid catalysts, *Appl. Catal. A-Gen.* **425–426** (2012) 199–204.

Figueiredo H. and Quintelas C., Tailored zeolites for the removal of metal oxyanions: Overcoming intrinsic limitations of zeolites, *J. Hazard. Mater.* **274** (2014) 287–299.

Freundlich H.M.F., Over the adsorption in solution, *J. Phys. Chem.* **57** (1906) 385–470.

Garcia Y, Rodriguez-Iznaga I., de Menorval L.C., Llewellyn P., Maurin G., Lewis D.W., Binions R., Autie M., Ruiz-Salvador A.R., Step-wise dealumination of natural clinoptilolite: Structural and physicochemical characterization, *Micropor. Mesopor. Mat.* **135** (2010) 187–196.

Gavrilović B., Popović S., Ćirić M., Gotovina Ž., Pantelić A., Subakov–Simić G., Vidović M., Seasonal aspects of water quality in the Grlište reservoir, Eastern Serbia, *The Environment* **1** (2014) 17–21.

Gedik K. and Imamoglu I., Removal of cadmium from aqueous solutions using clinoptilolite: Influence of pretreatment and regeneration, *J. Hazard. Mater.* **155** (2008) 385–392.

Gennaro B., Catalanotti L., Cappelletti P., Langella A., Mercurio M., Serri C., Biondi M., Mayol L., Surface modified natural zeolite as a carrier for sustained diclofenac release: A preliminary feasibility study, *Colloid. Surface. B* **130** (2015) 101–109.

Girisuta B., Danon B., Manurung R., Janssen L.P.B.M., Heeres H.J., Experimental and kinetic modelling studies on the acid-catalysed hydrolysis of the water hyacinth plant to levulinic acid, *Bioresource Technol.* **99** (2008) 8367–8375.

Godelitsas A. and Armbruster T., HEU-type zeolites modified by transition elements and lead, *Microporous and Mesoporous Materials* **61** (2003) 3–24.

Gómez Bernal H., Benito P., Rodríguez-Castellón E., Raspolli Galletti A. M., Funaioli T., Synthesis of isopropyl levulinate from furfural: Insights on a cascade production perspective, *Appl. Catal. A-Gen.* **575** (2019) 111–119.

Gouran–Orimi R., Mirzayi B., Nematollahzadeh A., Tardast A., Competitive adsorption of nitrate in fixed-bed column packed with bio-inspired polydopamine coated zeolite, *J. Environ. Chem. Eng.* **6** (2018) 2232–2240.

Grahovac J.A., Dodić J.M., Dodić S.N., Popov S.D., Vučurović D.G., Jokić A.I., Future trends of bioethanol co-production in Serbian sugar plants, renew, *Sust. Energ. Rev.* **16** (2012) 3270–3274.

Grand view survey: https://europe.iza-structure.org/IZA-SC/ftc_table.php (Accessed on 4th July 2019)

Guan F.F., Ma T.T., Yuan X., Zeng H.Y., Wu J., Sn-modified NaY zeolite catalysts prepared by post-synthesis methods for Baeyer–Villiger oxidation, *Catal. Lett.* **148** (2018) 443–453.

Guan H., Bestland E., Zhu C., Zhu H., Albertsdottir D., Hutson J., Simmons C.T., Ginic-Markovic M., Tao X., Ellis A.V., Variation in performance of surfactant loading and resulting nitrate removal among four selected natural zeolites, *J. Hazard. Mater.* **183** (2010) 616–621.

Guaya D., Valderrama C., Farran A., Armijos C., Cortina J.L., Simultaneous phosphate and ammonium removal from aqueous solution by a hydrated aluminum oxide modified natural zeolite, *Chem. Eng. J.* **271** (2015) 204–213.

Guaya D., Valderrama C., Farran A., Cortina J.L., Modification of a natural zeolite with Fe(III) for simultaneous phosphate and ammonium removal from aqueous solutions, *J. Chem. Technol. Biotechnol.* **91** (2016) 1737–1746.

Guo T., Qiu M., Qi X., Selective conversion of biomass-derived levulinic acid to ethyl levulinate catalyzed by metal organic framework (MOF)-supported polyoxometales, *Appl. Catal. A-Gen* **572** (2019) 168–175.

Gutiérez-Báez R., Toledo-Antonio J.A, Cortes-Jácome M.A., Sebastian P.J., Vázquez A., Effects of the SO_4 groups on the textural properties and local order deformation of SnO_2 rutile structure, *Langmuir* **20** (2004) 4265–4271.

Habuda-Stanić M., Kalajdžić B., Kuleš M., Velić N., Arsenite and arsenate sorption by hydrous ferric oxide/polymeric material, *Desalination*, **229** (2008) 1–9.

Hailu Y., Tilahum E., Brhane A., Resky H., Sahu O., Ion exchanges process for calcium, magnesium and total hardness from ground water with natural zeolite, *Groundwater for Sustainable Development* **8** (2019) 457–469.

Haque M.E., Nairuzzaman M., Hasan Imam H., X-Ray diffraction studies of some madhupur clay samples of Savar and Dhaka of Bangladesh with especial emphasis on clay minerals, *IJSTR* **2** (2013) 174–180.

Hayes D.J., Fitzpatrick S.W., Hayes M.H.B., Ross J.R.h., The Biofine Process-Production of levulinic acid, furfural, and formic acid from lignocellulosic feedstocks, In: Biorefineries-Industrial Processes and Products: Status Quo and Future Directions, Wiley-VCH VerlagGmbH, 2008 pp. 139–164.

Ho Y.S. and McKay G., Sorption of dye from aqueous solution by peat, *Chem. Eng. J.* **70** (1998) 115–124.

Ho Y.S., Review of second-order models for adsorption systems, *J. Hazard. Mater.* **136** (2006) 681–689.

Hou L., Liang Q., Wang F., Mechanisms that control the adsorption–desorption behavior of phosphate on magnetite nanoparticles: the role of particle size and surface chemistry characteristics, *RSC Adv.* **10** (2020) 2378–1388.

House J.E., Principles of chemical kinetics, Elsevier, Amsterdam, (2007), pp.1–23.

Hrenović J., Milenković J., Goic-Barisic I., Rajić N., Antibacterial activity of modified natural clinoptilolite against clinical isolates of *Acinetobacter baumannii, Micropor. Mesopor. Mat.* **169** (2013) 148–152.

https://www.rtk.rs/66965/celije-cvetanje-jezera-voda-iz-vodovoda-je-ispravna-za-pice/

Hu X., Wang S., Westerhof R.J.M., Wu L., Song Y., Dong D., Li C.Z., Acid-catalyzed conversion of C_6 sugar monomer/oligomers to levulinic acid in water, tetrahydrofuran and toluene: Importance of the solvent polarity, *Fuel* 141 (2015) 56–63.

Huo H., Lina H., Donga Y., Cheng H., Wang H., Cao L., Ammonia-nitrogen and phosphates sorption from simulated reclaimed waters by modified clinoptilolite, *J. Hazard. Mater.* **229-230** (2012) 292–297.

Inglezakis V.J., Loizidou M.D., Grigoropoulou H.P., Ion exchange of Pb^{2+},Cu^{2+},Fe^{3+}, and Cr^{3+} on natural clinoptilolite: selectivity determination and influence of acidity on metal uptake, *J. Colloid. Interf. Sci.* **261** (2003) 49–54.

Islam M. and Patel R., Nitrate sorption by thermally activated Mg/Al chloride hydrotalcite-like compound, *J. Hazard. Mat.* **169** (2009) 524–531.

Islam M., Mishra C., Patel R., Physicochemical characterization of hydroxyapatite and its application towards removal of nitrate from water, *J. Environ. Manage.* **91** (2010) 1883–1891.

Jaskūnas A., Subačius B., Šlinkšienė R., Adsorption of potassium ions on natural zeolite: kinetic and equilibrium studies, *Chemija* **26** (2015) 69–78.

Jeon C.S., Baek K., Park J.K., Oh Y.K., Lee S.D., Adsorption characteristics of As(V) on iron-coated zeolite, *J. Hazard. Mater.* **163** (2009) 804–808.

Jevtić S., Arčon I., Rečnik A., Babić B., Mazaj M., Pavlović J., Matijašević D., Nikšić M., Rajić N., The iron(III)-modified natural zeolitic tuff as an adsorbent and carrier for selenium oxyanions, *Micropor. Mesopor. Mat.* **197** (2014) 92–100.

Jevtić S., Grujić S., Hrenović J., Rajić N., Surfactant-modified clinoptilolite as a salicylate carrier, salicylate kinetic release and its antibacterial activity, *Micropor. Mesopor. Mat.* **159** (2012) 30–35.

Jiménez-Cedillo J., Olguín M.T., Fall Ch., Colín A., Adsorption capacity of iron- or iron–manganese-modified zeolite-rich tuffs for As(III) and As(V) water pollutants, *Appl. Clay Sci.* **54** (2011) 206–216.

Jiménez-Cedillo M.J., Olguín M.T., Fall Ch., Adsorption kinetic of arsenates as water pollutant on iron, manganese and iron–manganese-modified clinoptilolite-rich tuffs, *J. Hazard. Mater.* **163** (2009) 939–945.

Joshi H., Moser B.R., Toler J., Smith W.F., Walker T., 2011. Ethyl levulinate: a potential bio-based diluent for biodiesel which improves cold flow properties, *Biomass Bioenerg.* **35** (2011) 3262–3266.

Kang S., Fu J., Zhang G., From lignocellulosic biomass to levulinic acid: A review on acid-catalyzed hydrolysis, *Renew. Sust. Energ. Rev.* **94** (2018) 340–362.

Kaplanec I., Rečnik A., Mali. G. Rajic N., Study of the iron(III)-modified clinoptilolite in the adsorption of phosphate from aqueous medium: mechanism and kinetics, *Desalin. Water Treat.* **78** (2017) 231–240.

Karadžić V., Subakov-Simić G., Krizmanić J., Natić D., Phytoplankton and eutrophication development in the water supply reservoirs Garaši and Bukulja (Serbia), *Desalination*, **255** (2010) 91–96.

Karge H.G., Geidel E., in: H.G. Karge, J. Weitkamp (Eds.), Molecular Sieves 4, Characterization I, Springer, Berlin, 2003, pp. 1–201.

Katsou E., Malamis S., Tzanoudaki M., Haralambous K.J., Loizidou M., Regeneration of natural zeolite polluted by lead and zinc in wastewater treatment systems, *J. Hazard. Mater.* **189** (2011) 773–786.

Khder A.S., El-Sharkawy E.A., El-Hakam S.A., Ahmed A.I., Surface characterization and catalytic activity of sulfated tin oxide catalyst, *Catal. Commun.* **9** (2008) 769–777.

Kim J., Li W., Philips B.L., Grey C.P., Phosphate adsorption on the iron oxyhydroxides goethite (α-FeOOH), akaganeite (β-FeOOH), and lepidocrocite (γ-FeOOH): a ^{31}P NMR Study, *Energy Environ. Sci.* **4** (2011) 4298–4305.

Kiran B. and Kaushik A., Chromium binding capacity of *Lyngbya putealis* exopolysaccharides, *Biochem. Eng. J.*, **38** (2008) 47–54.

Kolahchi Z. and Jalali M., Effect of water quality on the leaching of potassium from sandy soil, *J. Arid Environ.* **68** (2007) 624–639.

Kragović M., Daković A., Marković M., Krstić J., Diego Gatta G., Rotiroti N., Characterization of lead sorption by the natural and Fe(III)-modified zeolite, *Appl. Surf. Sci.* **283** (2013) 764–774.

Kucherova A.E., Shubina I.N., Pas'koa T.V., Perspective sorbents based on zeolite modified with nanostructures for the purification of aqueous media from organic impurities, *Nanotechnologies in Russia*, **13** (2018) 327–330.

Kuwahara Y., Fujitani T., Yamashita H., Esterification of levulinic acid with ethanol over sulfated mesoporous zirconosilicates: influences of the preparation conditions on the structural properties and catalytic performances, *Catal. Today* **237** (2014) 18–28.

Kuwahara Y., Kaburagi W., Nemoto K., Fujitani T., Esterification of levulinic acid with ethanol over sulfated Si-doped ZrO_2 solid acid catalyst: Study of the structure–activity relationships, *Appl. Catal. A-Gen.* **476** (2014) 186–196.

Lagergren S., About the theory of so-called adsorption of soluble substances, K. Sven. Vetenskapsakad. Handl. 24 (1898) 1–39.

Lalley J., Han C., Li X., Dionysiou D.D., Nadagouda M.N., Phosphate adsorption using modified iron oxide-based sorbents in lake water: kinetics, equilibrium, and column tests, *Chem. Eng. J.* **284** (2016) 1386–1396.

Langmuir I., The constitution and fundamental properties of solids and liquids, *J. Am. Chem. Soc*. **38** (1916) 2221–2295.

Lassoued A., Dkhil B., Gadri A., Ammar S., Control of the shape and size of iron oxide (α-Fe_2O_3) nanoparticles synthesized through the chemical precipitation method, *Results Phys.* **7** (2017) 3007–3015.

Latifah O., Ahmed O.H., Muhamad N., Majid A., Enhancing nitrogen availability from urea using clinoptilolite zeolite, *Geoderma* **306** (2017) 152–159.

Lei T., Wang Z., Chang X., Lin L., Yan X., Sun Y., Shi X., He X., Zhu J., Performance and emission characteristics of a diesel engine running on optimized ethyl levulinate-biodiesel-diesel blends, *Energy* **95** (2016) 29–40.

Li M., Liu J., Xu Y., Qian G., Phosphate adsorption on metal oxides and metal hydroxides: A comparative review, *Environ. Rev.* **24** (2016) 319–332.

Li Z., Wnetrzak R., Kwapinski W., Leahy J.J., Synthesis and characterization of sulfated TiO_2 nanorods and ZrO_2/TiO_2 nanocomposites for the esterification of biobased organic acid, *ACS Appl. Mater. Inter.* **4** (2012) 4499–4505.

Lin H., Liu Q., Dong Y., He Y., Wang L., Physicochemical properties and mechanism study of clinoptilolite modified by NaOH, *Micropor. Mesopor. Mat.* **218** (2015) 174–179.

Lin H., Strull J., Liu Y., Karmiol Z., Plank K., Miller G., Guo Z., Yang L., High yield production of levulinic acid by catalytic partial oxidation of cellulose in aqueous media, *Energy Environ. Sci.* **5** (2012) 9773–9777.

Lippmaa E., Samoson A., Magi M., High-resolution aluminum-27 NMR of aluminosilicates, *J. Am. Chem. Soc.* **108** (1986) 1730–1735.

Liu J., Wang X-Q., Yang B.B., Liu C.L., Xu C.L., Dong W.S., Highly efficient conversion of glucose into methyl levulinate catalyzed by tin-exchanged montmorillonite, *Renew. Energ.* **120** (2018) 231–240.

Liu T., Feng J., Wan Y., Zheng S., Yang L., ZrO_2 nanoparticles confined in metal organic frameworks for highly effective adsorption of phosphate, *Chemosphere* **210** (2018) 907–916.

Liu X. and Zhang L., Removal of phosphate anions using the modified chitosan beads: Adsorption kinetic, isotherm and mechanism studies, *Powder Technol.* **277** (2015) 112–119.

Mahabadi A.A., Hajabbasi M.A., Khademi H., Kazemian H., Soil cadmium stabilization using an Iranian natural zeolite, *Geoderma* **137** (2007) 388–393.

Maheria K.C., Kozinski J., Dalai A., Esterification of levulinic acid to *n*-butyl levulinate over various acidic zeolites, *Catal. Lett.* **143** (2013) 1220–1225.

Malekian R., Abedi-Koupai J., Eslamian S.S., Influences of clinoptilolite and surfactant-modified clinoptilolite zeolite on nitrate leaching and plant growth, *J. Hazard. Mater.* **185** (2011) 970–976.

Mallesham B., Sudarsanam P., Raju G., Reddy B.M., Design of highly efficient Mo and W-promoted SnO_2 solid acids for heterogeneous catalysis: Acetalization of bio-glycerol, *Green Chem.* **15** (2013) 478–489.

Matsuhashi H., Miyazaki H., Kawamura Y., Nakamura H., Arata K., Preparation of a solid superacid of sulfated tin oxide with acidity higher than that of sulfated zirconia and its applications to aldol condensation and benzoylation, *Chem. Mater.* **13** (2001) 3038–3042.

Melero J.A., Morales G., Iglesias J., Paniagua M., Hernández B., Penedo S., Efficient conversion of levulinic acid into alkyl levulinates catalyzed by sulfonic mesostructured silicas, *Appl. Catal.A-Gen.* **466** (2013) 116–122.

Mihaly-Cozmuta L., Mihaly –Cozmuta A., Peter A., Nicula C., Tutu H., Silipas D., Indrea E., Adsorption of heavy metal cations by Na-clinoptilolite: Equilibrium and selectivity studies, *J. Environ. Manage.* **137** (2014) 69–80.

Mitrogiannis D., Psychoyou M., Baziotis I., Inglezakis V.J., Koukouzas N., Tsoukalas N., Palles D., Kamitsos E., Oikonomou G., Markou G., Removal of phosphate from aqueous solutions by adsorption onto $Ca(OH)_2$ treated natural clinoptilolite, *Chem. Eng. J.* **320** (2017) 510–522.

Mohorami S. and Jalali M., Phosphorus leaching from a sandy soil in the presence of modified and un-modified adsorbents, *Environ. Monit. Assess.* **186** (2014) 6565–6576.

Monazam E.R., Shadle L.J., Miller D.C., Pennline H.W., Fauth D.J., Hoffman J.S., Gray M.L., Equilibrium and kinetics analysis of carbon dioxide capture using immobilized amine on a mesoporous silica, *AlChE J.* **59** (2013) 923–935.

Mood S.H., Golfeshan A.H., Tabatabaei M., Jouzani G.S., Najafi G.H., Gholami M., Ardjmand M., Lignocellulosic biomass to bioethanol, a comprehensive review with a focus on pretreatment, *Renew. Sust. Energ. Rev.* **27** (2013) 77–93.

Moore D.M. and Reynolds R.C., X-ray Diffraction and the Identification and Analysis of Clay Minerals, Oxford University Press, Oxford, 1997, pp. 227–258.

Moradzadeh M., Moazed H., Sayyad G., Khaledian K., Transport of nitrate and ammonium ions in a sandy loam soil treated with potassium zeolite – Evaluating equilibrium and non-equilibrium equations, *Acta Ecol. Sin.* **34** (2014) 342–350.

Moraetis D., Papagiannidou S., Pratikakis A., Pentari D., Komnitsas K., Effect of zeolite application on potassium release in sandy soils amended with municipal compost, *Desalin. Water Treat.* **57** (2015) 1–12.

Moreno J.I., Jaimes R., Gómez R., Niño-Gómez M.E., Evaluation of sulfated tin oxides in the esterification reaction of free fatty acids, *Catal. Today* **172** (2011) 34–40.

Morone A., Apte M., Pandey R.A., Levulinic acid production from renewable waste resources: Bottlenecks, potential remedies, advancements and applications, *Renew. Sust. Energ. Rev.* **51** (2015) 986–997.

Moulder J.F., Stickle W.F., Sobol P.E., Bomben, K.D. Handbook of X-Ray Photoelectron Spectroscopy, Physical Electronics Inc. Eden Prairie, third ed., Minnesota, USA, 1995.

Mozgawa W., Krol M., Pichor W., Use of clinoptilolite for the immobilization of heavy metal ions and preparation of autoclaved building composites, *J. Hazard. Mater*. **168** (2009)1482–1489.

Naghash A. and Nezamzadeh-Ejhieh A., Comparison of the efficiency of modified clinoptilolite with HDTMA and HDP surfactants for the removal of phosphate in aqueous solutions, *J. Ind. Eng. Chem.* **31** (2015) 185–191.

Nairat M., Shahwan T., Eroğlu A.E., Fuchs H., Incorporation of iron nanoparticles into clinoptilolite and its application for the removal of cationic and anionic dyes, *J. Ind. Eng. Chem.* **21** (2015) 1143–1151.

Najfi-Ghiri M., Effects of zeolite and vermicompost applications on potassium release from calcareous soils, *Soil Water Res.* **9** (2014) 31–37.

Nandiwale K.Y., Bokade V.V., Esterification of renewable levulinic acid to *n*-butyl levulinate over modified H-ZSM-5, *Chem. Eng. Technol.* **38** (2015) 246–252.

Nandiwale K.Y., Sonar S.K., Niphadkar P.S., Deshpande S.S., Bokade V.V., Esterification of renewable levulinic acid to ethyl levulinate biodiesel catalyzed by highly active and reusable desilicated H-ZSM-5, *J. Chem. Technol. Biot.* **89** (2014) 1507–1515.

Nandiwale K.Y., Sonar S.K., Niphadkar P.S., Joshi P.N., Deshpande S.S., Patil V.S., Bokade V.V., Catalytic upgrading of renewable levulinic acid to ethyl levulinate biodiesel using dodecatungstophosphoric acid supported on desilicated H-ZSM-5 as catalyst, *Applied Catal. Gen-A* **460-461** (2013) 90–98.

Nandiwale K.Y., Yadava S.K., Bokade V.V., Production of octyl levulinate biolubricant over modified H-ZSM-5: Optimization by response surface methodology, *J. Energy Chem.* **23** (2014) 535–541.

Nekhunguni P.M., Tavengwa N.T., Tutu H., Investigation of As(V) removal from acid mine drainage by iron (hydr) oxide modified zeolite, *J. Environ. Manage.* **197** (2017) 550–558.

Nezamzadeh-Ejhieh A. and Khodabakshi-Chermahini F., Incorporated ZnO onto nano clinoptilolite particles as the active centers in the photodegradation of phenylhydrazin, *J. Ind. Eng. Chem.* **20** (2014) 695–704.

Noda L., De Almeida R., Probst L.F., Goncalves N., Characterization of sulfated TiO_2 prepared by the sol–gel method and its catalytic activity in then-hexane isomerization reaction, *J. Mol. Catal. A-Chem* **225** (2005) 39–46.

Øgaard A.F. and Krogstad T., Release of interlayer potassium in Norwegian grassland soils, *J. Plant. Nutr. Soil Sci.* **168** (2005) 80–88.

Oh J., Yang S., Kim C., Choi I., Kim J.H., Lee H., Synthesis of biolubricants using sulfated zirconia catalysts, *Appl. Catal.A-Gen.* **455** (2013) 164–671.

Omotude I., Okoronkwo A., Oluwashina O., Derived and thiourea-functionalized silica for cadmium removal: isotherm, kinetic and thermodynamic studies, *Appl. Water Sci.* **8** (2018) 21–34.

Ostojić A., Čurčić S., Čomić Lj., Topuzović M., Estimate of the Eutrophication Process in Gruža Reservoir (Serbia and Montenegro), *Acta Hydrochim. Hydrobiol.* **33** (2005) 605–613.

Oumabady A.C., Rajendran N.M., Selvaraju R., Mineralogical identification on polluted soils using XRD method, *J. Environ. Nanotechnol.* **3** (2014) 23–29.

Özcan A., Sahin M., Özcan A.S., Adsorption of nitrate ions onto sepiolite and surfactant-modified sepiolite, *Adsorpt. Sci. Technol.* **23** (2005) 323–34.

Padilla F.M., Gallardo M., Manzano-Agugliaro F., Global trends in nitrate leaching research in the 1960–2017 period, *Sci. Total Environ*. **643** (2018) 400–413.

Pantelić N., Dramićanin A.M., Milovanović D.B., Popović-Đorđević J.B., Kostić A.Ž., Evaluation of the quality of drinking water in Rasina district, Serbia: Physicochemical and bacteriological viewpoint, *Rom. J. Phys.* **62** (2017) 818.

Pasquale G., Vázquez P., Romanelli G., Baronetti G., Catalytic upgrading of levulinic acid to ethyl levulinate using reusable silica-included Wells-Dawson heteropolyacid as catalyst, *Catal. Commun.* **18** (2012) 115–120.

Patil C.R., Niphadkar P.S., Bokade V.V., Joshi P.N., Esterification of levulinic acid to ethyl levulinate over bimodal micro-mesoporous H/BEA zeolite derivatives, *Catal. Commun.* **43** (2014) 188–191.

Pavelić K., Hadžija M., Bedrica Lj., Pavelić J., Đikić I., Katić M., Kralj M., Bosnar M.H., Kapitanović S., Poljak-Blaži M., Križanac Š., Stojković R., Jurin M., Subotić B., Čolić M., Natural zeolite clinoptilolite: new adjuvant in anticancer therapy, *J. Mol. Med.* **78** (2001) 708–720.

Pederstad K. and Jørgensen P., Weathering in a marine clay during postglacial time, *Clay Miner.* **20** (1985) 477–491.

Peng L., Lin L., Li H., Yang Q., Conversion of carbohydrates biomass into levulinate esters using heterogeneous catalysts, *Appl. Energ.* **88** (2011) 4590–4596.

Peng L., Lin L., Zhang J., Shi J., Liu S., Solid acid catalyzed glucose conversion to ethyl levulinate, *Appl. Catal. A-Gen.* **397** (2011) 259–265.

Peng L., Lin L., Zhang J., Zhuang J., Zhang B., Gong Y., Catalytic conversion of cellulose to levulinic acid by metal chlorides, *Molecules*, **15** (2010) 5258–5272.

Pešić S., Eutrophication and aquatic weevils (Coleoptera: Curculionoidea, Curculionidae), *Kragujevac J. Sci.* **28** (2006) 129–138.

Platero E.E., Mentruit M.P., Areán C.O., Zecchina A., FTIR studies on the acidity of sulfated zirconia prepared by thermolysis of zirconium sulfate, *J. Catal.* **162** (1996) 268–276.

Popova M., Shestakova P., Lazarova H, Dimitrov M., Kovacheva D., Szegedi A., Mali G., Dasireddy V., Likozar B., Wilde N., Gläser R., Efficient solid acid catalysts based on sulfated tin oxides for liquid phase esterification of levulinic acid with ethanol, *Appl. Catal. A-Gen.* **560** (2018) 119–131.

Popova M., Szegedi A., Lazarova H., Ristić A., Kalvachev Y., Atanasova G., Wilde N., Novak Tušar N., Gläser R., Synthesis of biomass derived levulinate esters on novel sulfated Zr/KIL-2 composite catalysts, *Micropor. Mesopor. Mat.* **235** (2016) 50–58.

Pravilnik o higijenskoj ispravnosti vode za piće, Službeni list SRJ, br. 42/98 i 44/99 i br. 28/2019.

Pulidindi I.D. and Kim T.H., Conversion of levulinic acid from various herbaceous biomass species using hydrochloric acid and effects of particle size and delignification, *Energies* **11** (2018) 621–633.

Rackemann D.W., Doherty W.O.S, The conversion of lignocellulosics to levulinic acid, *Biofuels, Biprod. Bior.* **5** (2011) 198–214.

Rajalakshmi R., Vasudevan Srinivasan V., Pachamuthu M.P., Maheswari R., Characterizations of tin (SnO_2) doped KIT-5 by direct synthesis, *Mater. Chem. Phys.* **154** (2015) 164–169.

Rajic N., Stojakovic Đ., Jevtic S., Zabukovec Logar N., Kovac J., Kaucic V., Removal of aqueous manganese using the natural zeolitic tuff from theVranjska Banja deposit in Serbia, *J. Hazard. Mater.* **172** (2009) 1450–1457.

Rajić N., Stojaković Đ., Jovanović M., Zabikovec Logar N., Mazaj M., Kaučić V., Removal of nickel(II) ions from aqueous solutions using the natural clinoptilolite and preparation of nano-NiO on the exhausted clinoptilolite, *Appl. Surf. Sci.* **257** (2010) 1524 –1532.

Rajic N., Stojakovic Dj., Daneu N., Recnik A., The formation of oxide nanoparticles on the surface of natural clinoptilolite, *J. Phys. Chem. Solids*, **72** (2011) 800–803.

Rajić N., Zabukovec Logar N., Rečnik A., El-Roz M., Thibault-Starzyk F., Sprenger P., Hannevold L., Andersen A., Stocker M., Hardwood lignin pyrolysis in the presence of nano-oxide particles embedded onto natural clinoptilolite, *Micropor. Mesopor. Mat.* **176** (2013) 162–167.

Ramli N.A.S., Sivasubramaniam D., Amin N.A.S., Esterification of levulinic acid using ZrO_2-supported phosphotungstic acid catalyst for ethyl levulinate production, *Bioenerg. Res.* **10** (2017) 1105–1116.

Reháková M., Čuvanová S., Dzivák M., Rimár J., Gaval'ová Z., Agricultural and agrochemical uses of natural zeolite of the clinoptilolite type, *Curr. Opin. Solid St. M.* **8** (2004) 397–404.

Rezaei M. and Movahedi Naeini S.A.R., Kinetics of potassium desorption from the loess soil, soil mixed with zeolite and the clinoptilolite zeolite as influenced by calcium and ammonium, *J. Appl. Sci.* **9** (2009) 3335–3342.

Rivera A., Farías T., Clinoptilolite–surfactant composites as drug support: A new potential application, *Micropor. Mesopor. Mat.* **80** (2005) 337–346.

Roginsky S.Z. and Zeldovich J., The catalytic oxidation of carbon monoxide on manganese dioxide, *Acta Physicochim. URSS* **1** (1934) 554–575.

Salvi H.M. and Yadav G.D., Surface functionalization of SBA-15 for immobilization of lipase and its application in synthesis of alkyl levulinates: Optimization and kinetics, *Biocatal. Agric. Biotechnol.* 18 (2019) 101038.

Saravanamurugan S. and Riisager A., Solid acid catalysed formation of ethyl levulinate and ethyl glucopyranoside from mono- and disaccharides, *Catal. Commun.* **17** (2012) 71–75.

Schick J., Caullet P., Paillaud J.L., Patarin J., Mangold-Callarec C., Batch-wise nitrate removal from water on a surfactant-modified zeolite, *Micropor. Mesopor. Mat.* **132** (2010) 39–400.

Schick J., Caullet P., Paillaud J.L., Patarin J., Mangold-Callarec C., Nitrate sorption from water on a Surfactant-Modified Zeolite. Fixed-bed column experiments, *Micropor. Mesopor. Mat.* **142** (2011) 549–556.

Schollenberger C.J. and Simon R.H., Determination of exchange capacity and exchangeable bases in soil-ammonium acetate method, *Soil Sci.* **59** (1945) 13–24.

Sepehri S., Heidarpour M., Abedi-Koupai J., Nitrate Removal from Aqueous Solution Using Natural Zeolite-Supported Zero-Valent Iron Nanoparticles, *Soil Water Res.* **9** (2014) 224–232.

Shi W. and Li J., A new deactivation mechanism of sulfate-promoted iron oxide, *Catal. Lett.* **143** (2013) 1285–1293.

Shi W., Fu Y., Jiang W., Ye Y., Kang J., Liu D., Enhanced phosphate removal by zeolite loaded with Mg–Al–La ternary (hydr)oxides from aqueous solutions: Performance and mechanism, *Chem. Eng J.* **357** (2019) 33–44.

Šiljeg M., Cerjan Stefanović Š., Mazaj M., Novak Tušar N., Arčon I., Kovač J., Margeta K., Kaučić V., Zabukovec Logar N., Structure investigation of As(III)- and As(V)-species bound to Fe-modified clinoptilolite tuffs, *Micropor. Mesopor. Mat.* **118** (2009) 408–415.

Sing K.S.W., Everett D.H., Haul R.A.W., Moscou L., Pierotti R.A., Rouquerol J., Siemieniewska T., Reporting physisorption data for gas/solid systems with special reference to the determination of surface area and porosity, *Pure Appl. Chem.* **57** (1985) 603–619.

Singh N.B., Nagpal G., Agrawal S., Rachnaa, Water purification by using adsorbents: A review, *Environ. Technol. Inno.* **11** (2018) 187–240.

Songolzadeh M., Soleimani M., Takht Ravanchi M., Using Modified Avrami kinetic and two component isotherm equation for modelling of CO_2/N_2 adsorption over a 13X zeolite bad, *J. Nat. Gas Sci. Eng.* **27** (2015) 831–841.

Souza I.M.S., Gurgel G.C.S., Medeiros A.M., Zonta E., Ruiz J.A.C., Paskocimas C.A., Motta F.V., Bomio M.R.D., The use of clinoptilolite as carrier of nitrogened fertilizer with controlled release, *J. Environ. Chem. Eng.* **6** (2018) 4171–4177.

Souza V.C., Villarroel-Rocha J., Araújo M.J.G., Sapag K., Pergher S.B.C., Basic treatment in natural clinoptilolite for improvement of physicochemical properties, *Minerals-Basel* **8 (12)** (2018) 595–609.

Sowmiya M., Sharma A., Parsodkar S., Mishra B.G., Dubey A., Nanosized sulfated SnO_2 dispersed in the micropores of Al-pillared clay as an efficient catalyst for the synthesis of some biologically important molecules, *Appl. Catal. A-Gen.* **33** (2007) 272–280.

Soylu G.Z.P., Özcelik Z., Boz I., Total oxidation of toluene over metal oxides supported on a natural clinoptilolite-type zeolite, *Chem. Eng. J.*, **162** (2010) 380–387.

Stec M. and Grzebyk M., The implementation of the Strategy Europe 2020 objectives in European Union countries: The concept analysis and statistical evaluation, *Qual. Quant.* **52** (2018) 119–133.

Svirčev Z., Krstić S., Miladinov-Mikov M., Baltić V., Vidović M., Freshwater cyanobacterial blooms and primary liver cancer epidemiological studies in Serbia, *J. Environ. Sci. Heal. C* **27** (2009) 36–55.

Svirčev Z., Tokodi N., Drobac D., Review of 130 years of research on cyanobacteria in aquatic ecosystems in Serbia presented in a Serbian Cyanobacterial Database, *AIOL Journal* **8** (2017) 153–160.

Szymański W., Skiba M., Nikorych V., Kuligiewicz A., Nature and formation of interlayer fillings in clay minerals in Albeluvisols from the Carpathian Foothills, Poland, *Geoderma*, **235–236** (2014) 396–409**.**

Tarasevich Y.I., Krysenko D.A., Polyakov V.E., Aksenenko E.V., The heats of exchange of transition metal ions on the Na form of clinoptilolite, *Russ. J. Phys. Chem. A* **82** (2008) 1506–1511.

Teimouri A., Nasab Sh. Ghanavati, Vahdatpoor N., Habibollahi S., Salavati H., Najafi Chermahini A., Chitosan /Zeolite Y/Nano ZrO_2 nanocomposite as an adsorbent for the removal of nitrate from the aqueous solution, *Int. J. Biol. Macromol.* **93** (2016) 254–266.

Tejero M.A., Ramírez E., Fité C., Tejero J., Cunill F., Esterification of levulinic acid with butanol over ion exchange resins, *Appl. Catal.A-Gen.* **517** (2016) 56–66.

Temkin M.J. and Pyzhev V., Kinetics of ammonia synthesis on promoted iron catalysts *Acta Physicochim. URSS* **12** (1940) 217–222.

Thapa I., Mullen B., Saleem A., Leibig C., Baker T., Giorgi J.B., Efficient green catalysis for the conversion of fructose to levulinic acid, *Appl. Catal. A-Gen.* **539** (2017) 70–79.

The report on the environmental situation in the Republic of Serbia for 2017, Ministry of Environmental Protection, Serbian Environmental Protection Agency, Belgrade 2018, pp.40–53.

Thomas G.W., Methods of Soil Analysis, Part 3-Chemical Methods, Soil Science Society of America, Madison, WI, 1996, pp. 475–490.

Thomas G.W., Methods of Soil Analysis, Part 3-Chemical Methods, Soil Science Society of America, Madison, WI, 1996, pp. 961–1009.

Tokodi N., Drobac D., Meriluoto J., Lujić J., Marinović Z., Važić T., Nybom S., Simeunović J., Dulić T., Lazić G., Petrović T., Vuković-Gačić B., Sunjog K., Kolarević S., Kračun-Kolarević M., Subakov-Simić G., Miljanović B., Codd G.A., Svirčev Z., Cyanobacterial effects in Lake Ludoš, Serbia - Is preservation of a degraded aquatic ecosystem justified?, *Sci. Total Environ.* **635** (2018) 1047–1062.

Tomečková V., Reháková M., Mojžišová G., Magura J., Wadsten T., Zelenáková K., Modified natural clinoptilolite with quercetin and quercetin dihydrate and the study of their anticancer activity, *Micropor. Mesopor. Mat.* **147** (2012) 59–67.

Top A. and Ülkü S., Silver, zinc, and copper exchange in a Na-clinoptilolite and resulting effect on antibacterial activity, *Appl. Clay Sci.* **27** (2004) 13–19.

Tran H.N., You S.J., Hosseini-Bandegharaei A., Chao H.P., Mistakes and inconsistencies regarding adsorption of contaminants from aqueous solutions: A critical review, *Water Res.* **120** (2017) 88–116.

Treacy M.M.J. and Higgins J.B., Collection of Simulated XRD Powder Patterns for Zeolites, Elsevier, Amsterdam (2001), pp. 186–187.

Turan M., Mart U., Yüksel B., S. Çelik M.S., Lead removal in fixed-bed columns by zeolite and sepiolite, *Chemosphere* **60** (2005) 1487–1492.

Usman A.R.A., Kuzyakov Y., Lorenz K., Stahr K., Remediation of a soil contaminated with heavy metals by immobilizing compounds, *J. Plant Nutr. Soil Sci.* **169** (2006) 205–212.

Vargas A.M.M., Cazetta a.L., Kunita M.H., Silva T.L., Almeida V.C., Adsorption of methylene blue on activated carbon produced from flamboyant pods (*Delonix regia*): Study of adsorption isotherms and kinetic models, *Chem. Eng. J.* **168** (2011) 722–730.

Vasudevan P.T. and Briggs M., Biodiesel production-current state of the art and challenges, *J. Ind. Microbiol. Biotechnol.* **35** (2008) 421–430.

Vujasinović S., Zarić J., Kaluđerović D., Matić I., Mogućnosti anaerobne biodegradacije nitrata u podzemnim vodama požarevačkog izvorišta "Ključ" – primenom emulzifikovanog biljnog ulja, Zaštita materijala, **55** (2014) 69–75.

Wakerley D.W., Kuehnel M.F., Orchard K.L., Ly K.H., Rosser T.E., Reisner E., Solar-driven reforming of lignocellulose to H_2 with a CdS/CdO_x photocatalyst, *Nat. Energy* **2** (2017) 1–12.

Wang C., Leng S., Guo H., Cao L., Huang J., Acid and alkaline treatments for regulation of hydrophilicity/hydrophobicity of natural zeolite, *Appl. Surf. Sci.* **478** (2019) 319–326.

Wang S. and Peng Y., Natural zeolites as effective adsorbents in water and wastewater treatment, *Chem. Eng. J.* 156 (2010) 11–24.

Wang Y., Gao B.Y., Yue W.W., Yue Q.Y., Adsorption kinetics of nitrate from aqueous solutions onto modified wheat residue, *Colloids and Surfaces A: Physicochem. Eng. Aspects* **308** (2007) 1–5.

Weber W.J.Jr. and Morris J.C., Kinetics of adsorption on carbon from solution, *J. Sanit. Eng. Div. Am. Soc. Civ. Eng.* **89** (1963) 31–59.

Wei-yu S., Hong-bo S., Hua L., Ming-an S., Sheng D., Progress in the remediation of hazardous heavy metal-polluted soils by natural zeolite, *J. Hazard. Mater.* **170** (2009) 1–6.

Werpy T. and Petersen G., Top value added chemicals from biomass volume I - Results of screening for potential candidates from sugars and synthesis gas. U.S. Department of Energy, NREL/TP-510-35523 (2004).

WHO, Guidelines for drinking-water quality: fourth edition incorporating the first addendum, World Health Organization, Geneva, 2017.

World reference base for soil resources 2014, International soil classification system for naming soils and creating legends for soil maps Update 2015, Food and Agriculture organization of the United Nations, Rome, p. 192.

Xiong W., Tong J., Yang Z., Zeng G., Zhou Y., Wang D., Song P., Xu R., Zhang C., Cheng M., Adsorption of phosphate from aqueous solution using iron-zirconium modified activated carbon nanofiber: Performance and mechanism, *J. Coloid Interface Sci*. **493** (2017) 17–23.

Yan K., Wu G., Wen J., Chen A., One-step synthesis of mesoporous $H_4SiW_{12}O_{40}$-SiO_2 catalysts for the production of methyl and ethyl levulinate biodiesel, *Catal. Commun.* **34** (2013) 58–63.

Yan L., Yang N., Pang H., Liao B., Production of levulinic acid from bagasse and paddy straw by liquefaction in the presence of hydrochloride acid, *Clean- Soil, Air Water* **36** (2008) 158–163.

Yang G., Pidko E.A., Hensen E.J.M., Structure, stability, and Lewis acidity of mono and double Ti, Zr, and Sn framework substitutions in BEA zeolites: A periodic density functional theory study, *J. Phys. Chem.* **117** (2013) 3976–3986.

Yang H., Hu Y., Tang A., Jin S., Qiu G., Synthesis of tin oxide nanoparticles by mechanochemical reaction, *J. Allloy. Compd.* **363** (2004) 271–274.

Yang L., Yang M., Xu P., Zhao X., Bai H., Li H., Characteristics of Nitrate Removal from Aqueous Solution by Modified Steel Slag, *Water* **9** (2017) 757–774.

Yazdi F., Anbia M., Salehi S., Characterization of functionalized chitosan-clinoptilolite nanocomposites for nitrate removal from aqueous media, *Int. J. Biol. Macromol.* **130** (2019) 545–555.

Yi N., Wu Y., Fan L., Hu S., Remediating Cd-contaminated soils using natural and chitosan-introduced zeolite, bentonite, and activated carbon, *Pol. J. Environ. Stud.* **28** (2019) 1461–1468.

Zeng W., Cheng D.G., Zhang H., Chen F., Zhan X., Dehydration of glucose to levulinic acid over MFI-type zeolite in subcritical water at moderate conditions, *React. Kinet. Mech. Catal.* **100** (2010) 377–384.

Zhan Y., Lin J., Zhu Z., Removal of nitrate from aqueous solution using cetylpyridinium bromide (CPB) modified zeolite as adsorbent, *J. Hazard. Mater.* **186** (2011) 1972–1978.

Zhang D., Duan A., Zhao Z., Xu C., Synthesis, characterization, and catalytic performance of NiMo catalysts supported on hierarchically porous Beta-KIT-6 material in the hydrodesulfurization of dibenzothiophene**,** *J. Catal.* **274** (2010) 273–286.

Zhang G., Feng P., Zhang W., Liu H., Wang C., Ma H., Wang D., Tian Z., Single isomerization selectivity of glucose in methanol over Sn-BEC zeolite of homogenous Sn distribution, *Micropor. Mesopor. Mat.* **247** (2017) 158–165.

Zheng Y. and Chen K., Leaching kinetics of selenium from selenium-tellurium-rich materials in sodium solutions. *T. Nonferr. Metal. Soc.*, **24** (2014) 536–543.

Zhi Z., Li N., Qiao Y., Zheng X., Wang H., Lu X., Kinetic study of levulinic acid production from corn stalk at relatively high temperature using $FeCl_3$ as catalyst: A simplified model evaluated, *Ind. Corps Prod.* **76** (2015) 672–680.

Zhou L., He Y., Ma L., Jiang Y., Huang Z., Yin L., Gao J., Conversion of levulinic acid into alkyl levulinates: Using lipase immobilized on meso-molding three-dimensional macroporous organosilica as catalyst, *Bioresource Technol.* **247** (2018) 568–575.

Zhuang J.P., Pang C.S., Liu Y., The Synthesis of levulinic acid synthesis from glucose using ZSM-5 zeolite catalyst, *Appl. Mech. Mater.* **291–294** (2013) 782–785.

Zieliński J., Zglinicka I., Znak L., Kaszkur Z., Reduction of Fe_2O_3 with hydrogen, *Appl. Catal. A-Gen.* **381** (2010) 191–196.

BIOGRAPHY OF AUTHOR

Jelena Pavlović was born on 9 October 1988 in Brus, Serbia. She graduated in 2011 from the Department of Environmental Engineering at the Faculty of Technology and Metallurgy, University of Belgrade. She defended her master's thesis in 2012 at the Department of General and Inorganic Chemistry, where she started PhD studies in Chemistry in 2012 (mentor: Prof. dr Nevenka Rajić).

Since 2012, she has been employed in the Innovation Center of the Faculty of Technology and Metallurgy, first as Research Trainee and since 2015 as Research Assistant at the project entitled "Oxide-Based environmentally-friendly porous materials for genotoxic substances removal" funded by Ministry of Education, Science and Technological Development of Republic of Serbia. Her teaching activities are involved in the laboratory courses in General Chemistry I and General Chemistry II on basic studies.

J. Pavlović has been involved in the: 1) Innovation project "*Removal of ammonia from groundwater. Softening of groundwater rich in magnesium by using natural zeolite*"; 2) HERD project "*The use of natural zeolite (clinoptilolite) for treatment of farm slurry and as a fertilizer carrier*"; 3) COST Project: "*Valorisation of lignocellulosic biomass side streams for sustainable production of chemicals, materials & fuels using low environmental impact technologies"* and 4) Bilateral project between R. Serbia and Slovakia: "*Zeolite-based adsorbents for environmental remediation*".

As young research, she stayed at Faculty of Environmental Science and Technology, Norwegian University of Life Sciences, Ås; Institute of Organic Chemistry with Centre of Phytochemistry, Sofia and National Institute of Chemistry, Ljubljana.

Research areas of J. Pavlović include synthesis, modification, characterization and use of natural zeolites in adsorption and catalysis.

She is the author or co-author of: chapter in an international monograph, 6 publications in international journals, 2 publication in national journal and 1 in national journal with international significance, 12 abstracts presented in international conferences and 3 in national conferences.

J. Pavlović has been a member of the Serbian Zeolite Association since 2012.

BIOGRAFIJA AUTORA

Jelena Pavlović rođena je 9.10.1988. u Brusu, Srbija. Diplomirala je na Tehnološko-metalurškom fakultetu, Univerziteta u Beogradu 2011. god. na katedri za Inženjerstvo zaštite životne sredine. Master studije završila 2012. god. na katedri za Opštu i neorgansku hemiju gde je upisala i doktorske studije, studijski program Hemija, šk. 2012/2013. pod mentorstvom prof. dr Nevenke Rajić.

Od decembra 2012. god. zaposlena je u Inovacionom centru Tehnološko-metalurškog fakulteta kao istraživač pripravnik, a od maja 2015. kao istraživač-saradnik, u okviru projekta Ministarstva prosvete, nauke i tehnološkog razvoja „Porozni materijali na bazi oksida u zaštiti životne sredine od genotoksičnih supstanci". Angažovana je na izvođenju vežbi iz predmeta Opšta hemije I i Opšta hemija II na osnovnim studijama.

J. Pavlović bila je uključena u realizaciju: 1) Inovacionog projekata „Uklanjanje amonijaka iz podzemnih voda i omekšavanje sirove vode bogate magnezijumom pomoću prirodnog zeolita"; 2) HERD projekta „*The use of natural zeolite (clinoptilolite) for treatment of farm slurry and as a fertilizer carrier*"; 3) COST projekta „*Valorisation of lignocellulosic biomass side streams for sustainable production of chemicals, materials & fuels using low environmental impact technologies"* i 4) Projekta bilateralne saradnje između R. Srbije i R. Slovačke *„Zeolite-based adsorbents for environmental remediation"*.

Radi stručnog usavršavanja boravila je na: Fakultetu ekologije i tehnologije u Ås-u (Norveška), Institutu za organsku hemiju sa centrom za fitohemiju u Sofiji kao i Nacionalnom hemijskom institutu u Ljubljani.

Oblast naučnoistraživačkog rada J. Pavlović obuhvata sintezu, modifikaciju, karakterizaciju i primenu prirodnih zeolita u adsorpciji i katalizi.

J. Pavlović je autor ili koautor: poglavlja u monografskoj studiji međunarodnog značaja, šest radova u naučnim časopisima međunarodnog značaja, dva rada u časopisu nacionalnog značaja i jednog rada u nacionalnom časopisu međunarodnog značaja. Održala je predavanje po pozivu na skupu međunarodnog značaja. Autor je ili koautor dvanaest saopštenja na konferencijama međunarodnog značaja i tri saopštenja sa skupova nacionalnog značaja.

Od 2012. godine član je Zeolitskog društva Srbije.

LIST OF PUBLICATIONS BASED ON THIS DOCTORAL DISSERTATION

List of Publications:

1. **Pavlović J.**, Popova M., Mihalyi R.M., Mazaj. M., Mali G., Kovač J., Lazarova H., Rajic N., Catalytic activity of SnO_2- and SO_4/SnO_2-containing clinoptilolite in the esterification of levulinic acid, *Microporous and Mesoporous Materials* **279** (2019) 10–18.
2. **Pavlović J.,** Krogstad T. Rajić N., Applicability of zeolites in potassium and nitrate retention in different soil types, *Journal of Serbian Chemical Society* **82** (2017) 1303–1314.
3. **Pavlović J.**, Krogstad T., Rajić N., The use of natural zeolite (clinoptilolite) for the treatment of farm slurry and as a fertillizer carrier, Chapter in an international monograph, Norwegian University of Life Sciences, Faculty of Envoronmental Sciences and Technology, Department of Environmental Sciences, (2016) 34–47.
4. **Pavlović J.,** Krogstad T., Rajić N., Influence of the Fe(III)-modified clinoptilolite on phosphorus leaching from different soil types, *Materials Protection* **4** (2016) 539–544.
5. **Pavlović J.,** Krogstad T., Rajić N., Uticaj prirodnog zeolita kao suplementa na zadržavanje kalijuma u različitim vrstama zemljišta, Zbornik naučnih radova Instituta PKB Agroekonomik **21** (2015) 165–172.
6. **Pavlović J.**, Milenković J., Rajić N., Modification of natural clinoptilolite for nitrate removal from aqueous media, *Journal of Serbian Chemical Society* **79** (2014) 1309–1322.

List of Attended Conferences:

1. **Pavlović J**., Popova M., Mihalyi M., Mazaj M., Mali G., Kovač J., Lazarova H., Rajić N., Catalytic activity of clinoptilolite-based catalysts in the esterification of levulinic acid, *8th Serbian-Croatian-Slovenian Symposium on Zeolites*, 3–5 October 2019, Belgrade, Serbia.
2. **Pavlović J**., Popova M., Mihalyi M.R., Mazaj M., Mali G., Kovač J., Lazarova H., Rajic N., Clinoptilolite as a solid catalyst for the esterification of levulinic acid to

octyl levulinate, *4th Euro Asia Zeolite Conference*, 27–30 January 2019, Taormina, Italy.

3. Rajic N., Milenkovic J., **Pavlovic J.**, Jevtic S., Kaplanec I., Rečnik A., Hrenovic J., Adsorptive, catalytic and antimicrobial applications of Serbian natural clinoptilolite, *ZEOLITE 2018–10th International Conference on the Occurrence, Properties and Utilization of Natural Zeolites*, 24–29 June 2018, Cracow, Poland.
4. **Pavlović J**., Krogstad T., Rajić N., A study of potassium and nitrate leaching from different soil types in the presence of natural clinoptilolite, *7th FEZA Conference „The ZEOLITES: Materials with Engineered properties*", 3–7 July 2017, Sofia, Bulgaria.
5. **Pavlović J.**, Krogstad T., Rajić N., Influence of natural zeolite - clinoptilolite on potassium and nitrate retention in different soil types, *7th Slovenian-Serbian-Croatian Symposium on Zeolites*, 25–27 May 2017, Ljubljana, Slovenia.
6. **Pavlović J.**, Kaplanec I., Lazarević S., Rajić N., Phosphate adsorption from aqueous solution using iron-modified clinoptilolite, *6th Croatian-Slovenian-Serbian Symposium on Zeolites*, 1–3 October 2015, Šibenik, Croatia.
7. **Pavlović J.**, Milenković J., Stojaković Đ., Rajić N., Surface modification of the natural clinoptilolite for its potential use for the nitrate removal from water media, *5th Serbian-Croatian-Slovenian Symposium on Zeolites*, 30 May–02 June 2013, Zlatibor, Serbia.
8. Milovanović J., Jevtić S., Milenković J., **Pavlović J.**, Hrenović J., Rajić N., Efikasnost srbijanskog prirodnog zeolita u poboljšanju kvaliteta pijaće vode, *XIII međunarodna konferencija "Vodovodni i kanalizacioni sistemi"*, 22–24 Maj 2013, Jahorina, Bosna i Hercegovina.

APPENDIX A

Изјава о ауторству

Име и презиме аутора Јелена Павловић

Број индекса 4006/2012

Изјављујем

да је докторска дисертација под насловом

"Синтеза и карактеризација нових адсорбенаса и катализатора на бази природног зеолита применљивих у процесу коришћења биомасе"

"Synthesis and characterization of novel adsorbents and catalysts based on natural zeolite, applicable in use of biomass"

- резултат сопственог истраживачког рада;
- да дисертација у целини ни у деловима није била предложена за стицање друге дипломе према студијским програмима других високошколских установа;
- да су резултати коректно наведени и
- да нисам кршио/ла ауторска права и користио/ла интелектуалну својину других лица.

Потпис аутора

У Београду, _____

_____

APPENDIX B

Изјава о истоветности штампане и електронске верзије докторског рада

Име и презиме аутора Јелена Павловић

Број индекса 4006/2012

Студијски програм Хемија

Наслов рада "Синтеза и карактеризација нових адсорбенаса и катализатора на бази природног зеолита применљивих у процесу коришћења биомасе"

"Synthesis and characterization of novel adsorbents and catalysts based on natural zeolite, applicable in use of biomass"

Ментор Проф. др Невенка Рајић

Изјављујем да је штампана верзија мог докторског рада истоветна електронској верзији коју сам предао/ла ради похрањена у **Дигиталном репозиторијуму Универзитета у Београду.**

Дозвољавам да се објаве моји лични подаци везани за добијање академског назива доктора наука, као што су име и презиме, година и место рођења и датум одбране рада.

Ови лични подаци могу се објавити на мрежним страницама дигиталне библиотеке, у електронском каталогу и у публикацијама Универзитета у Београду.

Потпис аутора

У Београду, _____

_____

APPENDIX C

Изјава о коришћењу

Овлашћујем Универзитетску библиотеку „Светозар Марковић“ да у Дигитални репозиторијум Универзитета у Београду унесе моју докторску дисертацију под насловом:

“Синтеза и карактеризација нових адсорбенаса и катализатора на бази природног зеолита применљивих у процесу коришћења биомасе“

“Synthesis and characterization of novel adsorbents and catalysts based on natural zeolite, applicable in use of biomass“

која је моје ауторско дело.

Дисертацију са свим прилозима предао/ла сам у електронском формату погодном за трајно архивирање.

Моју докторску дисертацију похрањену у Дигиталном репозиторијуму Универзитета у Београду и доступну у отвореном приступу могу да користе сви који поштују одредбе садржане у одабраном типу лиценце Креативне заједнице (Creative Commons) за коју сам се одлучио/ла.

1. Ауторство (CC BY)

2. Ауторство – некомерцијално (CC BY-NC)

3. Ауторство – некомерцијално – без прерада (CC BY-NC-ND)

4. Ауторство – некомерцијално – делити под истим условима (CC BY-NC-SA)

5. Ауторство – без прерада (CC BY-ND)

6. Ауторство – делити под истим условима (CC BY-SA)

(Молимо да заокружите само једну од шест понуђених лиценци.
Кратак опис лиценци је саставни део ове изјаве).

Потпис аутора

У Београду, _____

_____

1. **Ауторство.** Дозвољавате умножавање, дистрибуцију и јавно саопштавање дела, и прераде, ако се наведе име аутора на начин одређен од стране аутора или даваоца лиценце, чак и у комерцијалне сврхе. Ово је најслободнија од свих лиценци.

2. **Ауторство – некомерцијално**. Дозвољавате умножавање, дистрибуцију и јавно саопштавање дела, и прераде, ако се наведе име аутора на начин одређен од стране аутора или даваоца лиценце. Ова лиценца не дозвољава комерцијалну употребу дела.

3. **Ауторство – некомерцијално – без прерада**. Дозвољавате умножавање, дистрибуцију и јавно саопштавање дела, без промена, преобликовања или употребе дела у свом делу, ако се наведе име аутора на начин одређен од стране аутора или даваоца лиценце. Ова лиценца не дозвољава комерцијалну употребу дела. У односу на све остале лиценце, овом лиценцом се ограничава највећи обим права коришћења дела.

4. **Ауторство – некомерцијално – делити под истим условима**. Дозвољавате умножавање, дистрибуцију и јавно саопштавање дела, и прераде, ако се наведе име аутора на начин одређен од стране аутора или даваоца лиценце и ако се прерада дистрибуира под истом или сличном лиценцом. Ова лиценца не дозвољава комерцијалну употребу дела и прерада.

5. **Ауторство – без прерада**. Дозвољавате умножавање, дистрибуцију и јавно саопштавање дела, без промена, преобликовања или употребе дела у свом делу, ако се наведе име аутора на начин одређен од стране аутора или даваоца лиценце. Ова лиценца дозвољава комерцијалну употребу дела.

6. **Ауторство – делити под истим условима**. Дозвољавате умножавање, дистрибуцију и јавно саопштавање дела, и прераде, ако се наведе име аутора на начин одређен од стране аутора или даваоца лиценце и ако се прерада дистрибуира под истом или сличном лиценцом. Ова лиценца дозвољава комерцијалну употребу дела и прерада. Слична је софтверским лиценцама, односно лиценцама отвореног кода.

APPENDIX D

ОЦЕНА ИЗВЕШТАЈА О ПРОВЕРИ ОРИГИНАЛНОСТИ ДОКТОРСКЕ ДИСЕРТАЦИЈЕ

На основу Правилника о поступку провере оригиналности докторских дисертација које се бране на Универзитету у Београду, коришћењем програма iThenticate извршена је провера оригиналности докторске дисертације кандидата Јелене Павловић, под називом **„Синтеза и карактеризација нових адсорбенаса и катализатора на бази природног зеолита применљивих у процесу коришћења биомасе (Synthesis and characterization of novel adsorbents and catalysts based on natural zeolite, applicable in use of biomass)”.**

Извештај који садржи резултате провере оригиналности ментор је добио дана 21.05.2020. Утврђени проценат подударности је 14%. Овај степен подударности последица је претходно публикованих резултата докторандових истраживања, који су проистекли из његове дисертације, што је у складу са чланом 9. Правилника.

На основу свега изнетог, а у складу са чланом 8. став 2. Правилника о поступку провере оригиналности докторских дисертација које се бране на Универзитету у Београду, изјављујем да извештај указује на оригиналност докторске дисертације, те се прописани поступак припреме за њену одбрану може наставити (позитивна оцена).

Датум 28. мај 2020. године Ментор

_____

Проф. др Невенка Рајић, редовни професор
Универзитет у Београду, Технолошко-металуршки факултет